**UNIVERSITÀ DEGLI STUDI DI PADOVA**

DIPARTIMENTO DI INGEGNERIA INDUSTRIALE

CORSO DI LAUREA MAGISTRALE IN INGEGNERIA CHIMICA E DEI PROCESSI INDUSTRIALI

Tesi di Laurea Magistrale in
Ingegneria Chimica e dei Processi Industriali

# MICRO-CHANNEL ARRAYS BY TWO PHOTON LITHOGRAPHY FOR CELL MIGRATION STUDIES

***Relatore: Prof.ssa Elisa Cimetta***
***Correlatore: Ing. Sara Micheli***

***Laureanda: ELISA VARASCHIN***

ANNO ACCADEMICO 2019 – 2020

# Riassunto

Lo studio della migrazione di cellule tumorali è di primaria importanza nel panorama biologico e medico, in quanto evento chiave nella metastasi tumorale. Quest'ultima è un processo dinamico in cui cellule tumorali iniziano a muoversi nel microambiente circostante, guidato principalmente da differenti stimoli meccanici e chimici. Pertanto, capire come queste cellule possano muoversi diventa un obiettivo importante. Fino ad oggi i classici studi di migrazione avvengono *in vitro*, nelle piastre di coltura, dove vengono trattati aggregati e popolazioni cellulari. Tuttavia, recenti studi hanno però dimostrato come le informazioni legate allo stadio iniziale della migrazione, con una risoluzione a cellula singola "*single-cell",* giochi un ruolo esclusivo nella metastasi. Di conseguenza, La necessità di un dispositivo che permetta di studiare la migrazione a questa scala diventa fondamentale. Ed è qui che la nuova frontiera della microfluidica gioca un ruolo fondamentale. Questa tecnologia è basata sulla manipolazione di fluidi su scala nano- e micro-metrica, governati da forze differenti rispetto alla macroscala. A differenza delle colture *in vitro*, questi dispositivi migliorano i tempi sperimentali, possono riprodurre un ambiente più fedele a quello *in vivo* e ridurre il numero di reagenti e sostanze necessarie per gli studi.

Pertanto, l'obiettivo di questa tesi è quello di produrre un dispositivo microfluidico che permetta lo studio della chemiotassi delle cellule di Neuroblastoma. Nella fase iniziale è stata studiata e modellata una possibile geometria. Il dispositivo è stato fabbricato utilizzando un'innovativa tecnologia di polimerizzazione a due fotoni (2PP) che consente di riprodurre con precisione nanometriche strutture 3D.

Più in dettaglio, sono stati studiati diversi progetti proposti, sia *in silico* tramite simulazioni CFD, che sperimentalmente. È stato concluso che è necessaria la produzione di un master in resina con tecnologia 2PP, combinata con stampaggio *replica molding* in materiali polimerici.

# Abstract

The study of tumor cell migration is of paramount importance in biological and medical research, as it is a key event in cancer metastasis. Metastasis is a dynamic process in which cancer cells begin to move in the surrounding microenvironment, driven mainly by different mechanical and chemical stimuli. Therefore, understanding how these cells acquire increased motility is a stimulating and necessary goal. Nowadays, classical migration studies are performed *in vitro,* in culture plates where aggregates and cell populations are treated. However, recent studies have shown that initial stage migration information with "*single-cell*" resolution plays an exclusive role in metastasis. Therefore, the need for a device that allows to study migration at this scale and resolution becomes crucial. The new frontier of microfluidics plays here a fundamental role. This technology is based on the manipulation of fluids at the nano- and micro-metric scales, where they are governed by different forces than at the macroscale. Unlike *in vitro* cultures, these devices improve experimental times, can reproduce an environment more faithful to the *in vivo* one, and reduce the number of reagents and substances needed for studies. Therefore, the goal of this thesis is to produce a microfluidic device that allows the study of chemotaxis of Neuroblastoma cells. In the initial phase, a geometry was studied and modeled. The device was fabricated using an innovative two-photon polymerization (2PP) technology that allows to accurately reproduce nanometric 3D structures.

More in detail, different proposed designs have been studied, both *in silico* via CFD simulations, and experimentally. It has been concluded that the production of a resin master with 2PP technology, combined with and *replica molding* in polymeric materials, is required for the production of the final platform. Finally, the device was biologically tested to see if it could actually generate a favorable environment from a cellular point of view for these types of study.

# Table of Contents

# List of Figures

# List of Tables

# Introduction

Microfluidics is a science that studies the behavior of fluids at the nano- and micro-scales. Its application to the biological and biomedical fields is useful to improve various issues related to traditional cell cultures. Thanks to microfluidic devices, it is possible to improve experimental times, reproduce an environment more faithful to the cellular one, and reduce the quantities of reagents and substances needed for studies. All of this contributes to an improved understanding of what happens *in vivo*, inside our bodies.

Metastasis is a dynamic process in which cancer cells begin to move in the surrounding microenvironment, mainly driven by different mechanical and chemical stimuli. A microfluidic platform with micro-channel arrays and a *"single-cell"* resolution, could be a suitable instrument to investigate tumor cell migration in Neuroblastoma, an aggressive cancer that develops during childhood. Modern 3D printers can realize precise micro and nano structures with a fast turnaround, overcoming the limitations of traditional methods to produce microfluidic platform (photolitigraphy and micromolding techniques). Micro-channel arrays can be successfully fabricated using the two-photon polymerization (2PP) technique.

The focus of the thesis is to design a micro-channels arrays geometry enabling migration studies at *"single-cell"* resolution under a controlled concentration gradient, the chosen chemotactic stimulus.

The first stages of design and modeling were carried out in the BIAMET laboratory, as well as all subsequent biological and fluid dynamic validations. The fabrication was made with the collaboration of the research group Lab.Tesi, based in Rovigo, using the *Nanoscribe Photon Professional GT*, a 3D printer that exploits the technology of two-photon photopolymerization.

The thesis is composed of four Chapters.

In the first one, the state of the art about microfluidics and two-photon polymerization physics and its application to the biomedical and biological fields are presented, focusing on microfluidic devices. Moreover, brief descriptions of Neuroblastoma, the metastasis process, and classical migration study are given.

In the second chapter, the different platform geometries and corresponding CFD simulations will be presented. A functional design of the platform must lead to the formation of a suitable concentration gradient. Afterward, the results will be discussed. Then, all the procedures for the master production using Nanoscribe technology will be described. Finally, *replica molding* and plasma treatment processes for the production of the final platform in PDMS will be presented. In the fourth chapter, all biological tests performed using the SK-N-AS

Neuroblastoma cell line are explained and discussed. Initially, the aim is to verify if cells can attach and grow inside the produced platform, and then verify if they move through the channels. In the final part of the chapter, the tests to induce migration inside the microfluidic platform are reported.

# Chapter 1

# State of the Art

In this Chapter, the theory of microfluidics, Two-photons-polymerization, and their role in biomedical research will be introduced, with specific attention to the fabrication methods. Afterward, a brief description of the importance of migration in cancer cell study, in particular for Neuroblastoma, is presented. Finally, the motivation and aim of the thesis will be explained.

## 1.1 Microfluidics

Microfluidics is the science and technology that studies the behavior of systems that differ from conventional flow theory due to the nano- and micro- length scale.[1] This field allows us to manipulate small ($10^{-9}$ and $10^{-10}$ liters) amount of fluids, using a channel with a dimension of tens to hundreds of micrometers, providing several advantages. Indeed, not only the dimensions of the devices but also the quantities of samples and reagents are dramatically decreased (accurate control of the low volume of fluids), leading to the shorter time of experiments[2], the possibility of running multiple parallel operations, and fewer costs. For these reasons, "Lab-on-a-chip" (an example is reported in Figure1.1) devices can gather various laboratory functions in a single chip. The early applications of microfluidic engineering can be found in the analysis area, in particular in microanalytical methods such as gas-phase chromatography (GPC), high-pressure liquid chromatography (HPLC) and capillary electrophoresis (EC)[2]. Another support to the development of this discipline was from silicon microelectronics and micro-electromechanical systems (MEMS). Some of the first works in the microfluidics platform system used silicon and glass. Still, these materials have largely been displaced by plastic, because of silicon optical properties (opaque material) and its high cost. Much of the exploratory research in microfluidic systems has been carried out using polymers such as polydimethylsiloxane (PDMS)[2] and other particular resins.

**Figure 1.1** *Example of a microfluidic device. A microbioreactor composed of a matrix of microwells arranged in lines and connecter to two lateral channels. The Device is filled with a color tracer that allows the visualization of the structure. Adapted from*[3].

It is evident that microfluidics is an extraordinarily interdisciplinary and versatile science, and for this reason, the motivation for the development of this technique is very high. Microfluidics finds support also in the field of heat management, energy generation, and display technology. Other specific applications include protein crystallization, proteomics, micropumps, separations techniques in general and DNA separation, chemical synthesis, and *single-cell* analysis.[4]

Despite all the advantages explained previously, the potential of microfluidic devices has not been fully exploited, mainly due to the fact that the control of flows at the micro- and nanometric scale is still an issue[5].

Nevertheless, it is essential to underline that, with accurate theoretical and experimental analysis of the microfluidic system, it is possible to achieve very high precision and high-throughput data.

### *1.1.1 The physics of microfluidic*

It is crucial to underline that the fluid behavior in microfluidic systems differs from conventional flow theory. First of all, some meaningful equations that express the principal mechanism of transport are explained. The velocity field for a Newtonian fluid follows the Navier-Stokes equations, reported in Equation (1.1):

$$\rho \frac{Dv}{Dt} = \rho\left(\frac{\partial v}{\partial t} + (v \cdot \nabla)v\right) = -\nabla p + \mu \nabla^2 v + \rho g, \tag{1.1}$$

In the case of microfluidic devices, inertial forces are small compared to viscous ones, so that the non-linear term can be discarded. In essence, the term $\rho(v \cdot \nabla)v$ can be neglected when the flow is hugely slow[6], leaving the Stokes equation, reported in Equation (1.2):

$$\rho \frac{Dv}{Dt} = -\nabla p + \mu \nabla^2 v + \rho g \ , \tag{1.2}$$

A variety of physical phenomena occur in these devices, and for this reason, it becomes useful to understand how a particular phenomenon prevails on others. For this purpose, dimensionless numbers can be used, and the most relevant ones are listed in Table 1.1.

**Table 1.1** *Dimensionless numbers used in microfluidics. Adapted from[4].*

| Acronym | Name | Phenomena compared |
|---|---|---|
| Re | Reynolds | Inertial/viscous |
| Pe | Péclet | Convection/diffusion |
| Ca | Capillary | Viscous/interfacial |
| Wi | Weissenberg | Polymer relaxation time/shear rate time |
| De | Deborah | Polymer relaxation time/flow time |
| El | Elasticity | Elastic effects/inertial effects |
| Gr | Grashof | Re for buoyant flow |
| Ra | Rayleigh | Pe for buoyant flow |
| Kn | Knudsen | Slip length/macroscopic length |

**Table 1.2** *Main properties of water at 20°C and 1 atm pressure in a microfluidic channel. Adapted from[4].*

| Parameter | Value |
|---|---|
| Velocity | $10^{-6}$-$10^{-4}$ m/s |
| Channel radius | $10^{-6}$-$10^{-4}$ m |
| Channel length | $5 \cdot 10^{-3}$-$10^{-1}$ m |
| Density | 1.0 g/cm$^3$ |
| Shera viscosity | $1.0 \cdot 10^{-2}$g/cm s |
| Viscosity | $1 \cdot 10^{-3}$ Pa·s |

These dimensionless numbers compare two different phenomena or length scales to find a physical meaning and to determine which is predominant. The calculation of the aforementioned dimensionless numbers is typically done considering a flux of water, flowing in microfluidic devices, with properties reported in Table.1.2

The Reynolds number gives information about how much inertial forces dominate over viscous ones and vice versa. It is also useful to easily characterize a fluid flow regime, and in particular whether it is laminar or turbulent[7]. In microfluidic devices, this number usually assumes small values due to the viscous forces overcoming the inertial ones. It can be demonstrated that, for a tubular pipe, the flow is laminar if Re < 2300, and for Reynolds between 2300 and 5000, there is a transition region from the laminar to the turbulent. The Reynolds number can be calculated by Equation 1.3:

$$Re \equiv \frac{\rho v D_{eq}}{\mu} , \tag{1.3}$$

where $\rho$ is the fluid density, $v$ is the characteristic velocity of the fluid, $\mu$ is the fluid viscosity and $D_{eq}$ is the equivalent diameter, calculated from Equation (1.4):

$$D_{eq} = \frac{2S}{4P} , \tag{1.4}$$

where S is the area available from the passage of the fluid, and P is the semi-perimeter. However, the literature notices that values of Re, especially for the transition from laminar to turbulent channels, might be different than those predicted by theory[7]. With high-Re we are in the presence of random eddies that stretch and fold fluid elements chaotically, speeding up the mixing[4]. It means that low Reynolds numbers characterize the microfluidic devices and laminar flows. For this reason, the transport of species takes place mainly due to diffusion. Therefore, Péclet number, Pe, gives information about these behaviors, comparing the convective and diffusive mass transport by the Equation (1.5):

$$Pe \equiv \frac{vD}{D_i} , \tag{1.5}$$

where $\nu$ is the velocity inside the pipe [m/s], $D$ is the diameter [m], and $D_i$ is the diffusion of the coefficient of the specie $i$ [$m^2$/s].

The smaller Pe, the higher the contribution of the diffusion component to the overall mass transport. Typical Pe values for a microfluidic channel, considering the diffusion of low protein in water ($D_i \approx 4 \cdot 10^{-11}$ $m^2$/s), are between 0.05 and 500[8].

Therefore, in microfluidic devices, the convective contribution is small compared to the diffusion that is dominant and typically slow. Thanks to this feature and careful design, a stable concentration gradient can be generated inside the platform. The conservation equation of species $i$ can be considered in Equation (1.6):

$$\frac{\partial c_i}{\partial t} = -\nabla(c_i v) - \nabla(J_i) + R_i , \tag{1.6}$$

where the left-hand side represents the variation in concentration of species $i$ with time, the first right-hand-side represents the convective flux, then there is the diffusive flux and at least the production/consumption of the species $i$ during a chemical reaction.

Highlighting what we considered before, given that the diffusive term is predominant, reactions are not involved, and the steady state is achieved, Equation (1.7) can be simplified as:

$$0 = -\nabla(J_i) . \tag{1.7}$$

From Equation (1.8) is it possible to say that the diffusive flux is constant, assuming constant condition across the device. Fick's law expresses the diffusive flux:

$$J_i = - D_i \nabla c_i , \tag{1.8}$$

where $D_i$ is the diffusion coefficient of $i$ in the medium [m$^2$/s] and $\nabla c_i$ is the gradient of concentration of species $i$ [mol/ m$^3$].

The diffusion coefficient of a generic particle can be evaluated thanks to the Einstein-Smoluchowski equation:

$$D_i = \nu k_B T, \tag{1.9}$$

where $\nu$ is the mobility of the particle [kg/s], $k_B$ the Boltzmann constant [J/K], and $T$ is the temperature [K]. In the particular assumption where the particle shape is comparable to a sphere, the Equation (1.10) becomes:

$$D_i = \frac{k_B T}{6\pi \nu r}, \tag{1.10}$$

also known as the Stokes-Einstein equation, where $r$ [m] is the radius of the particle.

Lastly, another dimensionless number that we consider in detail is the Capillary number Ca, expressing the competition between the interfacial and viscous stresses. In the microscale, compared to the macro scale, the interfacial stress has a more dominant role. Ca is useful to estimate the possibility of producing mono-disperse droplets and is defined as:

$$Ca = \frac{\nu \mu}{\gamma} , \tag{1.11}$$

where $\gamma$ is the surface tension of the fluid (usually at the interface with air)[4].

When two immiscible fluids are present, surface tension and viscous stress have a specific role: the first reduces the interfacial area, the second extends, and pulls the interface downstream. These contributions can be balanced to obtain droplets with radius $R$:

$$R \sim \frac{\gamma}{\nu \mu} h = \frac{h}{Ca} . \tag{1.12}$$

### *1.1.2 Microfluidics in biology*

With the aim of carefully studying biological systems and analyzing intra- and intercellular molecular interactions, it is of paramount importance to reproduce the complex biological world as close as possible.

The conventional culture method in biology is *in vitro* and made using Petri dishes. This "flat environment" cannot be representative of the real state of the physiologic system and could therefore lead to unrealistic results[3]. The most common restriction in standard biological experiments is the lack of spatial proximity, which causes the presence of

"potential false positives" interaction between molecules that usually may not interact *in vivo*[9].It means that they are not data about interaction dynamics between molecules using this technique.

Thanks to microfluidics, these limitations can be overcome. The main advantages of microfluidic devices are reported below[5,9]:

- the small volume that improves the cell dosage, providing a more accurate quantity or reagents and of cells in the experiment;
- Precise control of cell number and density in a given area and volume. These devices can also provide a cell placement in a specific position;
- Reduction of a cell population from $10^4$-$10^7$ to a few hundred or dozens;
- The laminar flow that allows establishing precise conditions and concentration gradients;
- Possibility to rearrange the cells into spatially-controlled geometries both in 2D and 3D;
- Possibility of controlling the microenvironment using membrane valves;
- Possibility of using optically transparent materials to observe the experiment with the microscope, thanks to the usage of fluorescent molecular imaging.

However there also some drawbacks with microfluidics in biology[9]:

- lack of experimental compatibility with established laboratory methodologies.
- faster consumption of nutrients and an increase of the concentration of metabolites due to the small volumes;
- lack of culture protocols;
- cell attachment can induce some problems such as channels clogging and malfunctioning of valves.

Despite these disadvantages, microfluidics still is an excellent opportunity for the progress of biology experimentation thanks to the ability to recreate finely-tuned cell culture conditions.

### *1.1.3 Microfluidic devices technologies*

Regarding production methods of microfluidic platforms, micromachining, soft lithography, embossing, in situ construction, injection molding, and laser ablation are the most commonly used[10]. Depending on the specific application, a suitable production method is chosen. An important common stage is the design and production of the master mold, where a geometry is proposed and visualized with CAD software, and possibly simulated with a software for fluid dynamic simulation. The production of the microfluidic platform follows, usually by *replica molding*, micromachining, and micromolding.

#### 1.1.3.1 Design and production of master

Two of the most consolidated production techniques are presented in more detail below:

- Soft lithography: The first step is the production of a master mold, from which the platform will be replicated using a suitable material. The structure design is printed onto a polymer sheet creating a photomask (made in a few hours). The printed 2D features are then positioned over a photoresist film (polymeric substance that reacts to UV and X electronic and ionic rays) in order to induce a selective polymerization following light exposure. The photoresist film is uniformly dispersed on a silicon wafer through spin coating. Subsequently, the master obtained can be employed to fabricate the platform through *replica molding*[8];
- Micromilling: This technique allows to obtain more precise structures by "removing bulk material" from a raw workpiece (usually made of metallic material, such as aluminum). In microfluidic, it is mainly used for micro-channel fabrication. It is not employed as frequently as soft lithography because of the higher costs[11].

## 1.2 Two photon polymerization technologies

The Two-photon polymerization (2PP) is a process where the photo-polymerization takes place as a consequence of a quasi-simultaneous absorption of two photons. Molecules that absorb photons are excited to an energetic state in which they can produce reactive species able to trigger the photo-polymerization. It is a non-linear phenomenon of the third order in which the molecule energy absorption rate and thus the two-photon absorption (TPA) takes places. The rate of energy absorbed in a two-photon process is shown in Eq. 1.13 and is proportional to the square of the light intensity[12]:

$$\frac{dW}{dt} = \frac{8\pi^2\omega}{n^2 c^2} I^2 Im(\chi^{(3)}) \tag{1.13}$$

where $\omega$ is the singular frequency, $c$ the speed of light in vacuum, $n$ the refractive index of the medium, $I$ the laser intensity and $\chi^{(3)}$ the imaginary part of the third-order susceptibility tensor.

In this specific case, the photons belong to the infrared region (IR) (Figure1.2). Their energy, combined with the quadratic dependence of the TPA probability with the laser intensity, implies very high photon densities and huge radiation intensities to trigger the polymerization. IR laser that works in continuous is not able to obtain enough photon density value without thermal damaging the material.

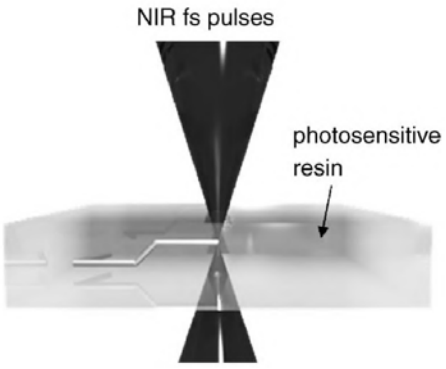


**Figure 1.2** *NIR light is focused into the volume of the UV-sensitive resin allowing the 3D fabrication. Adapted from* [13]

The minimum photon density needed to trigger the 2PP is achieved only in the laser focal spot, while in the outer regions, no radiation absorption occurs. This peculiarity allows a precise and selective polymerization in the photoresist volume. The obtained polymerized volume is much smaller. The volume is called voxel; it has an ellipsoidal shape elongated along the axial direction and an aspect ratio generally higher than 3[14]

### *1.2.1 3D fabrication technique*

In recent years, three-dimensional (3D) micro-/nanofabrication technologies have attracted increasing attention due to their potential use in a wide range of applications, including integrated optics, plasmonics, microbiology, and microelectromechanical systems.[15] The reasons why 3D printing, or additive manufacturing, has become routinely feasible are the freedom in design and the elimination of most cost-, time- and labor-intensive stages of the product development processes. 3D printing is more precise, faster, and typically less expensive than traditional forms of manufacturing.[16] These advantages have favored not only the industrial but also R&D processing. Two-Photon Polymerization (TPP) offers a new possibility in that means, with a sub-micrometers scale resolution.

Nanoscribe is the gold-standard machine able to do this and, also thanks to the enormous potential of modern femtosecond near-infrared laser for microfabrication, has gained considerable attention over the past year due to the following reason:

- near-infrared laser can fabricate complex and arbitrary 3D microstructures using computer-generated 3D models;
- The mechanism is coherent and repeatable;
- 100 nm spatial resolution can be obtained;
- diverse 2D-3D microstructures can be integrated directly into complex experimental microdevices.[17]

## 1.2.2 The physics of 2PP

Two photon-polymerization (2PP) technology is based on the two-photon-absorption (2PA). This theory was first formulated by Maria Göpper-Mayer in 1931 and demonstrated in an experiment by Kaiser in 1961. This happened following the invention of the laser, which enabled the generation of two-photon excited fluorescence in a europium-doped crystal.[18] Two photons can be absorbed sequentially or simultaneously as shown in Figure1.3.

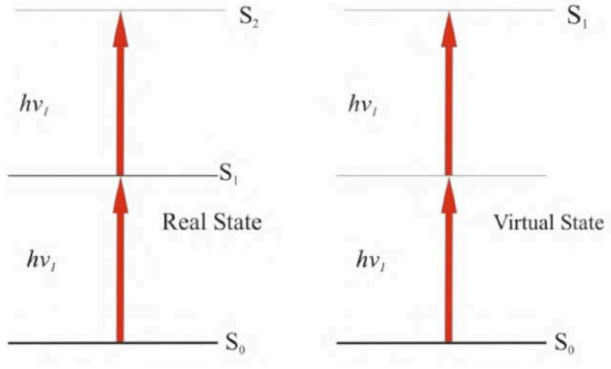


**Figure 1.3** *Two photon-absorption. (a): sequential absorption; (b): simultaneous absorption. Adapted from [19].*

In the sequential absorption, a two-level system in ground state $S_0$ is excited to an intermediate real state $S_1$ by the first photon. Then another photon excites the material to the final state $S_2$. An intermediate state energy is required. In simultaneous absorption, there is no real intermediate energy state, i.e., the material is transparent at that wavelength. Instead, there is a virtual intermediate energy state, and two-photon absorption happens only if another photon arrives within the virtual state lifetime. For this to happen, it is essential to have high intensities, which can exclusively be provided by a tightly focused femtosecond laser beam.[19] 2PA is a threshold effect. It means that we need a peak power more elevated than a certain threshold to activate it. The femtosecond laser can emit very short pulses of tens to hundreds of femtoseconds with high pulse peak power allowing to reach the threshold while maintaining low average power.

## 1.2.3 Polymerization process

Photopolymerization is the light-induced reaction principle used by 3D printing with Nanoscribe. It can convert liquid or solid gel monomer into a solid polymer. These reactions require the use of an appropriate photo-initiator which is a light-sensitive molecule that produces an active species upon irradiation with UV, visible or infrared light, as in our case. The photo-initiators that have been most extensively employed so far are divided into two main categories depending on the nature of the generated active species (radicals or cations). The most commonly used are the cationic initiators, photo-acid generators that produce cations upon light irradiation. The photolysis of these initiators has been shown to result in

the generation of free radicals allowing the combination of monomers to be polymerized. A capable initiator has a high quantum yield in the generation of the active moieties, high thermal stability. Free-radical polymerizations are chain reactions in which the addition of a monomer molecule to an active chain-end regenerates the active site at the chain-end. The free-radical photopolymerization mechanism involves at least three different kinds of reaction:

Initiation $$I \xrightarrow{2\,h\nu} I^{*} \longrightarrow \dot{R} \quad (1.a)$$

Propagation $$\dot{R}+M \longrightarrow R\dot{M} \xrightarrow{M} RM\dot{M}\ldots \longrightarrow R\dot{M}_n \quad (1.b)$$

Termination $$R\dot{M}_n+R\dot{M}_m \longrightarrow RM_{n+m}R \quad (1.c)$$

- Initiation step: the photo-initiator molecule, *I*, is decomposed with light, *hv* is a photon, in the presence of a monomer, *M*, to form an active species, $\dot{R}$ (1a);
- Propagation step: the initiator fragment reacts with a monomer molecule to form the first active adduct that is capable of being polymerized. Monomers continue to add in the same manner resulting in the formation of micro radicals which are end-active polymers (1.b);
- Termination step: the growth center is deactivated ad the final polymer molecules are formed. This step involves typically the reaction between two polymers bearing active centers and can proceed by two different mechanisms, combination or disproportionation, leading to the formation of one or two polymer chains(1c).[19]

#### 1.2.3.1 2PP Bio-applications

The capability to produce 2D and 3D complex highly resolute structures and the possibility to different broad biomaterials in different conditions have made the direct laser writing two-photon polymerization (DLW-2PP) an appealing technology for the development of several bioengineering environments. DLW-2PP can create and represent a better environment for cells and all the microorganisms involved in a particular study. It has been used for the fabrication of micro-channels in microfluidic (also as a master for the platform production), in micro-robotic applications, in tissue engineering for studying cell behavior.

#### 1.2.3.2 2PP in microfluidics

The ability to create a micro-meter platform in a single step through 3D printing has the potential to change the field of microfluidics significantly. The approaches to fabricate a chip are different; for example, it is possible to make a master for casting PDMS or open

and closed devices composed of micro-channels. Figure1.4 reports the schematic illustrations of a 3D micro-channel structure fabricated by two-photon using positive (a,b) and negative (b,c) photoresists.

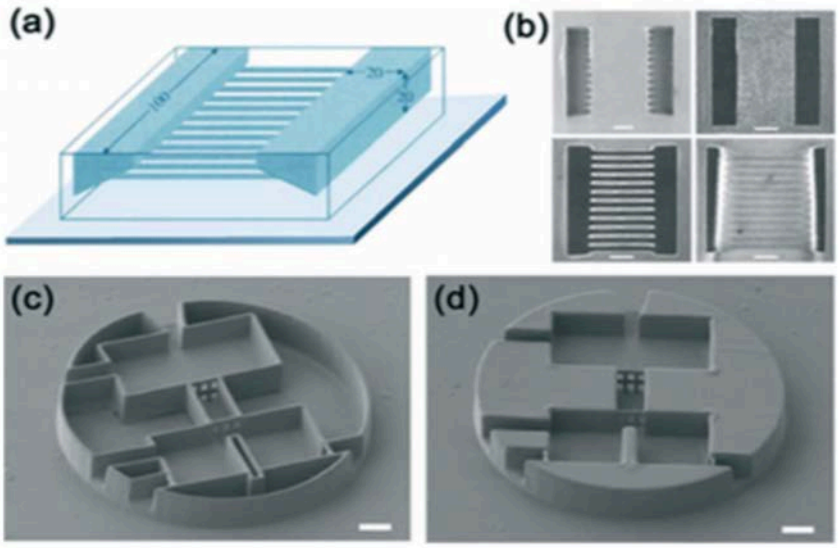


**Figure 1.4** *Schematic illustration of a 3D micro-channel structure fabricated by two-photon using positive photoresists (a,b) and negative (c,d). Adapted from*[20].

## 1.3 The role of migration in cancer cells and study

Metastatic disease is common in cancer and especially in Neuroblastoma tumor and targets mainly cortical bone, bone marrow, and lymph nodes.[21] Cell migration is the ability of a cell to move across varying distances depending on intrinsic and extrinsic cues from the environment[22], and it is an essential dynamic cell behavior that drives cancer metastasis[23]. What makes a malignant cancer cell lethal is its dissemination and seeding of metastatic foci.[24] Therefore cell motility, the migratory/invasive ability, is a critical aspect of this process that needs an accurate and thorough study aimed at investigating what can block or promote this mechanism.

### *1.3.1 Cancer metastasis and its diagnosis*

As mentioned above, the process of metastasis relies on the movement of cells from one point to another, in an intrinsically dynamic process. Tissue biopsies and examination of the morphology of the cells and the molecular composition of the microenvironment in static microscopy images are included in the traditional diagnosis pathology methods. These types of diagnoses are not able to control and define the dynamic cellular processes. Therefore a link between it and the static microenvironment inputs must be made [25].

#### 1.3.1.1 Traditional cell migration study

The Boyden chamber assay is the most widely accepted cell migration technique in conventional studies. It was initially introduced by Boyden for the analysis of leukocyte chemotaxis and is composed of a hollow plastic chamber of two medium-filled compartments separated by a microporous membrane[26]. This chamber is suspended over a larger plate, well-containing medium, and chemo-attractants. Cells are present inside the chamber and are allowed to migrate through the porous membrane (Figure1.5)[27]. This is a classic study *in vitro* that allows to study chemotaxis, that corresponds to a migration process that describes cell motility toward increasing concentrations of a soluble attractant or repulsive substances within the extracellular matrix. It is possible to examine the effect of an inhibitor that is specifically an intercellular signaling molecule[26]. In a standard Boyden assay, the pore diameter of the membrane varies between 3 to 12 µm. In Table 1.3 are reported the recommended dimensions of pore diameters for the most important microorganisms involved in these studies.

**Table 1.3** *Recommended dimensions of the diameter of the microporous membrane for the most critical microorganisms involved in the Boyden Chamber assay. Adapted from [27].*

| Microorganism | Pore Diameter [$\mu$m] |
|---|---|
| Leukocyte or lymphocyte | 3 |
| Fibroblast cells or cancer cells | 5 |
| Most cells type | 8 |

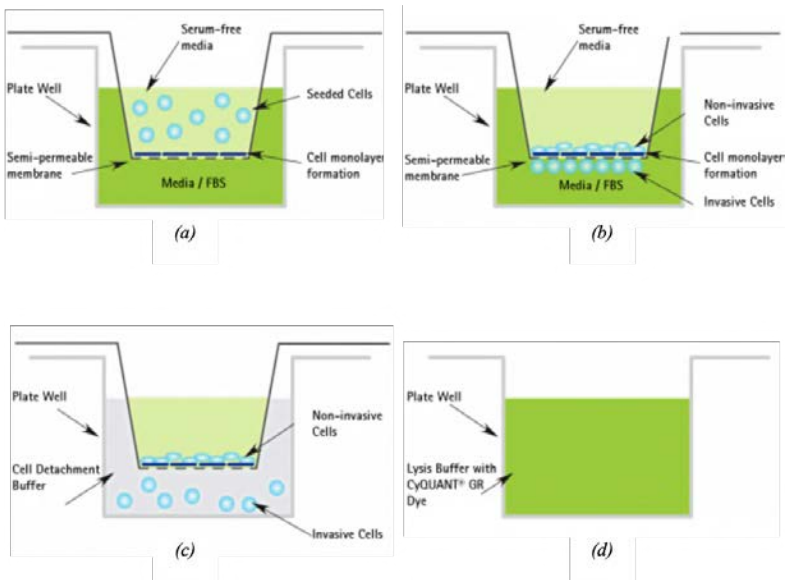


**Figure 1.5** *Illustration of Boyden Chamber assay: (a) Load cell suspension into plate well insert; (b) Invading cells migrate and attach to bottom brane; (c) Detach invading cells in cell detachment; (d) Lyse cells in cell Lysis Buffer and detect cell numbers. Adapted from[27].*

However, as was said before, *in vitro* studies present a significant limitation: the environment of study is completely different from reality, and for this reason is not possible to achieve an accurate analysis that could be obtained thanks to more *in vivo*-like techniques.

## 1.4 Neuroblastoma

Neuroblastoma (NB), defined as immature (blast) tumor of the sympathetic nervous system, is one of the embryonal malignancies in infants during fetal or postnatal life. The occurrence of this tumor is strongly age-dependent, with the median age of onset of 2 years and the peak age of 18 months[28]. It is the most common malignant tumor in infants: in the United States, the incidence is 1 case per 100000 children. Moreover, it represents about 8% of all malignancies diagnosed in pediatric patients, and it causes 15% of the pediatric cancer deaths[29].

Neuroblastoma arises during fetal or early postnatal life[29], generically, it is primarily located in lymph nodes, bone, bone marrow, and liver skin. As a result of this, Neuroblastoma can occur everywhere along the sympathetic chain, from the neck to the groin,[28] defining itself as an extremely heterogeneous disease. Different biological and molecular factors can highly predict the clinical behavior, necessary when it is time to consider the specific procedure to cure the patient.

### *1.4.1 The role of exosomes in cancer detection*

Exosomes are 40-100 nm extracellular vesicles (EVs) secreted by various living cells in all body fluids and recently turned out to be important cancer biomarkers[30]. Their composition is very complicated; indeed, they contain proteins, lipids, mRNA, and microRNAs. Cell communication is essential to understand the mechanism that transforms the normal in cancer cells. Accordingly, exosomes are key elements that facilitate intercellular communication. They can influence the major cellular pathways such as those regulating metastasis and apoptosis[31] and are involved in initiation, growth, progression, and drug-resistance, transferring oncogenic protein and nucleic acids[30]. In cancer cells, exosomes are secreted ten times more than in normal cells[30] causing and increasing in the number of exosomal proteins and miRNA that can be used as a new biomarker for cancer monitoring[30].

## 1.5 Motivation and aim of the thesis

The behavior of a cell relies crucially on the mechanical, chemical, and geometric properties of its environment[32]. In this sight, it is clear that standard methodologies and techniques *in vitro* present limitations to study cell migration especially the intravasation of a tumor cell from the tumor stroma to a lymphatic vessel or a capillary bed. Thanks to bioengineering

knowledge, 2D (two-dimensional) and 3D (three-dimensional) systems can be produced to mimic elements in environments in which cells move *in vivo*[22].

For this reason, as described in the first chapter, the construction of 3D devices with an innovative technique of 2PP combined with microfluidics is a promising science for studying cell culture in a specific and controlled environment. These devices could be suitable for the study of the Neuroblastoma's migration under gradient concentration, also known as chemotaxis. For this reason, the goal is to build a device that allows the study of cell migration to a single-cell resolution, with micro-channel arrays that recall the shape and size of the lymphatic vessels. In this project, mechanical and chemical engineering knowledge can be coupled with the biotechnological ones to achieve a better comprehension of this disease.

# Chapter 2

# Platform design, CFD simulations and manufacturing

In this Chapter, the different platform geometries and CFD simulations applied to these will be presented. Simulations are performed using an efficient tool routinely used for engineering problems, COMSOL Multiphysics®. A functional design of the platform must lead to the formation of a suitable concentration gradient Afterward, the result will be discussed. Then, all the procedures for the master production using Nanoscribe technology will be presented. The master production was made in collaboration with the TE.SI laboratory of the Department of Industrial Engineering located in Rovigo.

## 2.1 Platform description and geometry

The main components in a microfluidics platform are the micro-channels that are arranged to achieve the desired performance. In this work of thesis, the generation of a stable concentration gradient inside the micro-channels to study the chemotaxis, is simulated. The general platform design in consists in Figure 2.1:

- Two lateral channels and chambers used to introduce the fluids at different concentrations;
- Micro-channels that connect the lateral chambers, and in which the gradient is established.

First of all, studies have been carried out for different configurations (geometries) in order to have the best stable concentration gradient.

### *2.1.1 First prototype microfluidic platform*

The relevant dimension of the first prototype microfluidic platform are listed in Table 2.1 and the relevant element highlighted in Figure 2.1

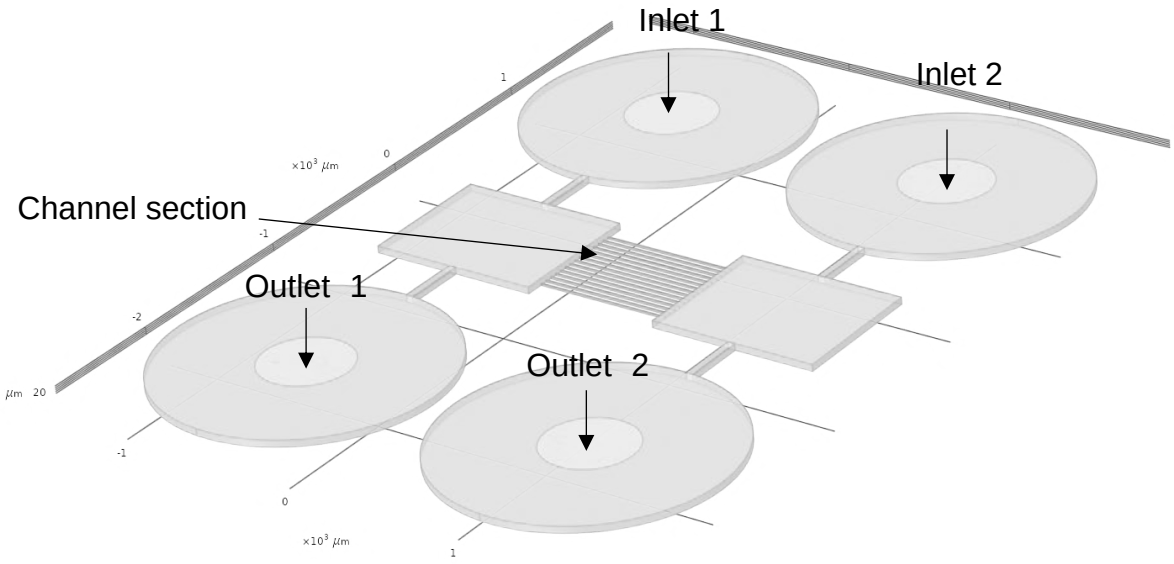


**Figure 2.1** *Relevant dimension of the first prototype microfluidic platform.*

**Table 2.1** Relevant dimension of the first prototype microfluidic platform.

| Quantity | Value | Unit of measure |
|---|---|---|
| Number of µ-channels | 15 | µm |
| Section of µ-channels (no choke) | 20x10 | µm |
| Length of µ-channels | 750 | µm |
| High of µ-channels | 10 | µm |
| High lateral channels | 40 | µm |

## *2.1.2 Optimization of different geometry*

Starting from the existing configuration several details are modified to simplify it and make it easier to produce and to model with the 3D printing machines and cellular lines available. The key point of this new structure is the particular shape of channels. The migration channels are modified to resemble lymphatic capillaries to better understand how cancer cells are able to move through geometrically confining spaces[38]. By recalling the classic pore sizes of the membranes used for migration studies, the channels with various dimensions have been simulated, as seen in Table 2.2 and Figure 2.2.

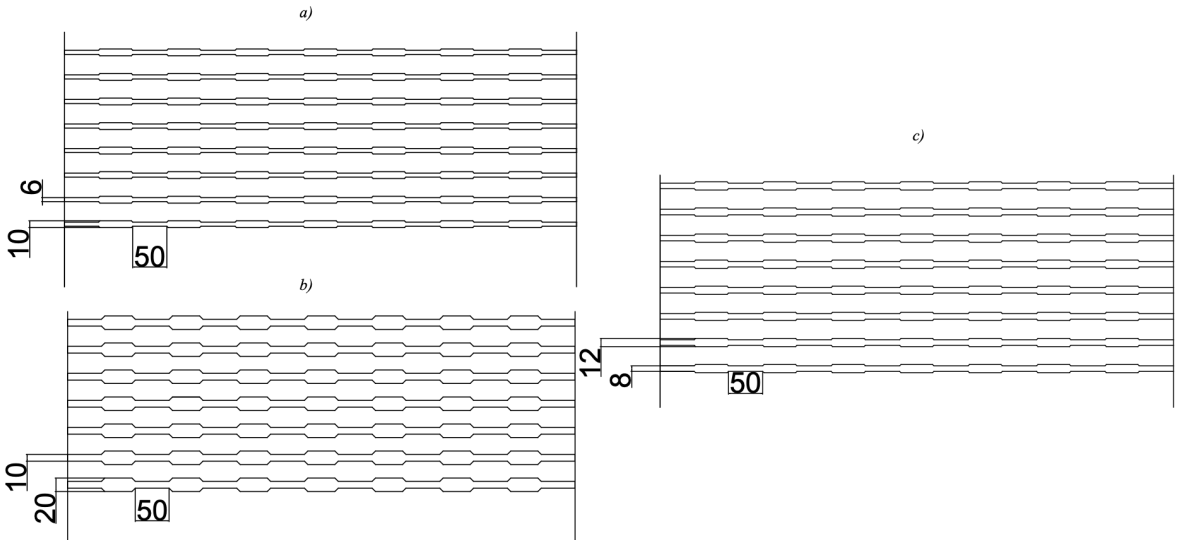


**Figure 2.2:** *Cad Geometry 2 (a), Geometry 3 (b), Geometry 4 (c); dimension in µm.*

**Table 2.2** Simulated geometries.

| | # µ-channels rows | µ-channels section [µm] | µ-channels section (narrowest) [µm] | µ-channels length [µm] | Lateral channels high [µm] |
|---|---|---|---|---|---|
| **Geometry 1** | 15 | 10x10 | - | 10 | 40 |
| **Geometry 2** | 15 | 10x10 | 6x10 | 10 | 40 |
| **Geometry 3** | 15 | 12x10 | 8x10 | 10 | 40 |
| **Geometry 4** | 15 | 20x10 | 10x10 | 10 | 40 |

### *2.1.3 Optimization of lateral channel*

The simulation of the lateral channel is useful to predict the behavior of the entire platform. Starting from the initial configuration, the dimensions of the channels which connect the two main chambers are modified to study changes in the velocity field. We speculated that this initial geometry may cause problems in cell seeding. The variations are shown Table 2.3 and Figure 2.3

**Table 2.3** Simulated Geometry of the lateral channel that connect the inlet/outlet to the other one.

| Lateral channel | µ-channels section (narrowest) [µm] |
|---|---|
| **Channel 1** | 70 |
| **Channel 2** | 400 |
| **Channel 3** | 500 |
| **Channel 4** | 550 |

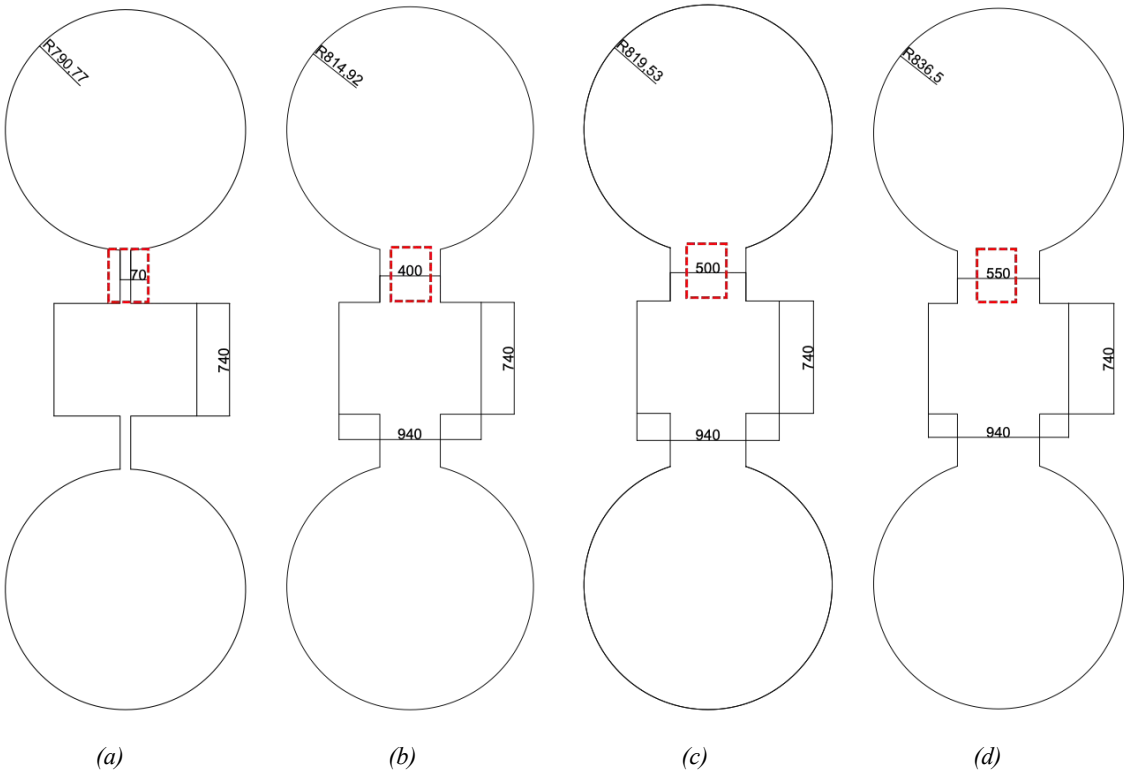


**Figure 2.3** *Cad Channel 1 (a), Channel 2 (b), Channel 3 (c), Channel 4 (d); dimensions in µm.*

## 2.2 CFD simulation applied to microfluidic

Computational fluid dynamics (CFD) is a numerical technique able to analyze systems involving fluid flow, heat transfer, and associated phenomena such as chemical reactions employing solution of balance equations in a generic domain. This analysis is very powerful and spans a wide range of industrial and non-industrial application areas. To name a few examples: the Aerospace industry, evaluating lift and drag forces on aircraft and vehicles;

Chemical Engineering, solving mixing issues by better designing impellers and mixers, or heat transfer in heat exchangers and furnaces; and Biomedical Engineering, studying blood flow through arteries and veins[51]. CFD codes are structured around the numerical algorithms that can hold fluid flow problems leading to a discrete solution, which is only an approximation of the real behavior.

There are various advantages of CFD over experiment-based approaches to fluid system design:

- Substantial reduction o lead times and cost of design;
- Ability to study systems where controlled experiments are difficult or impossible to perform;
- Ability to work under hazardous conditions;
- Less expensive and more efficient than conventional approaches.

At the same time, the main drawbacks are:

- An approximate solution, that is not completely faithful to reality;
- CFD simulations require physical and laboratory validation[11].

CFD codes are structured around the numerical algorithms that can tackle fluid flow problems. Hence all codes contain three main elements:

1. Pre-processor: this involves the definition of the geometry of the region of interest, divided into several smaller non-overlapping sub-domain (meshing technique). The problem must be defined (inlets, outlets, reactions) and selection of physical and chemical phenomena, appropriate boundary condition and fluid properties must be specified;
2. Solver: it represents the core of the program. Briefly, the numerical algorithm consists of the integration of the equations of fluid flow over the finite control volumes, the conversion of the resulting integral equations into a system of algebraic equations, AEs, and their solution by an iterative method;
3. Post-processor: this allows to get a visualization of the domain geometry and grid display. Results are represented through vectors, trajectory, 2D and 3D surface plots and animations (see Figure 2.4).

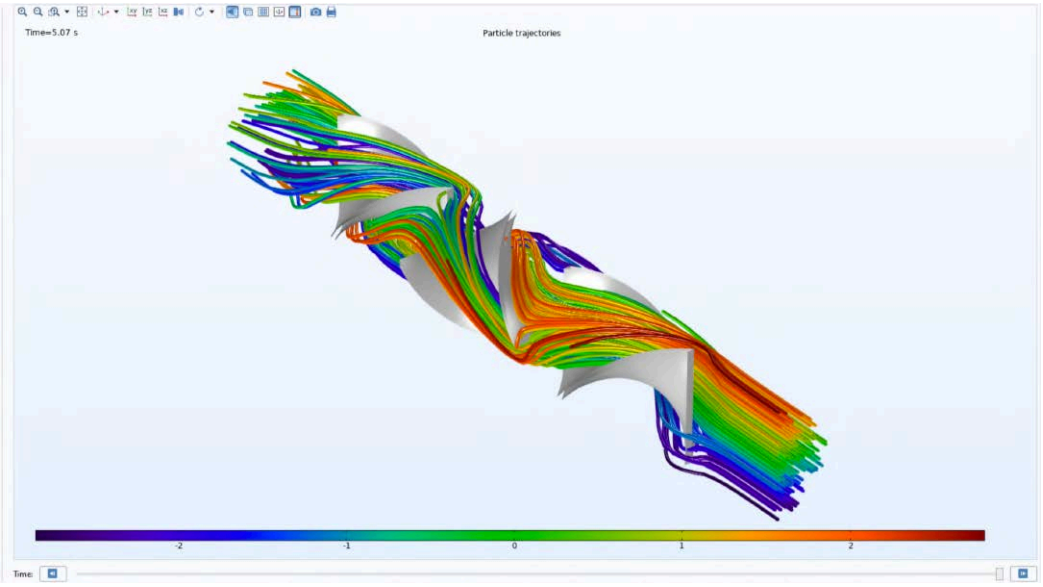


**Figure 2.4** *Laminar static particle mixer designer. Post processor results. Example of a CFD simulation using COMSOL Multiphysics ®. Adapted from*[52]

## 2.3 Main phenomena investigated

The goal of this modeling work is to aid the design of a microfluidic device that ensures the generation of a stable gradient inside micro-channels. The basic physics required to implement the model are laminar flow phenomena and diffusive mechanisms.

### *2.3.1 Laminar flow and Re number*

Laminar flow is a condition in which the velocity of a particle in a fluid system is not a random function of time[7]. A laminar regime ensues when two or more streams flowing in contact with each other will not mix except by diffusion, and flow as in a stack of layers. The dimensionless Reynolds number, defined by (Equation 1.3), is mainly used to characterize this regime. Considering a straight circular pipe, the transition to turbulence occurs for Re between 2000 and 3000. Microfluidic devices support very small values to ensure a laminar evolution of the flow field. In this case, considering water as the fluid , the typical working flow velocity is between $\mathcal{O}(10^{-5}), \mathcal{O}(10^{-4})$, radii of 1-100 µm and the Reynolds number between $\mathcal{O}(10^{-8}), \mathcal{O}(10^{-2})$.

The Newtonian fluid behavior is described with Newton's law of viscosity:

$$\tau_{yx} = \mu \frac{dv_x}{dy} \tag{2.1}$$

This equation relates shear stress, $\tau_{yx}$, to the local velocity gradient, $dv_x/dy$, along the y-direction. The proportional factor $\mu$ is the dynamic viscosity of the fluid expressed in Pa · s. Figure 2.5 reports characteristic shear stresses and velocity profiles.

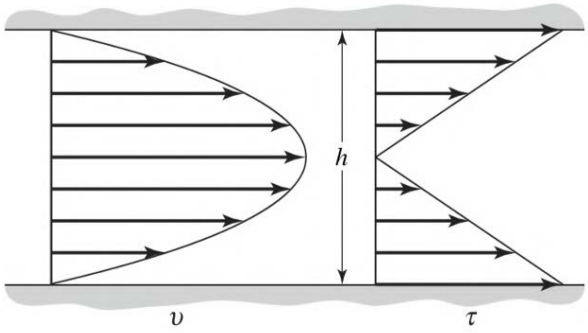


**Figure 2.5** *Velocity and shear stress profiles. Adapted from*[53]

Low values of Re affirm that viscous forces typically overwhelm inertial forces and the resulting flows are laminar.

## 2.3.2 Diffusion

Diffusion is the process by which a concentrated particles in a volume are transported; in a microfluidic device, due to low Reynolds number values and laminar regime, this is the determinant transport phenomena. The dimensionless number that better captures this phenomenon is the Peclet number, Pe. It expresses the relative importance of convection to diffusion[9] contribution (Equation 1.5).

For this microfluidic device, the calculated values are in the order of magnitude of $\mathcal{O}(10^{-4})$, considering the same values of diameter, velocity, and a diffusion coefficient equal to $10^{-9}$ $m^2/s$. Diffusive species transport is regulated by Fick's law (Equation 1.8) of stationary diffusion. The flux depends on the diffusion coefficient, of transport species and on a concentration gradient.

## 2.3.3 Physics interphase of system

COMSOL Multiphysics® has several built-in physics available that can be solved simultaneously to describe the aforementioned phenomena. Laminar flow and transport of diluted species are the basic physics involved in the microbioreactor's simulations.

### 2.3.3.1 Laminar flow

Laminar flow is used to model the velocity and the pressure fields for the flow of a single-phase fluid in the laminar flow regime. This physics supports incompressible flow (the density depends on temperature, not pressure). The equations solved by the laminar flow are the Navier-Stokes equation for conservation of momentum, and the continuity equation for

conservation of mass. The fluid that will be used in experimental validation is a fluorescein isothiocyanate-dextrans diluted in physiological solution. Its properties are comparable to water, assuming it as a constant density Newtonian fluid.

#### 2.3.3.2 Transport of diluted species

The transport of diluted species physic is applicable for solutions where the solute concentration is at least one order of magnitude lower than that of the solvent, and simulates the chemical species transport through diffusion (Fick's law). In this module, the convective term can be activated or excluded by the user [54]. The input parameters are:

- The diffusion coefficient, $D = 1 \cdot 10^{-9}$ m$^2$/s, isotropic;
- The initial concentration of the transported species, equal to 1 mol/ m$^3$.

This module is coupled with the laminar flow one in order to map the diffusion results according to the calculated flow field.

### *2.3.4 Constitutive equations, Boundary and Initial conditions*

Equations are numerically discretized and solved by a numerical scheme. COMSOL® takes a generalized form of the Navier-Stokes equation to allow for variable viscosity[11]. The equations are listed below.

$$\rho = \frac{\partial \mathbf{u}}{\partial t} + \rho(\mathbf{u} \cdot \nabla)\mathbf{u} = \nabla[-p + \mu(\nabla \mathbf{u} + (\nabla \mathbf{u})^T)] + \boldsymbol{F} \tag{2.2}$$

$$\nabla \mathbf{u} = 0 \tag{2.3}$$

where $\mu$ is the dynamic viscosity $\rho$ is the viscosity, $\mathbf{u}$ is the velocity field, $p$ the pressure, and $\boldsymbol{F}$ is a volume force field to which gravitational effects are applied. This general formulation could describe all types of non-compressible flow[54].

The boundary conditions (BCs) set are shown below:

- No-slip condition at the walls;
- Inlet velocity (in terms of mass flowrate);
- Outlet pression, whose gradient is equal to zero.

In transport of diluted species, physic is characterized by the material balance on a specified species $i$ (Equation 2.4) and total flux of species $i$ as defined in Equation (2.5)

$$\frac{\partial c_i}{\partial t} + \nabla \cdot (D_i \nabla c_i) + \mathbf{u} \cdot \nabla c_i = R_i, \tag{2.4}$$

where $c_i$ is the concentration of the species $i$, $D_i$ is the diffusion coefficient of the species $i$, $R_i$ is the reaction term, **u** is the velocity field and $\boldsymbol{N}_i$ is the total flux.
As for the initial conditions (ICs), they are related to the initial state of the simulated domain. The flow field is initialized with inlet flow rate fixed, and the transient simulation is thus run according to a pressure field and a quiescent velocity. In the initial configuration, the mass transport is initialized enforcing no transported species.

## 2.4 Modeling result

This section reports the main simulation results of paragraph §2.1.2. Concentration profiles inside the micro-channels are investigated.

### *2.4.1 First prototype geometry simulations*

A transient simulation was performed to highlight the fluid dynamic characteristics and the early stages of the generation of the concentration gradient inside the channels.

#### 2.4.1.1 Laminar flow

As explained in paragraph §2.3.3.1, the simulation is set on the entire platform to solve the Navier-Stokes equations for the single-phase fluid. The fluid enters from the two upper inlets and exits via the two lower sides. The value of the inlet velocity was a key variable for the gradient concentration generation, and a value of 20 µL/h, corresponding to an average velocity of $1.86 \times 10^{-4}$ m/s, was chosen. At the outlets, a condition of pressure is set, in which the relative pressure is assumed to be zero. The temperature is set to 331.15K (the temperature inside the incubator, perfect environment for cells). Figure 2.6 shows the surface plot of the absolute velocity inside the platform.

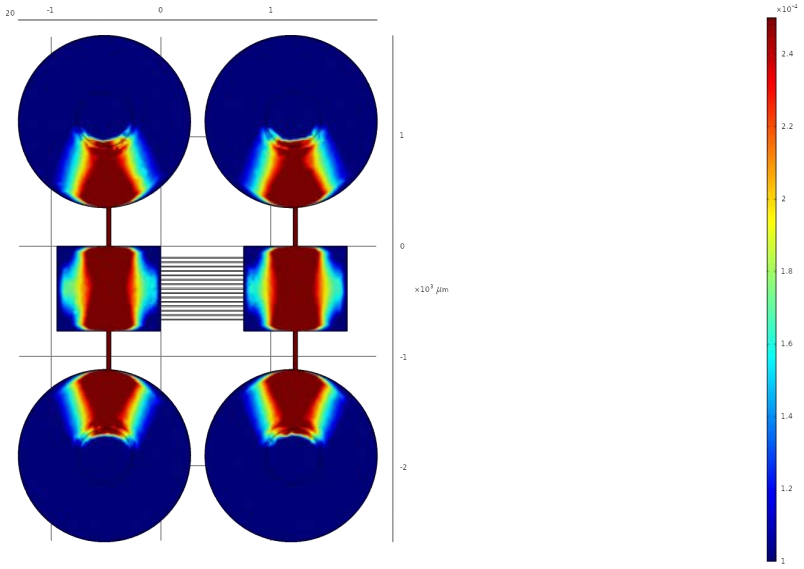


**Figure 2.6** *Results of the COMSOL simulation for the velocity magnitude.*

The velocity inside the rectangular chambers of the platform shows a parabolic profile, as shown in Figure 2.7, with a maximum value of 2.9 x$10^{-4}$ m/s at the center of the chamber, and tends to zero approaching the walls, and with this also the Reynolds number.

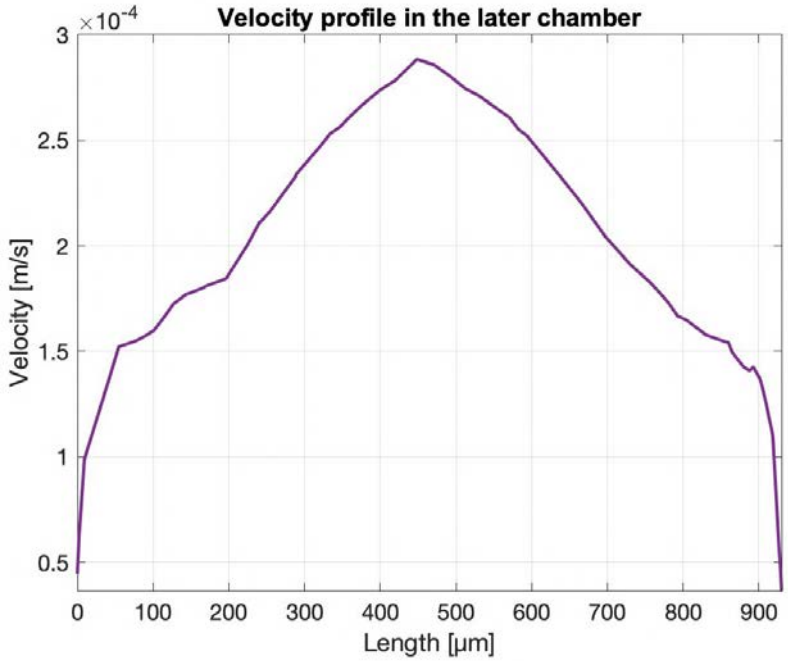


**Figure 2.7** *Velocity profile in the lateral chamber, using a 3D CFD simulation*

However, investigating what happens inside the micro-channels, the velocity is not zero, but has a maximum value of 4.51 x$10^{-9}$ m/s, five orders of magnitudes smaller than the average velocity in the lateral chambers. Then, the Peclet number is calculated using Equation 1.5, and the result is 1.88 x$10^{-4}$. It is <1, thus confirming the dominant effect of diffusive flux over the convective one. Figure 2.8 also shows how the flow is fully developed, showing a parabolic velocity profile.

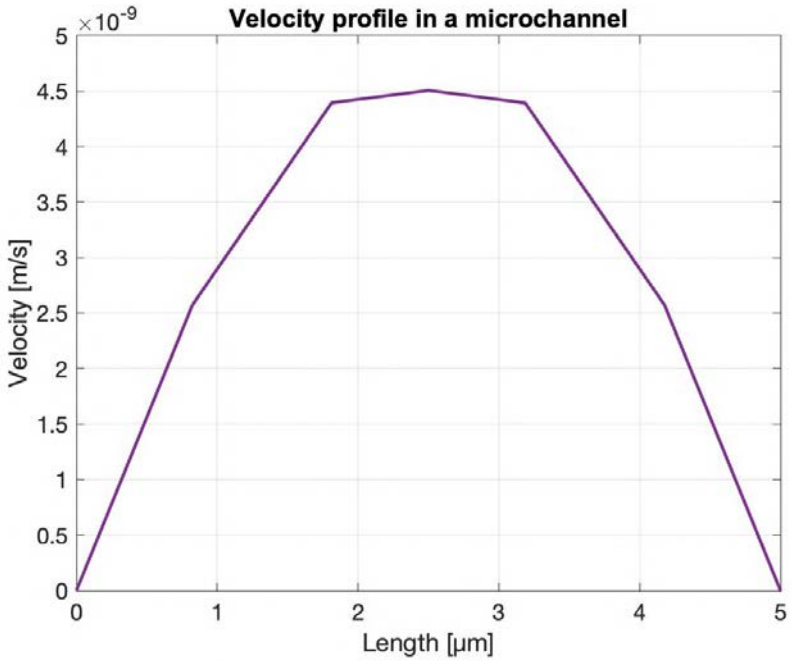


**Figure 2.8** *Velocity profile in a micro-channel, using a 3D CFD simulation.*

### 2.4.1.2 Transport of diluted species

Transport of diluted species interface is added to the study, and as explained in paragraph §2.3.3.2, it does not require the properties of species *i*, except for the diffusion coefficient. Since fluids with water-like behavior will spread within the channels, the diffusion coefficient of the latter has been considered ($D = 1 \cdot 10^{-9}$ m$^2$/s). Results of the concentration profile are shown in Figure 2.9.

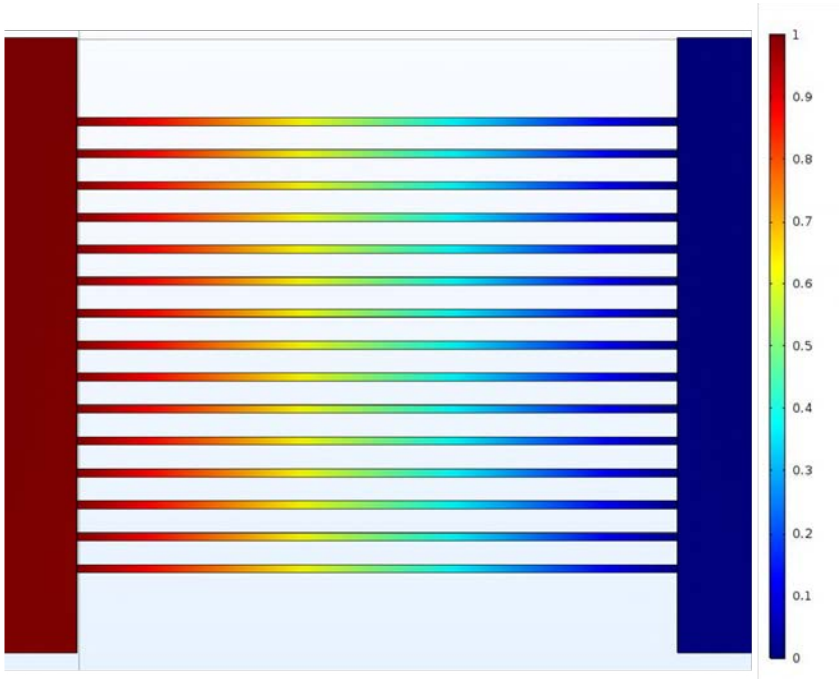


**Figure 2.9** *Geometry 1: Concentration slice result in the middle of the configuration. Time 30 min. Flowrate of 20μ L/h*

In order to get a general view of the trend along the channels, the concentration values of the first, eighth and fifteenth channels were plotted. Note that there are no substantial differences between these (possible calculation errors on simulations can be considered) and that the trend is linear, Figure 2.10

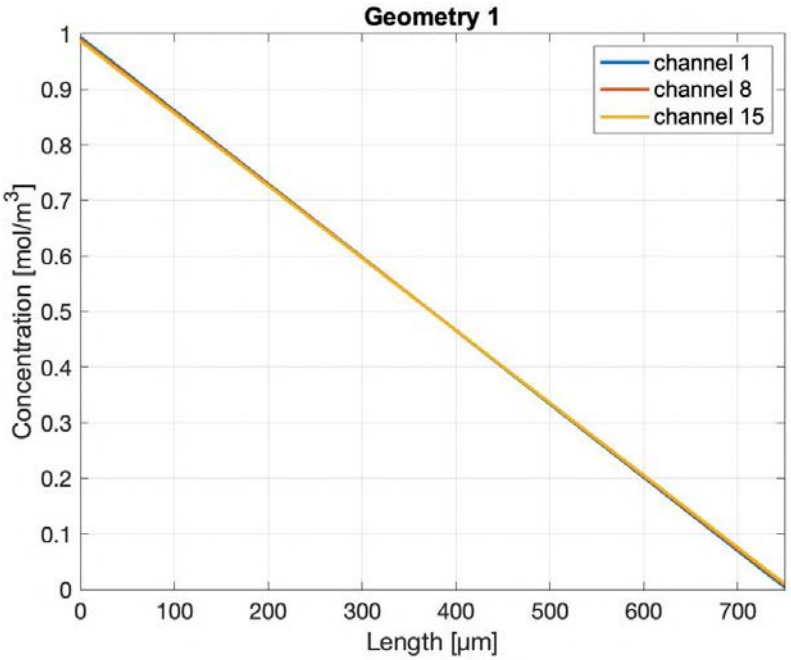


**Figure 2.10** Expected concentration along the first, eighth and fifteenth channels of the platform.

## *2.4.2 Channel 2 to 4: Simulations*

All the simulations are based on transient evolution in order to investigate the velocity profile inside the lateral channel. The velocity profile in the lateral chamber was analyzed at the height of the first micro-channel. The section of interest is highlighted for each design by the red line (Figure 2.10).

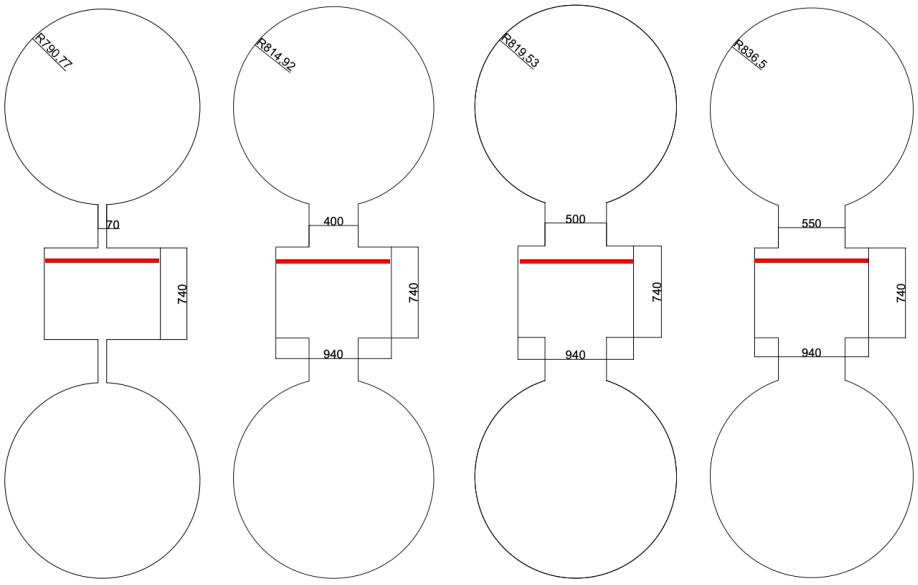


**Figure 2.10** *Cad Channel 1 (a), Channel 2 (b), Channel 3 (c), Channel 4 (d); velocity profile section highlighted by the red line; dimensions in µm.*

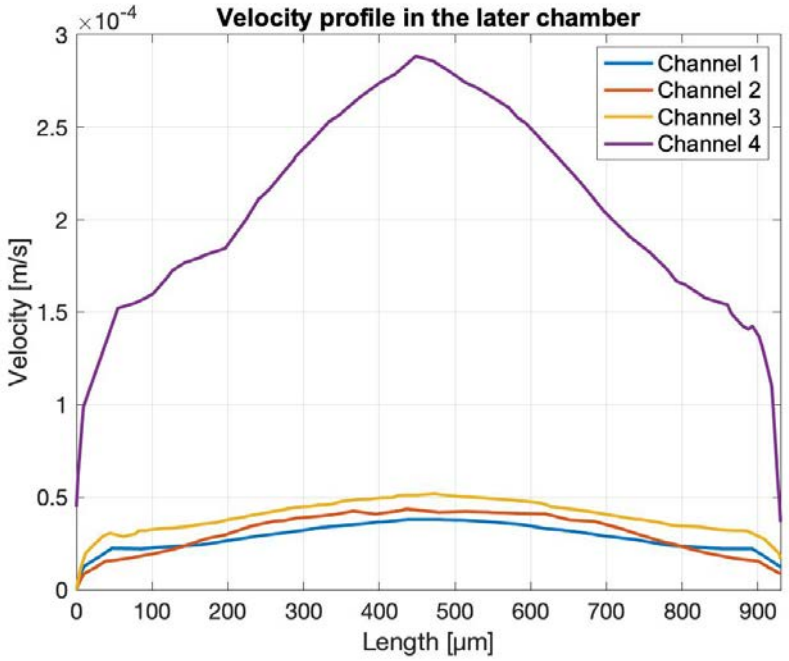


**Figure 2.11** *Velocity profile in the lateral channel with dimension of channel 1 to 4.*

Figure 2.11 shows how increasing the dimension of the channels which connect the two main cameras, the mean velocity decreases by an order of magnitude, improving the diffusive behavior within the channels.

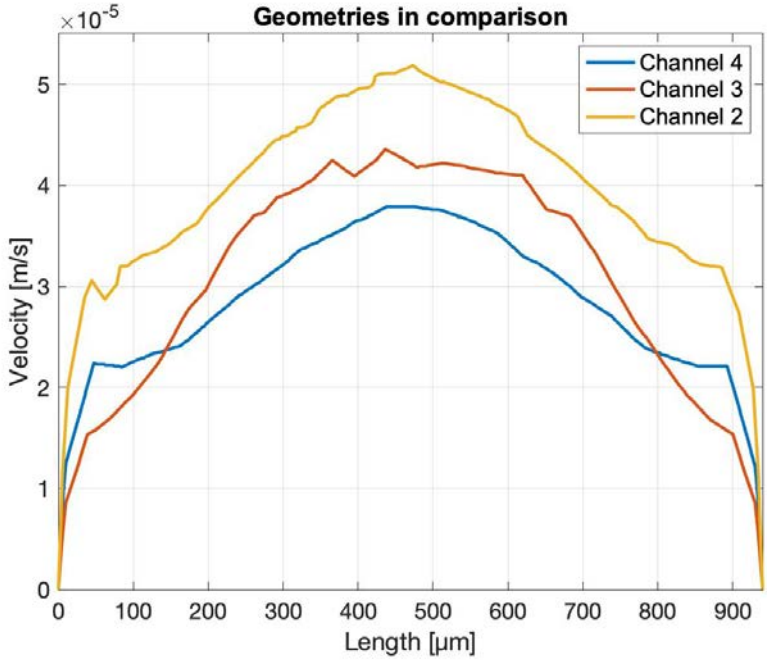


**Figure 2.12** *Velocity profile in the lateral channel with dimension of channel 2 to 4.*

Observing the velocity profile for each lateral channel design, dimension of channel number 3, allows the closest parabolic trend. For this reason, the design of channel number 3 is chosen (Figure 2.14).

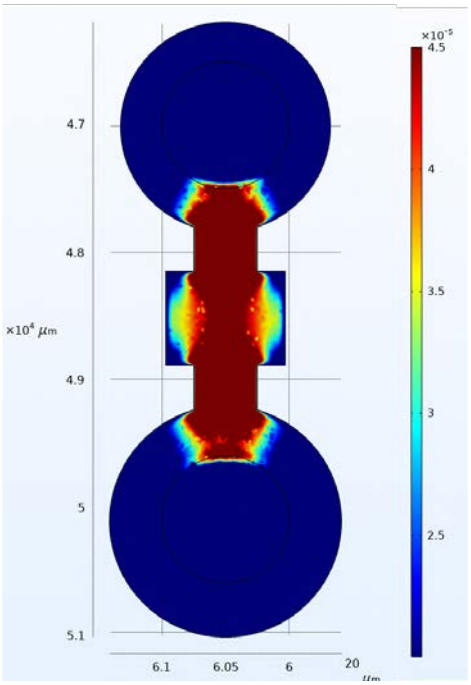


**Figure 2.14** Results of the COMSOL simulation for the velocity magnitude.

### *2.4.3 Micro-channel geometry 2 to 4: simulations*

All the simulations are based on transient evolution to investigate the time to get a stable concentration gradient. A simulated time limit of 3 hours is set with a step of 30 minutes. The results show that after 30 minutes the concentration gradient becomes stable.

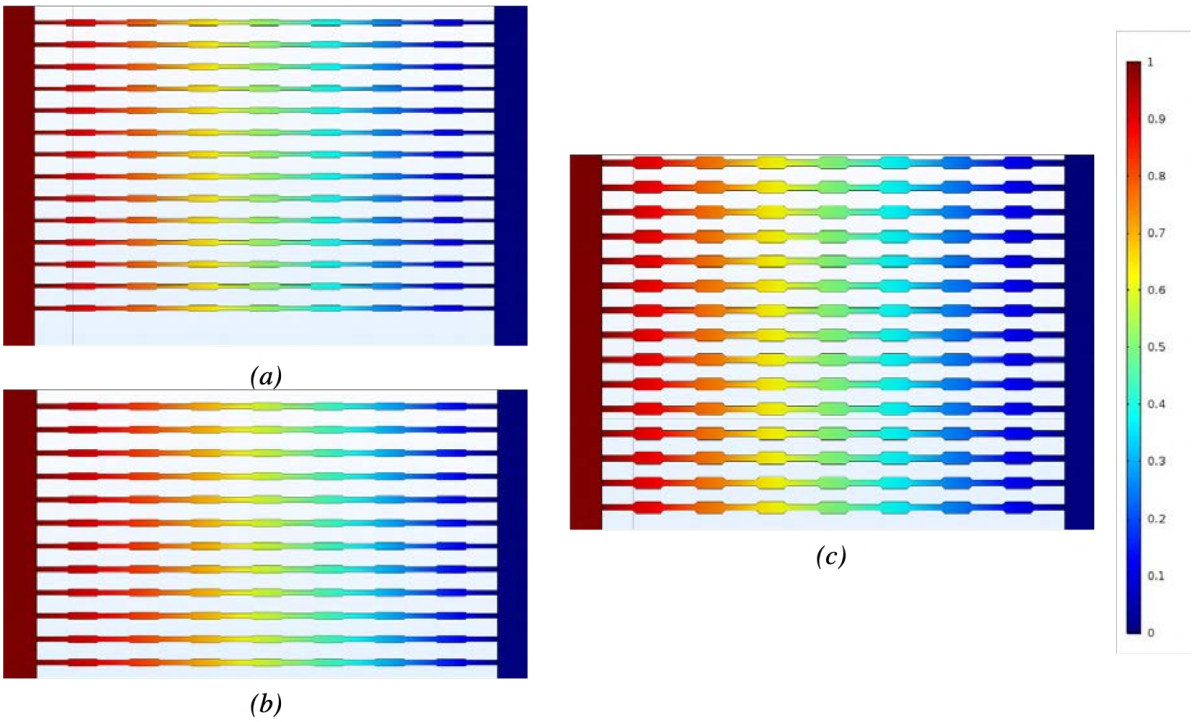


**Figure 2.13** *Geometry 2 (a), Geometry 3 (b), Geometry 4 (c): concentration slice in the middle of the configuration. Time 30 min. Flowrate of 20μ L/h.*

The expected concentration along the first, eighth and fifteenth channels of the platform for each geometry are reported in Appendix A.

Results considerations are reported below:

- A modification of the ratio between the channel and shrinkage changes the concentration profile;
- Increasing by double the size of the narrowest part of the channel the trend of the concentration is close to that of a channel without shrinkage;
- Geometry 3 trend deviates from the rest of the other geometries.

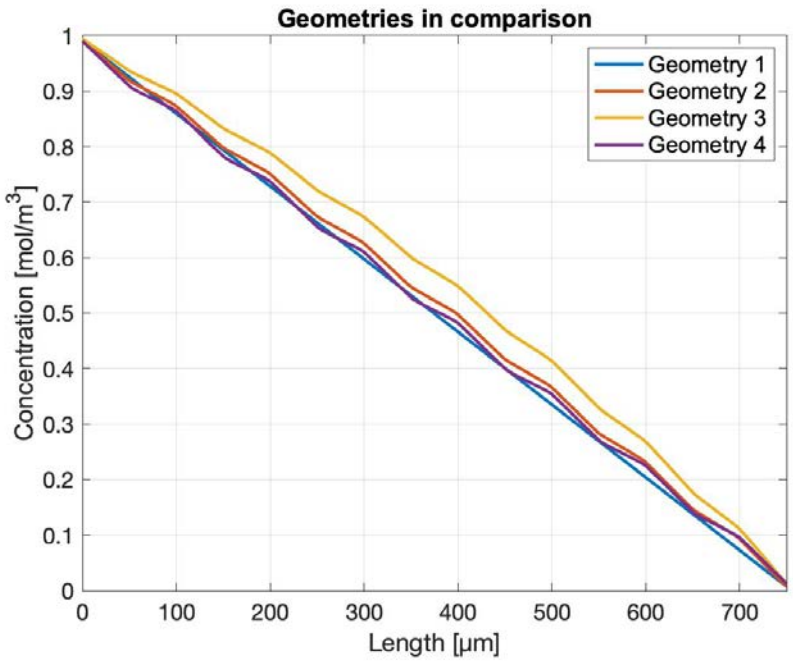


**Figure 2.14** *Expected concentration along the channel for all the geometries.*

In conclusion, by observing the results obtained from the simulations, and the dimensions used in the classical migration studies, Geometry 2 was chosen (Figure 2.15-16). This geometry will be printed through the innovative two-photon-polymerization technology.

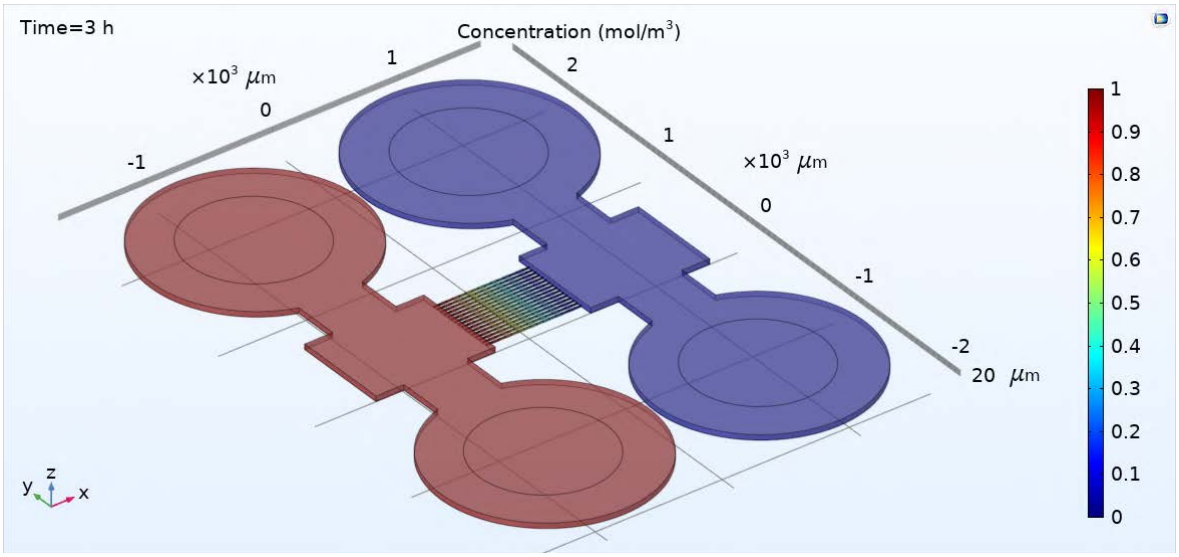


**Figure 2.15** *Concentration slice result. Time 30 min. Flowrate of 20µ L/h.*

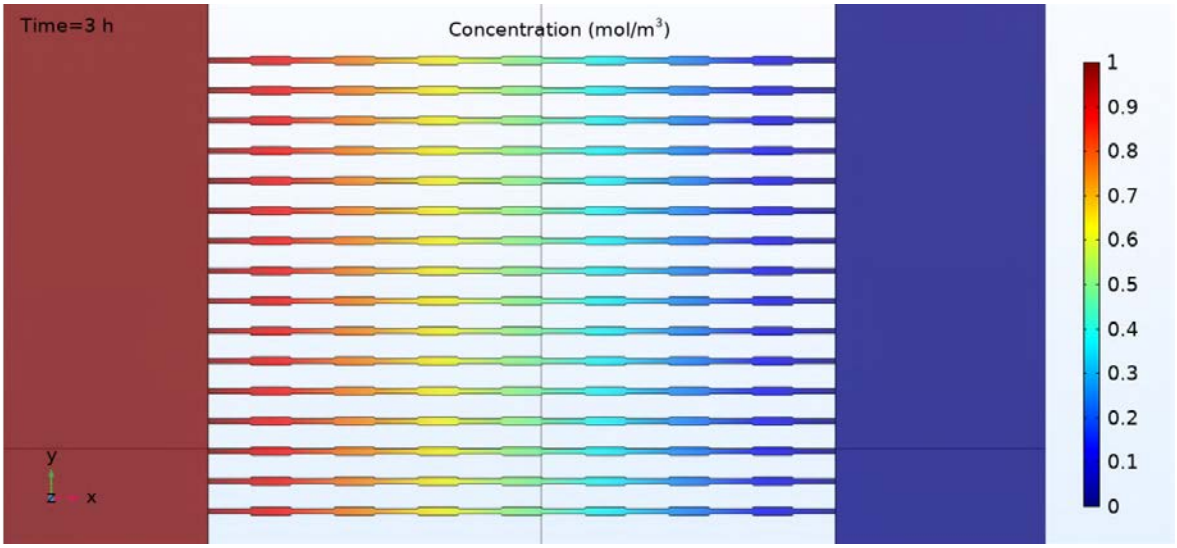


**Figure 2.16** *Concentration slice result in the channel section. Time 30 min. Flowrate of 20µL/h.*

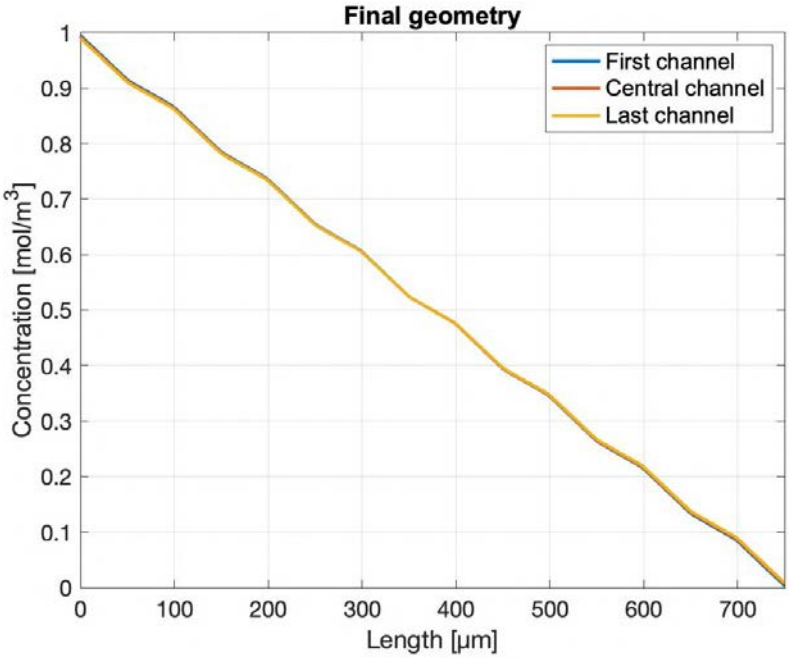


**Figure 2.17** *Expected concentration along the channel for the final geometry.*

Focusing on the values obtained inside the channels, a mean velocity of $1.18 \times 10^{-8}$ m/s and $2.78 \times 10^{-9}$ m/s for the lager and the narrowest section of the micro-channels are obtained (Figure 2.18-19). Péclet number is <1, once again confirming the dominant effect of diffusive flux over the convective one.

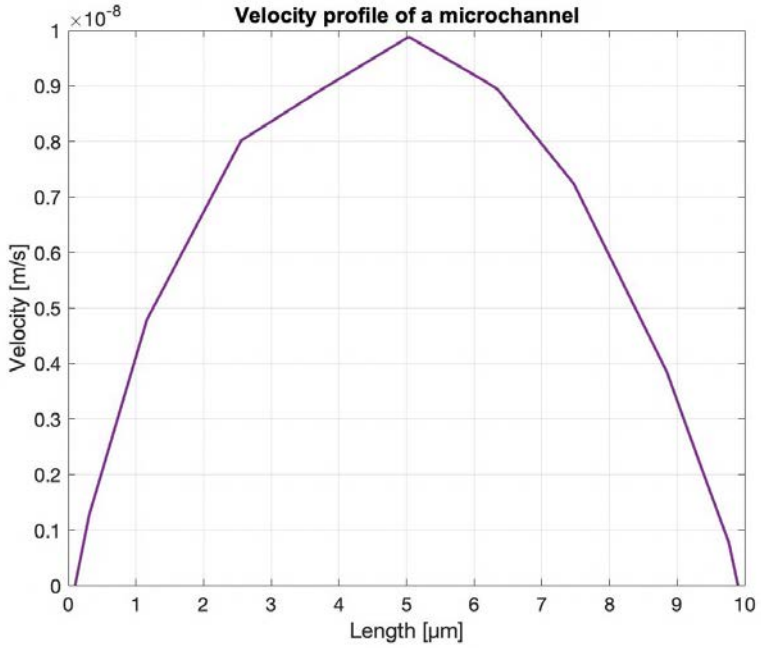


**Figure 2.18** *Velocity profile in a micro-channel, using a 3D CFD simulation.*

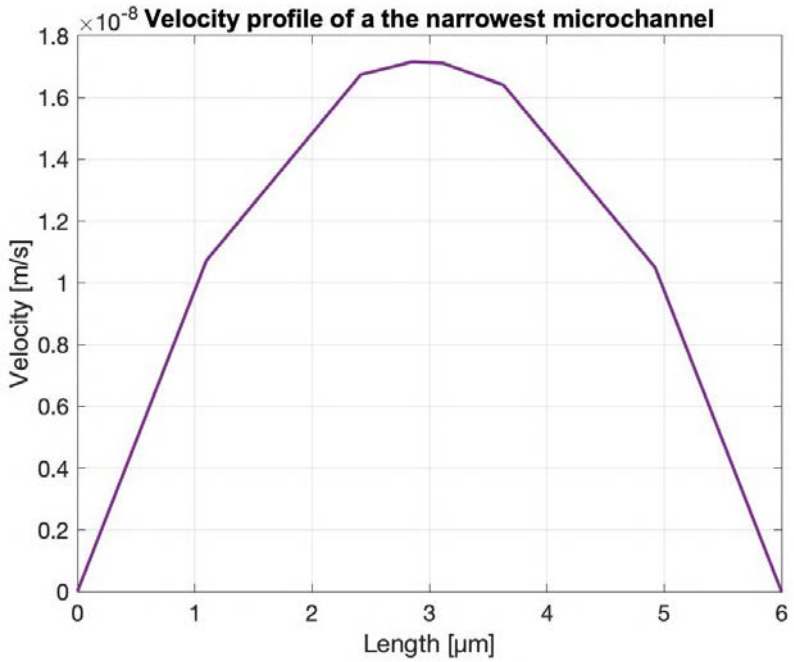


**Figure 2.19** *Velocity profile in the narrowest micro-channel section, using a 3D CFD simulation.*

## 2.5 Fabrication of micro-channel arrays through Nanoscribe

Nanoscribe is a German start-up born in 2001, and now a leader in 3D printing. In fact, the company has developed machines capable of writing complex structures, not achievable with other forms of lithography, which have only been marketed since 2006. These systems are based on the two-photon-polymerization technique. They are characterized by the presence of a laser focus system that can be detected by two materials that have very similar physical properties, guaranteeing that the 3D object is well attached to the substrate.

### *2.5.1 Nanoscribe Photonic Professional GT and operating principles*

The instrument with whom most of the work was performed for any type of micro-structure is the *Nanoscribe Photonic Professional GT*. It is a device for three-dimensional laser lithography, with the great benefit of not requiring any mask to polymerize the substrate. *Nanoscribe Photonic Professional GT* takes advantage on a series on lenses to focus a pulsed laser beam in a small volume called *voxel*, which is typically shaped as an ellipse and is the basic construction "brick" for printing. This integrated optical set directs the high-intensity pulsed laser directly into the photo-resin producing a multi-photonic absorption within the voxel. The movement and intensity of the laser are regulated by a computer program connected to the machine. Structures are created by moving the laser beam back and forth through the resin; voxels overlap gradually until you get the three-dimensional structure designed on the computer achieving excellent resolutions. In Figure 2.22 it is possible to see the process's scheme.

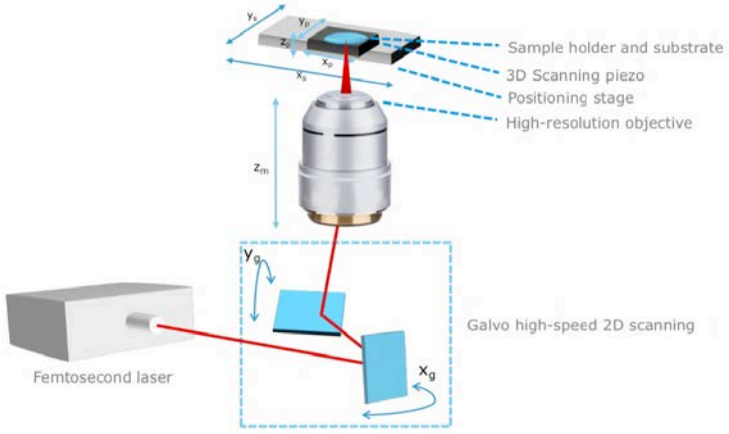


**Figure 2.22** *Process's scheme of direct laser writing. Adapted from*[40]

### *2.5.2 Principal components*

The system consists of a rack containing the processor and generator of the laser beam, a second cabinet containing the optics of the system, a micro-scope, and a terminal equipped with a graphical interface, which allows control by the user (Figure 2.20).


**Figure 2.20** *Nanoscribe Photonic Professional GT system. Adapted from*[40]

### 2.5.2.1 Laser

The femto-second fiber laser source generated must own specific characteristics that allow an exclusive two-photon-polymerization. The technical features are listed below (Table 2.4):

**Table 2.4** *Laser pulsed characteristic of Nanoscribe Professional GT.*

| Pulsed Laser Characteristic | Value | Unit of measure |
|---|---|---|
| **Center wavelength** | 780 | nm |
| **Pulse length** | 100 | fs |
| **Laser power** | 25 | kW |
| **Frequency** | 80 | MHz |

There are two different ways to control the laser intensity, coded in the commands implemented in the machine control software:

- Power scaling: allows to evaluate what is the maximum power expressed by the beam generator. The maximum values that can be obtained from the laboratory device are around 1.33;
- Laser power: is a parameter controlled directly by the beam generator and expresses the percentage of the maximum power established by the PowerScaling parameter. It varies between 0 and 100.

NanoScribe is set by default so that with PowerScaling of 1 and LaserPower equal to 100.

### 2.5.2.2 Printing configurations

In this paragraph we will shortly present and discuss the three main printing configurations of the Photonic Professional (GT) (Figure 2.21):

- Oil immersion: In this configuration the laser beam is focused through the substrate into the photoresist. Between the microscope objective and the substrate, the immersion oil is matching the refractive index to get the ideal focus on the substrate /resist interface. However, the worse gets the focus quality due to spherical aberrations.
- Dip-in Laser Lithography (DiLL): Here the microscope objective is directly dipped into the photoresist. The spherical aberrations are minimized and constant for the complete printing range. No interfaces limit the structure height in this configuration, the maximum structure height is limited only by the sample holder used and may be larger than 2mm.

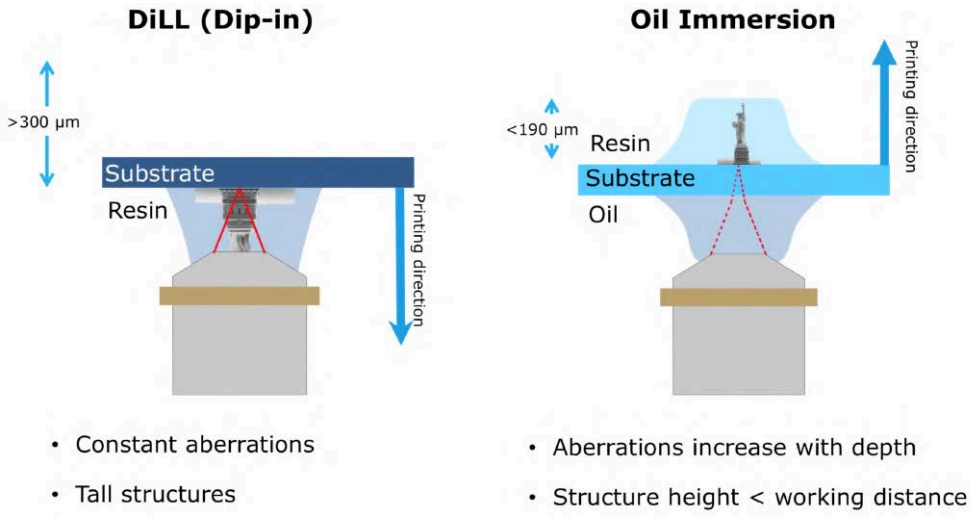


**Figure 2.21** *Comparison between DiLL and Oil immersion configurations. Adapted from*[40].

### 2.5.2.3 Objectives and softwares

The objectives allow both to focus the laser beam at a precise point, and also to have monitor the writing process in real time (as long as a lighting source is activated). The two objectives and their applications are listed in Table 2.5 :

**Table 2.5** *Objective and applications. Adapted from*[41]

| Objective | Resins | Substrate(s) | Working distances | NA |
|---|---|---|---|---|
| 25x | IP-S | ITO coated glass, silicon | 400 µm | 0.8 |
| 63x | IP-Dip | Fused silica | 600 µm | 1.4 |

Each objective has several advantages and disadvantages. Notable features include:

- A high numerical aperture (NA), among the highest achievable, which allows an excellent focus of the laser beam, especially for the 63x objective.
- The ability to work at Dip-in Laser Lithography (DiLL), a technology that consists of immersing the lens directly into the resist (Figure 2.21). This reduces spherical aberration and keeps it constant throughout the writing process. In addition, the height of the structure to be printed is only limited by the size of the sample holder, therefore it can reach more than 2000 µm.

The presence of an autofocus camera connected to the micro-scope, and lighting systems both in transmission and in reflection, allow to have a view of the processing in progress (Figure 2.22).

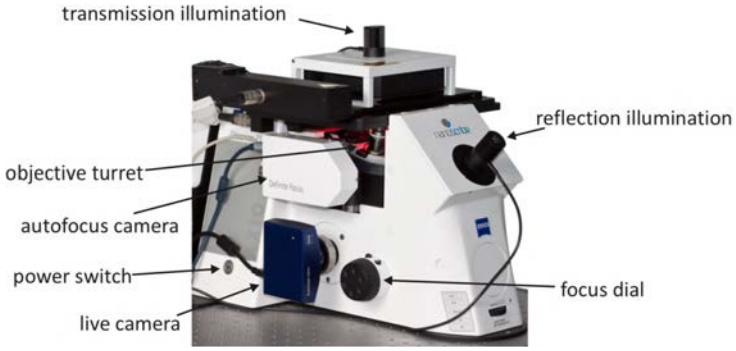


**Figure 2.22** *Micro-scope with major components. Adapted from*[41].

There are mainly three different softwares used to control and program NanoScribe:

- NanoWrite: it is the main software, which controls all the parameters of the machine and provides machine language instructions to the laser and the worktop. Among the various functions, there is also the ability to monitor write parameters, perform diagnostics, or set corrections systematic errors, such as worktop tilts or spherical aberration (Figure 2.23);

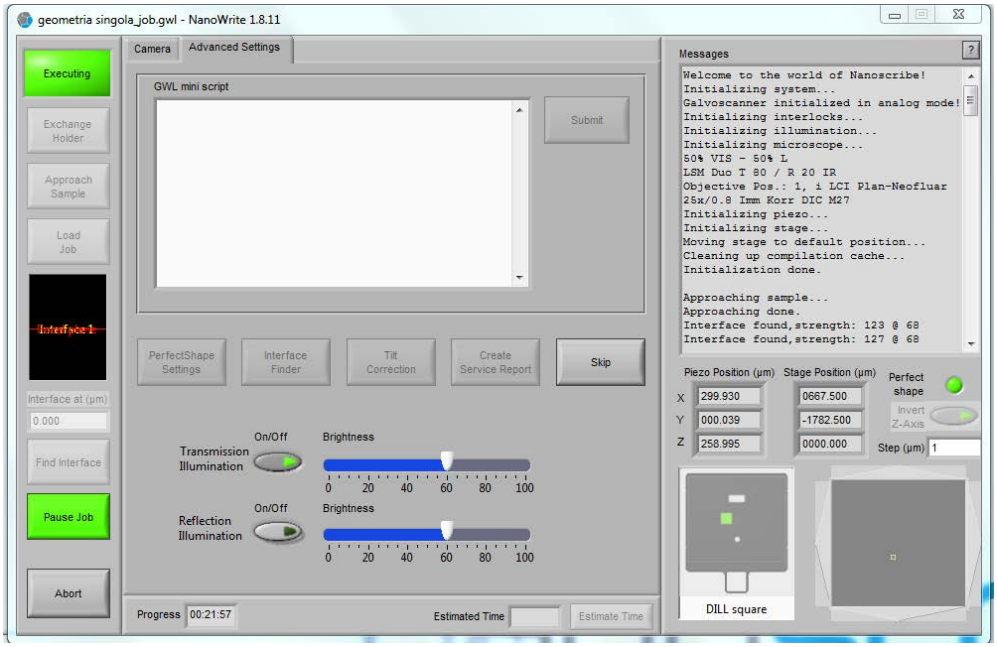


**Figure 2.23** *Principal Interface of Nanowrite.*

- Describe: this is the software through which the user translates the geometric figures into the language of the machine, the .gwl file. Among other functions is the ability to see a 3D virtual simulation of the print job, including process parameters and execution time estimation. It has also a tool that allows to easily import a 3D CAD drawing into GWL, so it is possible to create geometric models with third-party software, such as Autodesk Inventor or SolidWorks. Besides, there is a debugging system, which allows you to easily identify any operator compilation errors (Figure 2.24);

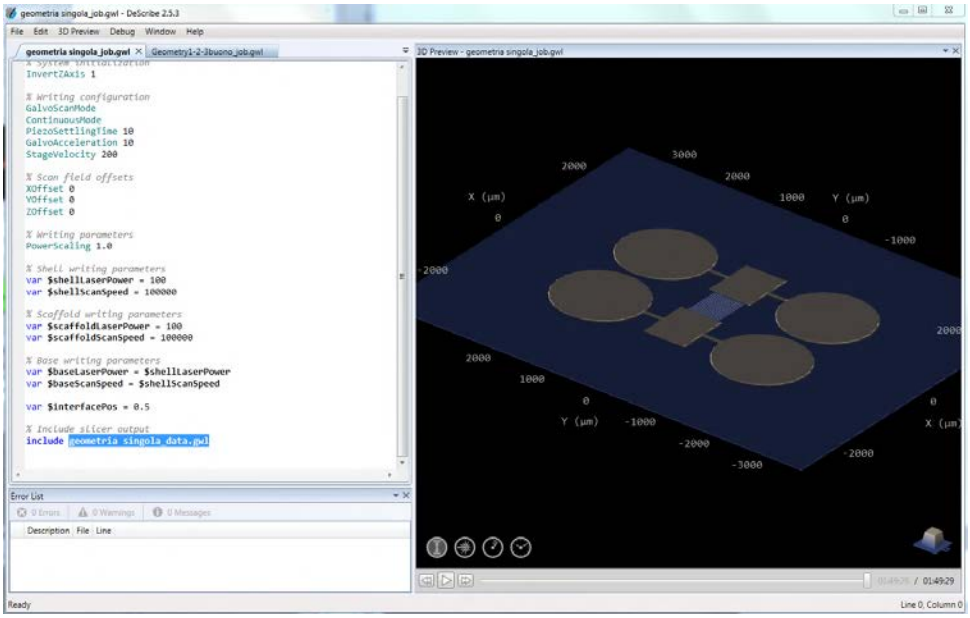


**Figure 2.24** *Graphic interface of DeScribe.*

- Axio Vision: it is a control system of the Carl Zeiss micro-scope included in the machine; In this way it is possible to observe in real-time what Nanoscribe Photonic Professional GT is printing, to acquire images and videos.

#### 2.5.2.4 Writing modes

In this section, three different writing modes of Photonic Professional GT are presented. A writing mode is the combination of scanning mode (which positioning is used) and an operation mode (how the laser beam is operated). The three scan modes corresponding to the three-positioning system are described as follow:

- Piezo Scan Mode: It is based on a fixed-beam moving-sample (FBMS) approach, meaning the complete sample holder is moved over the fixed laser beam to define structures. Since the center of the objective lens is used exclusively, and the Piezo stage has a high linearity throughout its range, this model yields accurate results within the full writing volume of 300x300x300 $\mu m^3$. It is used for high resolution writing with a positioning accuracy in the range of 10 nm within a writing area of 300$\mu m^2$;
- Galvo Scan Mode: it uses the fast beam scanning option via a galvo scanner and vertically the z-axis of the piezo or the z-drive. This mode is ideally suited for layer by layer fabrication of large surface and large-area structures. It is used for high-speed writing. Positioning accuracy and writing area depend on the objective in use. This represents the GT upgrade standard scanning mode;
- Stage Scan Mode: the programmed point lists are addressed in this coordinate system. Movements in z-direction are performed by the z-axis of the piezo. The main purpose of the stage is stationary positioning. It is used for coarse writing with a positioning repeatability in the range of 1.5 μm on a large area defined by the maximum writing area on the current substrate.

For all modes, the z-axis movements can be performed either with the Piezo z-axis or with the z-drive of the micro-scope for layer-by-layer writing.

### *2.5.3 Materials*

The correct selection of material in DWL-2PP is essential to produce nano/micro--structures suitable for each application. They provide the best performance for a broad range of applications, e.g., from micro-optic for rapid prototyping and small series production to biomedical devices. What is essential is the photoresist, a resin consisting mainly of monomers, oligomers, photo-initiators. Other primary materials are solvents, to ease the adhesion of the resin to the substrate and inhibitors, to control the quantum yield of polymerization.

Resins can be positive or negative. In positive resins, the irradiated part is not polymerized, and it is removed during the development. Instead, Nanoscribe provides a product line of negative resins, where the irradiated part is polymerized, and it is the only remaining part after the development. Negative resins are used the most because small structures are produced. In other words, the irradiated volume is smaller than the volume washed away, also decreasing the fabrication time.

### 2.5.3.1 IP-S and IP-Dip resins

In this project, two commercially available negative-tone acrylate-based photoresist were used: IP-S and IP-Dip (Nanoscribe GmbH). Both resins are used with "Dip-in" laser lithography (DiLL) technology. IP-Dip is more fluid than IP-S and for this reason, is suitable for higher resolution applications. On the other hand, IP-S is more viscous and designed for mesoscale printing. The key properties and elemental and components composition of resins are summarized in Table 2.6-7-8-9.

**Table 2.6** *IP-Dip and IP-S elemental composition. Adapted from*[42]

| Resins | Carbon (at.%) | Hydrogen (at.%) | Nitrogen (at.%) | Oxygen (at.%) | Empirical Formula |
|---|---|---|---|---|---|
| **IP-Dip** | 40.2 | 46 | 0.04 | 13.7 | $CH_2N_{0.001}O_{0.34}$ |
| **IP-S** | 31.5 | 54.1 | 5.8 | 11.8 | $CH_{1.72}N_{0.086}O_{0.37}$ |

**Table 2.7** *IP-Dip components composition. Adapted from*[43]

| Components | Quantity |
|---|---|
| Aliphatic alcohol, containing acrylate | 60-80% |
| Acrylate- and polyether, containing alicyclic hydrocarbon | <24% |
| Hydrocarbon acrylate | <24% |

**Table 2.8** *IP-S components composition. Adapted from*[44]

| Components | Quantity |
|---|---|
| Carbamate-methacrylate, mixture | >95% |
| Butyrolactone | <5% |
| Photoinitiator based on aromatic ketones | <1% |

**Table 2.9** *IP-Dip and IP-S physical and mechanical properties. Adapted from*[42]

| Properties | Unit of measure | IP-Dip | IP-S |
|---|---|---|---|
| **Density (liq)** | g/cm$^3$ | 1.14-1.19 | 1.16-1.19 |
| **Density (s)** | g/cm$^3$ | 1.2 | 1.2 |
| **Young's Modulus** | GPa | 0.75-4.5 | 4.6 |
| **Hardness** | MPa | 152 | 160 |
| **Poisson's ratio** | - | 0.35 | 0.35 |
| **Refractive index** | - | 1.52 | 1.48 |

## 2.6 Nanoscribe standard operating procedure

The standard operating procedure is divided into three basic steps and summarized in Figure 2.25:

- Preparation: including the 3D CAD realization and the conversion of .stl file to .gwl file through Describe software;
- Production: here the printing procedure, with Photonic Professional GT through Nanowrite, software takes place;
- Post-Processing: involving the development of the sample through the removal of excess resin.

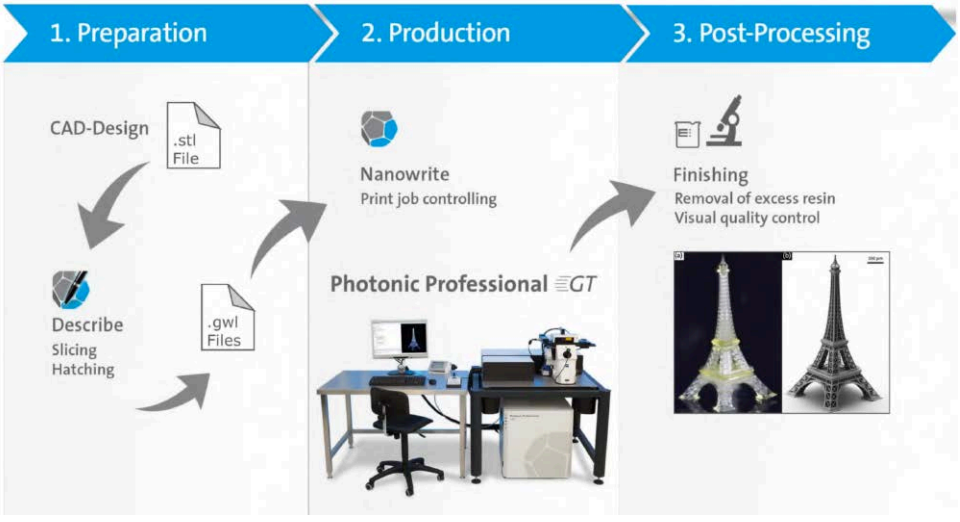


**Figure 2.25** *Software workflow overview. Adapted from*[40]

### *2.6.1 Designed 3D geometry*

The first phase of the 3D printing process requires the design and the micro-channels arrays in CAD model. AUTOCAD® software was used for this purpose; its 3D model and the final layout are shown Figure 2.26-27. After that the geometry was exported in .stl file.

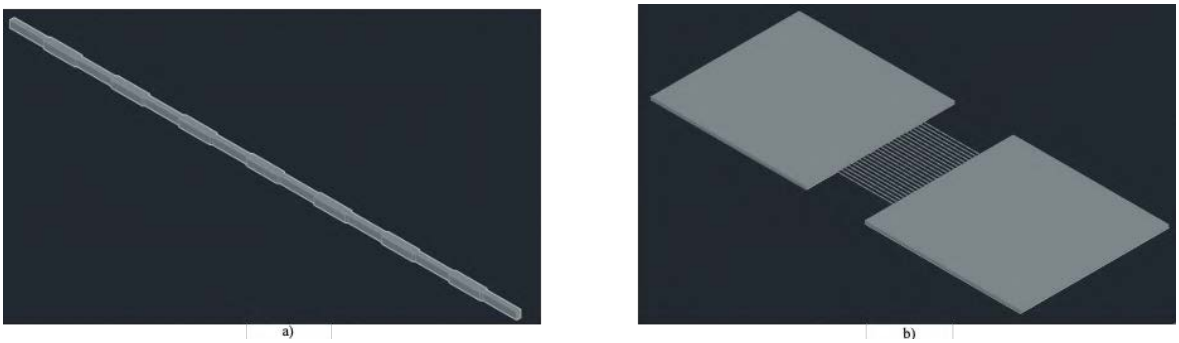


**Figure 2.26** *3D model of the final layout (b) and of a micro-channel (a)*

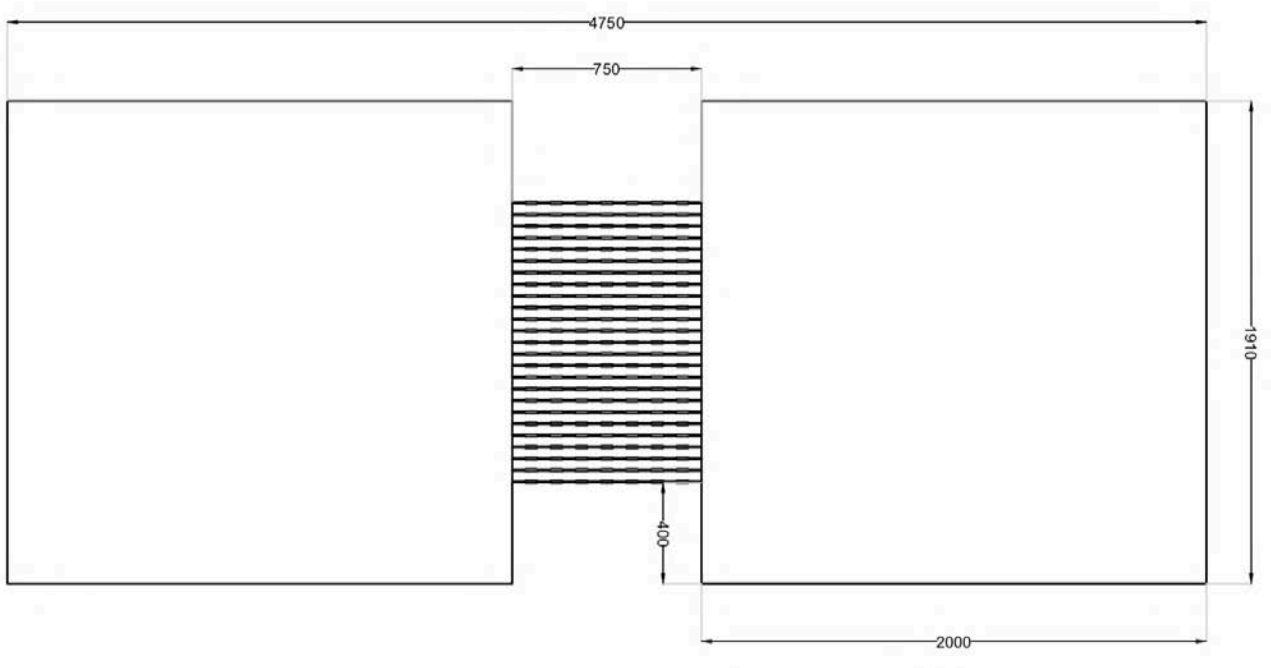


**Figure 2.27** *2D Cad of the final layout. The main dimensons are in μm.*

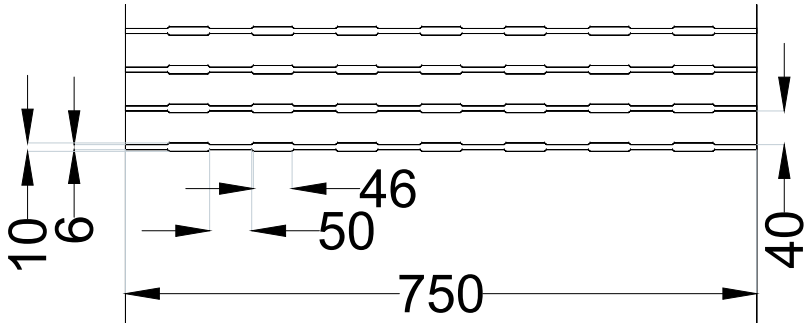


**Figure 2.28** *Measure of the final layout focusing on the micro-channel dimension in μm.*

The relevant dimensions of the microfluidic platform are listed in Table 2.10 and highlighted in Figure 2.28.

**Table 2.10** *Main dimension of former μ-bioreactor.*

| Quantity | Value | Unit of measure |
|---|---|---|
| Number of μ-channels | 15 | μm |
| Section of narrowest μ-channels | 6x10 | μm |
| Section of μ-channels | 10x10 | μm |
| Length of μ-channels | 750 | μm |
| High of μ-channels | 10 | μm |
| High lateral channels | 40 | μm |

## 2.6.2 Start Up/Shut Down tool and software initialization

Considering the Figure 2.29 where the entire elements of *Nanoscribe Photonic Professional GT* are shown, the Start Up procedure is described as follow:

1. Turn on the main power supply;
2. Turn on the microscope power supply;
3. Turn on the computer;
4. Turn on laser;
5. Turn on stage;
6. Log on the computer and open NanoWrite software. Select the desired object to print.

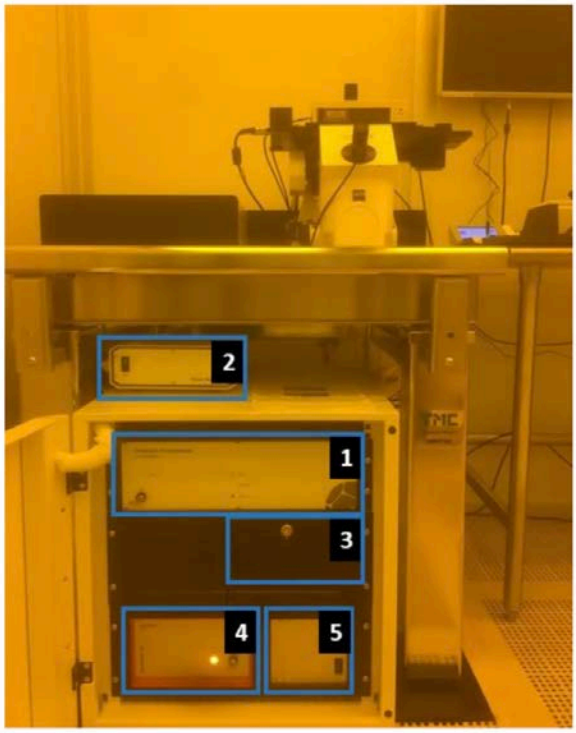


**Figure 2.29** *Elements of Nanoscribe Photonic Professional GT: 1) main power supply, 2) microscope power supply, 3) computer, 4) laser, 5) stage. Adapted from*[41].

After that, a stage calibration and sample holder choice (Figure 2.30) have to be performed, making sure that there is no objective in the system. The Shut Down procedure is nothing but the reverse of the start-up one. In this project we used the DiLL substrate model sample holder (with a dimension of 25mm x 25mm and thickness of 0.7mm).

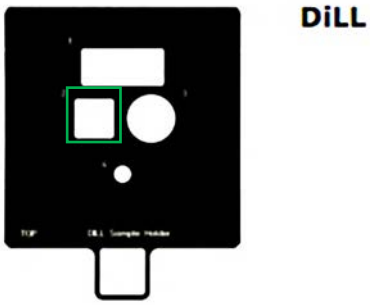


**Figure 2.30** *DiLL substrate model sample holder with the substrate used highlighted.*

The sample preparation procedure is described as follow:

1. Clean the substrate with acetone/IPA/distilled water. In this way a droplet of resist will not spread strongly over the surface;
2. Fix the substrate on the sample holder;
3. Put a drop of oil or/and resist on the substrate carefully;
4. Insert the sample holder into the microscope module.

After this, the object has to be installed on the objective turret of the microscope module.

### 2.6.3 3D Writing procedure

1. Switch on the transmission illumination;
2. Click the “Approach Sample” button. In this way the objective comes close to the sample;
3. When the right working distance is found the program is possible to observe the small interferences fringes in the “Interface Finder” window Figure 2.31;
4. Click Load Job and open the job.gwl file;
5. Start the job.

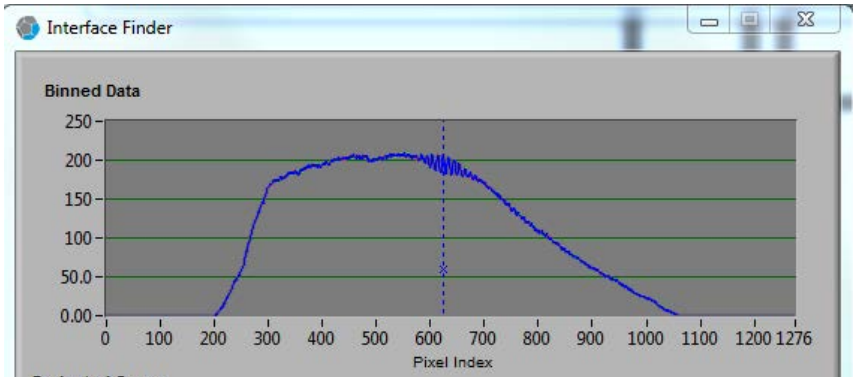


**Figure 2.31** *Small interferences fringes in the “Interface Finder”.*

### 2.6.4 Development of sample

The sample development procedure is described below:

1. Use a bath of propylene glycol monomethyl ether acetate (PEGMEA) in a 25ml beaker. To fix the substrate vertically in the beaker, use the vertical substrate holder. Allow the substrate to develop for at least 10 minutes. Depending on the size of the structure, this step can take up to 30 minutes. However, the development time is not very critical – structures can be kept in the developer for much longer without changing the structure. Click the “Approach Sample” button. In this way the objective comes close to the sample;
2. When development is done, carefully remove the holder from the PEGMEA and place it into a second beaker containing isopropanol (IPA) for 1-2 minutes. Do this carefully – the surface tension of the liquids can easily destroy fragile features.
3. Remove from the IPA and place the substrate on a clean surface to air dry. For more robust structures, methanol can be applied to the surface to expedite evaporation.

## 2.7 Micro-channel arrays production

It was necessary to decide how the proposed device could be created by means of this innovative technology. First of all, the choice fell on the material. After several printing simulations, through the software Describe, it was concluded to discard IP-Dip resin. Since the latter was created for nanoscale prints, its high-resolution leads to a greater printing time than that obtained using IP-S resin. Another thing evaluated was how the platform was printed. Until now, there are not many studies on the various printing methods with which these micro-channels can be made or on the resins used with this machinery. For this reason, three different production choices have been evaluated. Figure 2.32:

- 3D structure: which consist of reproducing exclusively the 3D structure of channels and the camera entirely in IP-S. The idea was that cells can migrate directly into the resin structure;
- Sandwich structure: it involves generating a rectangular hollow structure in which inside will be present the channels. Here too the intention is to migrate cells within this structure;
- 3D structure as a master: production of a non-hollow solid of the structure geometries and then being able to use it as a master for the fabrication of the device employing *replica molding*.

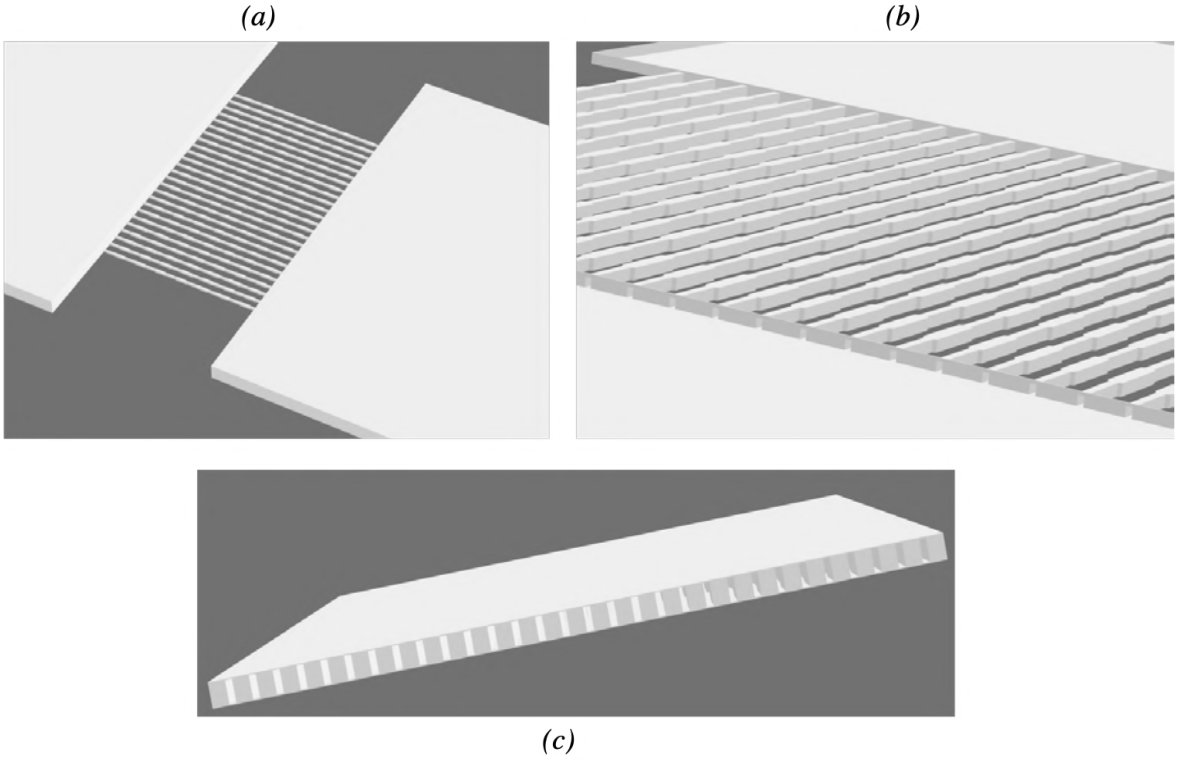


**Figure 2.32** *Different stl file of the 3D structure as a master (a); 3D structure (b); sandwich structure(c))*

# Chapter 3

# Platform characterization and hydraulic seal validation

This chapter analyzes all the three micro-channel arrays produced via 2PP using both optical microscopes and a profilometer, in collaboration with the TE.SI laboratory of the Department of Industrial Engineering located in Rovigo. The results of the analyses are commented. Then, the production of the platform was carried out through *replica molding*, and finally the protocol and the results of the hydraulic seal validation are described.

## 3.1 Metrologic characterization

Once the micro-channels arrays are printed, they are subjected to metrological characterization, to verify that printing was successful and corresponding to the nominal design. This operation is necessary since it is not possible to verify the success of the printing with the naked eye. By metrological characterization we mean visual and topographical analyses, and the quantification of the surface roughness of the micro-channels arrays. It also allows to evaluate the height of the micro-channels and highlight any critical area. The analysis was performed both on the printed devices and on the replicated PDMS platforms. In particular, the analysis was repeated after 5$^{th}$ and 10$^{th}$ PDMS replica. These analyses were performed using the Sensofar S Neox profilometer, shown in Figure 3.1


**Figure 3.1** *Sensofar S Neox profilometer with its supporting hardware. Adapted from*[45]

This device is a complete microscopy system for non-contact optical profilometry, particularly suitable for measurements in the nanometer and micrometer scale. The instrument is quite versatile thanks to the 3-in-1 technologies that are described below:

- Ai Focus Variation: Active illumination Focus Variation vertically scans either optics (with very low depth-of-field) or the sample to obtain a continuous set of images of the surface. An algorithm determines which points in each frame are in focus, and an entire image is built using all in-focus points from all frames. It has been improved with the use of active illumination to get more reliable focus location even on optically smooth surfaces;
- Confocal: the imaging technique included by the Confocal microscopes, utilizes an aperture at the confocal plane of the objective. Out-of-focus light is thus prevented from entering the imaging system and only the in-focus plane on the sample is captured. 2D profiles and 3D surface images can be captured by scanning the aperture mechanically or digitally;
- Interferometry: Optical Interferometry makes use of the optical path difference between light reflected in the two arms of the interferometer (reference and sample) to yield a spatial interference pattern (interferograms) that contains information on the surface topology of the sample. It boats a better vertical resolution.

The system is composed by a head placed on the objectives, and its movement on the plane can be motorized, for small shifts, or done by manual approach. Three objectives are available to measurements: 2.5x, 20x and 100x. The acquisition of the study area is done though the 2.5x objective, while for the actual measurements only 20x is used. It basically involves performing scans on XY plane, then increasing in Z, and rebuilding the structure in 3D, thus obtaining a single-resolution image of a more or less large surface. Some technical characteristics of the machine are showed in Table 3.1.

**Table 3.1** *Technical characteristics of the S Neox Profilometer. Adapted from*[46]

| Characteristics | Value | Unit of measure |
|---|---|---|
| Optical resolution | 0.31 | µm |
| Spatial sampling | 0.34 | µm |
| Working distance WD | 4.5 | mm |
| Field of view FOV | 845 x 707 | µm |

The steps to data acquisition phase relating to the metrological characterization of the micro-channels are:

1. Position of the sample to be analyzed in the XY plane and manually approaching the piece roughly for quick adjustment along the Z-axis, to re-enter the field of view;

2. Identify of the area to be analyzed with the 2.5x objective and making sure to see the area clearly enough. This is followed by the acquisition of a preview with the 2.5x objective;
3. Switch to the 20x objective and to Confocal mode, to set the Z min and Z max coordinates of the surface involved in the analysis. To impose a top and bottom range in which to perform the measurement;
4. By imposing a zero as a reference system and using a joystick for movement and rapid control, the upper and lower limits of the Z coordinate are then established for the analysis;
5. Move to the sketching area, where a preview of the surface to be observed is made. A grid is positioned on the preview, which must cover the entire area to be analyzed;
6. Choice of analysis technique and 3D mode. It is possible to set some parameters, such as brightness, sensitivity, overlap and speed factor to improve the acquisition of the measurement and the speed with which it is carried out;
7. Start the analysis and, at the end, display the measurement that were acquired[46].

## 3.2 Printing results

Before proceeding with the metrological analysis, the structures were observed with an optical microscope. As seen in Figure 3.2, the 3D structure presents some critical areas, especially in the lateral chamber where the upper walls, after the bath in PGMEA, have collapsed. This problem was probably caused by a lack of support within the lateral structures.

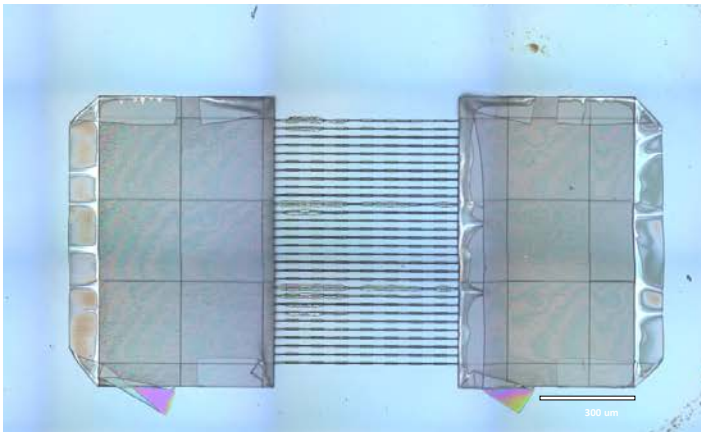


**Figure 3.2** *3D structure image obtained at the microscope 2.5x.*

The sandwich structure is shown in Figure 3.3. At first glance, it seems that the printing job was successful, however, from the reconstructed 3D image through Sensofar S Neox profilometer, we observe that the upper layer doesn't keep its starting structure, collapsing and obstructing the channels (Figure 3.3 b).

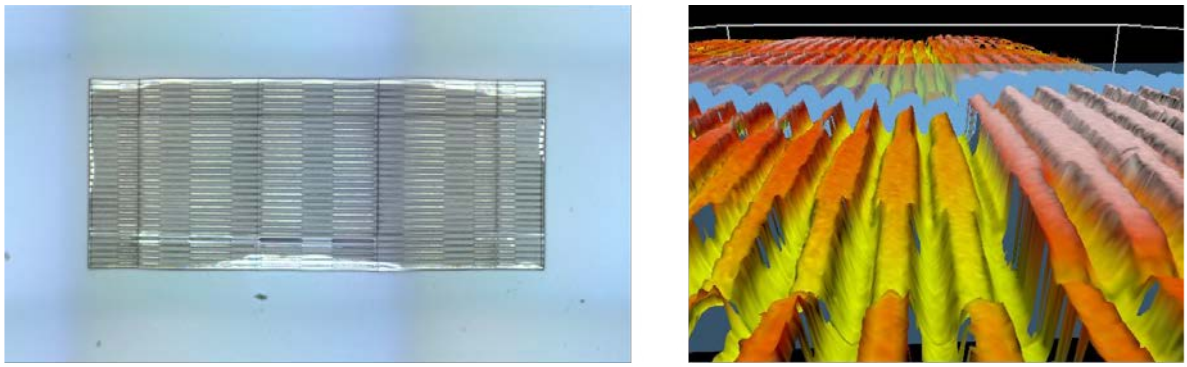

*(a)* *(b)*

**Figure 3.2** *(a) Sandwich structure image acquired by microscope 2.5x; (b) 3D reconstruction of sandwich structure acquired by the Sensofar S Neox profilometer.*

For this reason, the aforementioned structures are discarded, and a 3D structure as master, for the production of the microfluidic platform by means of *replica molding*, is considered. A preliminary printing of channel arrays is thus made, but the acquisition with the microscope shows that the channels detach from the surface and bend (Figure 3.4). To overcome this problem, two large side structures have been added, with the aim of providing greater stability to the entire device. The channels appear now much more aligned, but still have some critical issues as highlighted in the red box in Figure 3.5.A further improvement of the structure was introduced, namely the addition of a thin resin film as anchor base for the channels. Figure 3.6 shows that there is an improvement on the linear disposition of the channels.

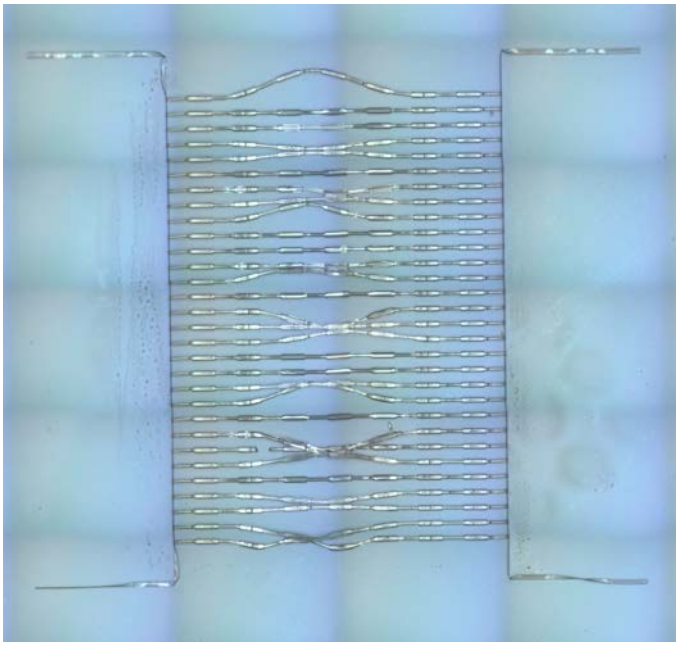

**Figure 3.4** *Channel arrays image acquired by microscope 2.5x.*

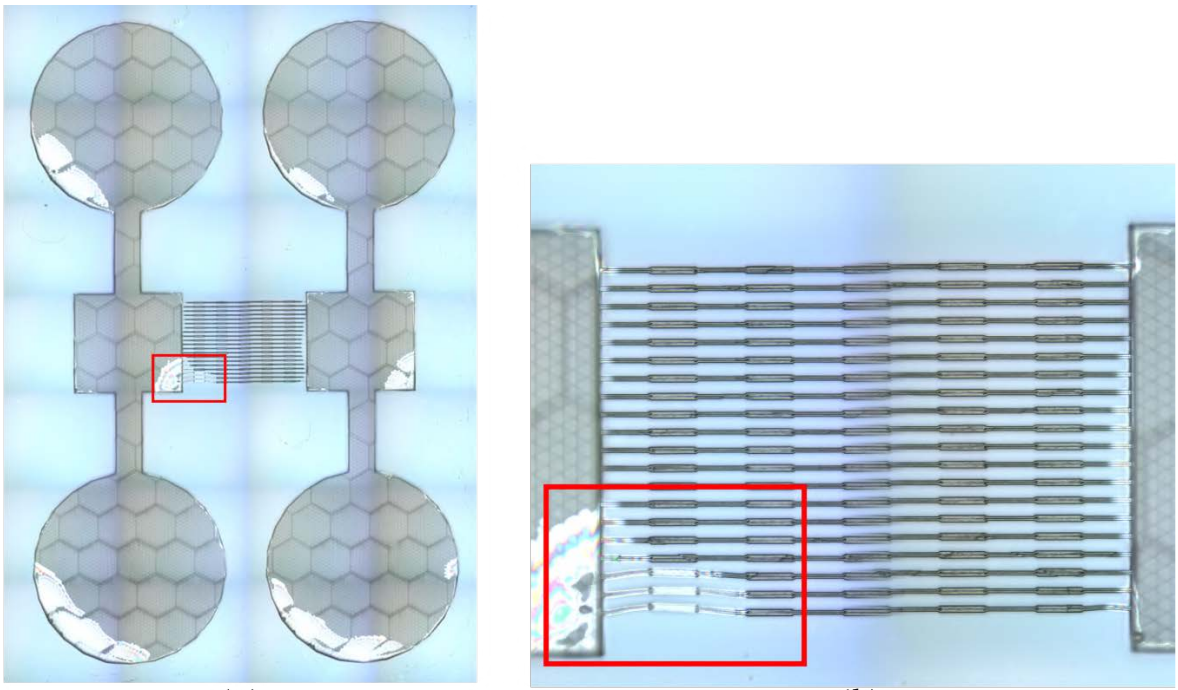


**Figure 3.5** *Channel arrays with two lateral structure. Images acquired by microscope 2.5x.*

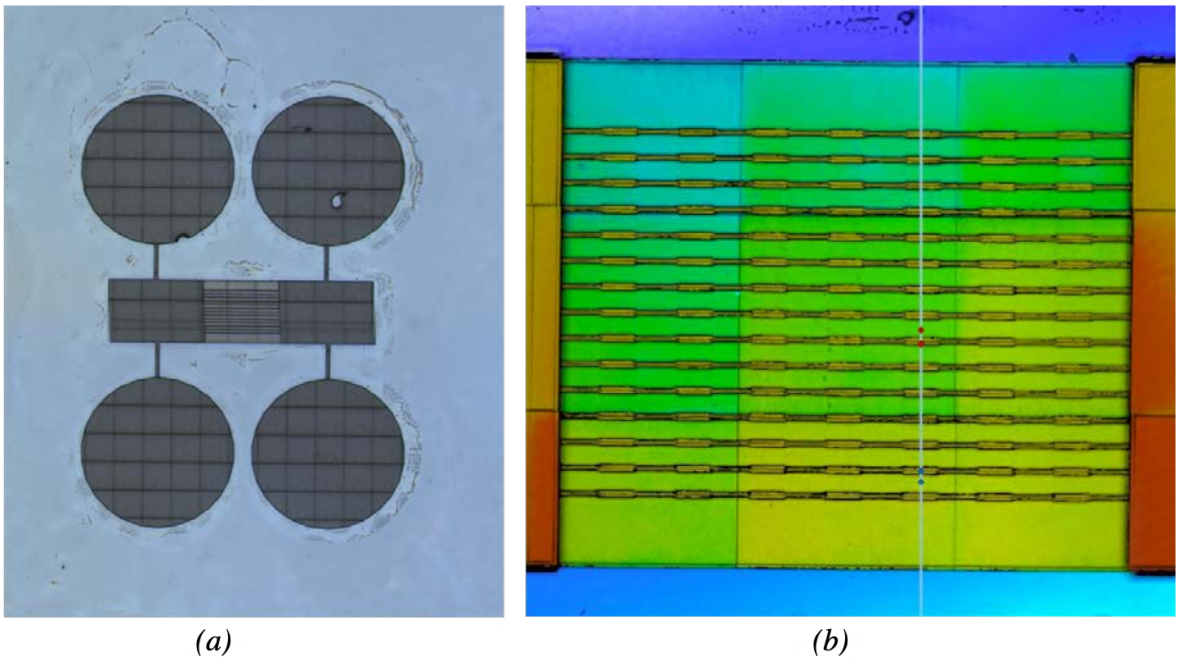


**Figure 3.6** *Channels arrays structure with lateral structure on a thin film of resin. Image acquired by microscope 2.5x (a) and by Sensofar S Neox profilometer (b).*

### 3.2.1 Analysis of IP-S Micro-channels arrays as a master

To verify the quality of the produced master, we performed an analysis using the 3D optical profilometer, giving information about the heights of the channels. The heights of specific area of interest are studied with the Confocal mode. Every channel is divided in three sections: top, center and bottom, as shown in Figure 3.7.

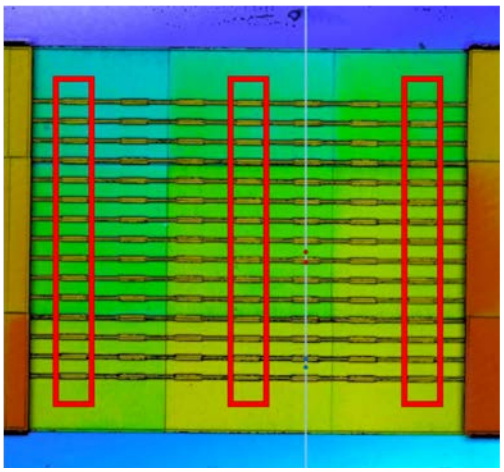

**Figure 3.7** *Section of interest used to carry out the profilometric analysis.*

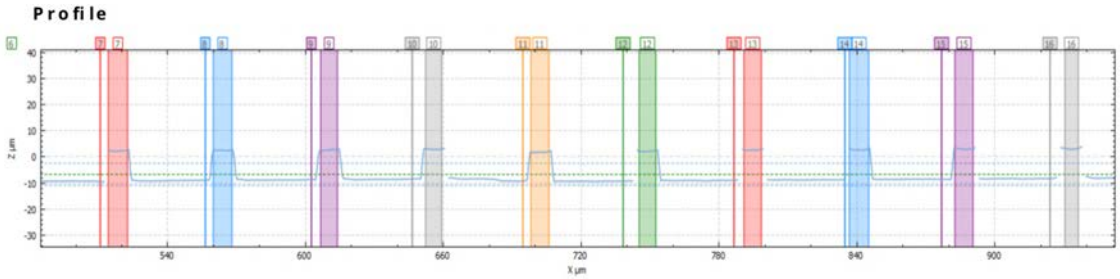


**Figure 3.8** *Section of interest used to carry out the profilometric analysis.*

The results of the analysis are shown in Figure 3.9 and data of mean height and standard deviation for each section are listed in Table 3.2.:

**Table 3.2** *Mean high and standard deviation for each section.*

| Section | Mean height [µm] | STD [µm] |
|---|---|---|
| Top | 10.63 | 0.12 |
| Center | 10.73 | 0.12 |
| Bottom | 10.59 | 0.22 |

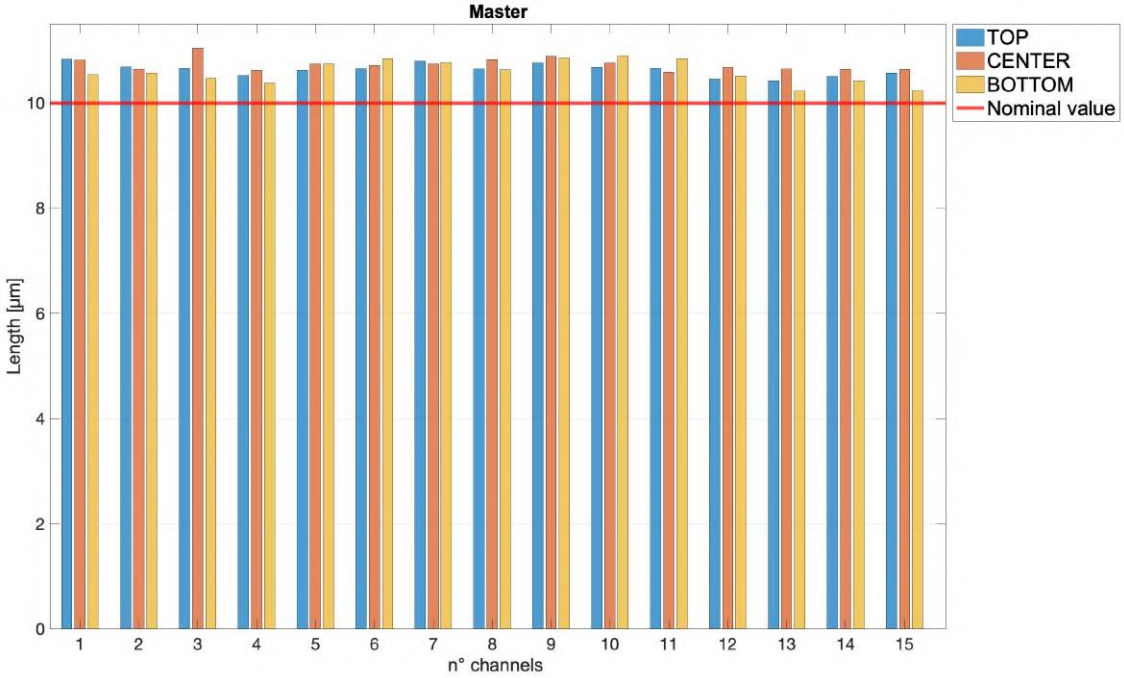


*(a)*

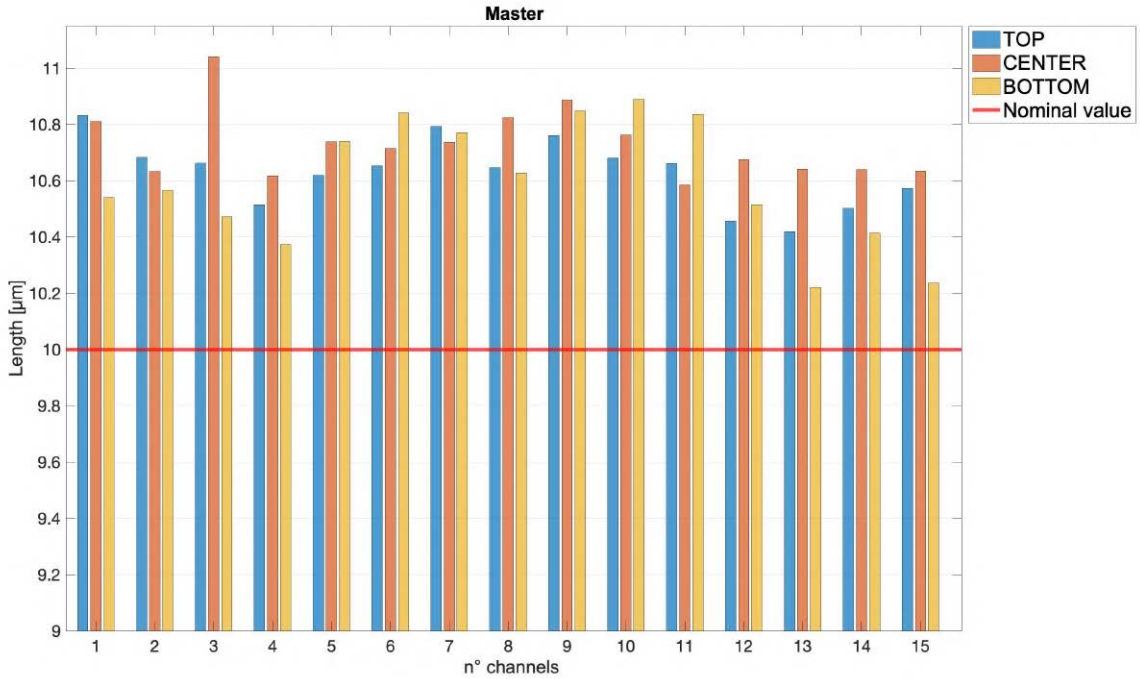


*(b)*

**Figure 3.9** *(a)Metrological characterization of the heights of all 15 channels: in blue the measures of the micro-channel top, in orange the one of the micro-channel center and in yellow the measures of micro-channel bottom. In red the line of the comparison CAD value;(b) Chart zoom.*

The bar chart illustrates results of the metrological characterization, demonstrating that the heights of each printed channel are higher than the nominal value. This can be attributed to a systematic error of the printer or to the scattering effect that occurs when the sample is

exposed to white light, altering its metrological measure. A statistical analysis, using the Anova one-way method, has been carried out to verify whether the variation in channel heights in the various sections is significant or not. The results, plotted in Figure 3.10, show that the difference between heights, in a 7% confidence interval, is not significant because the p-value is equal to 0.0696.

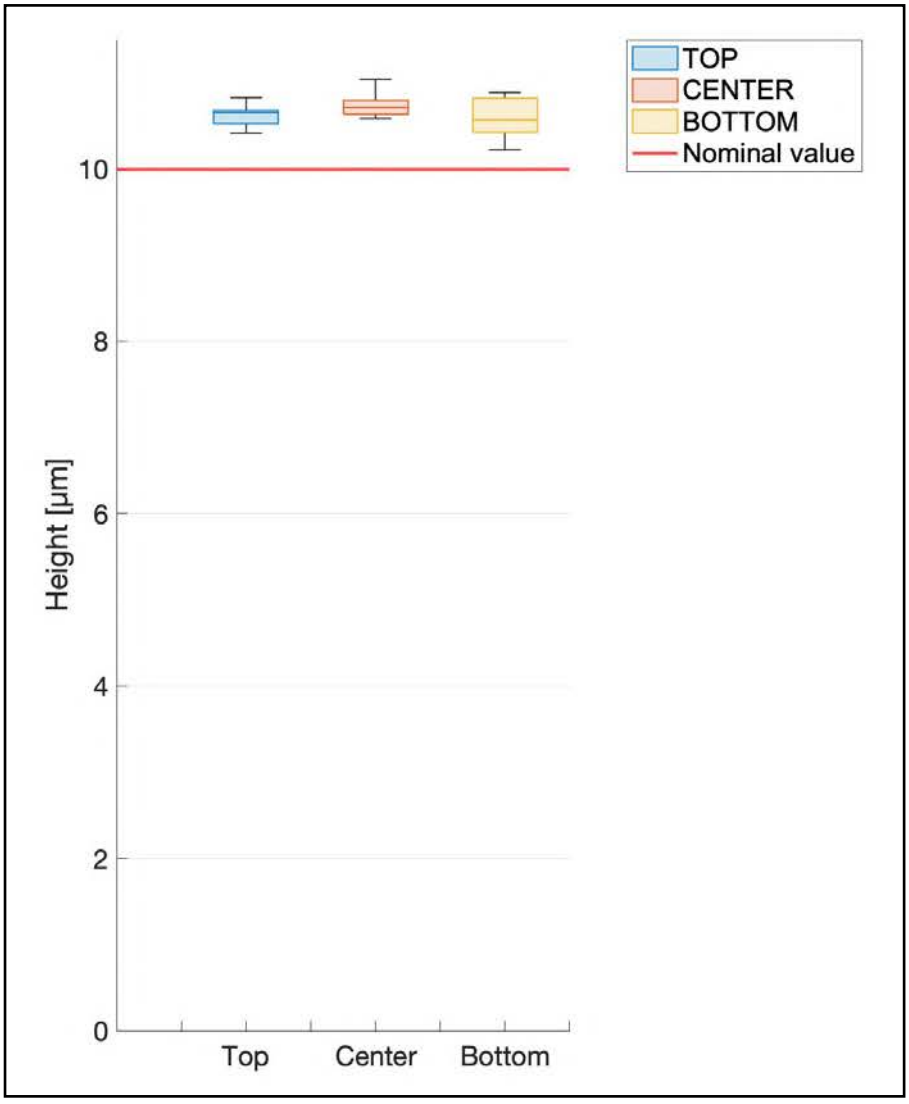


*(a)*

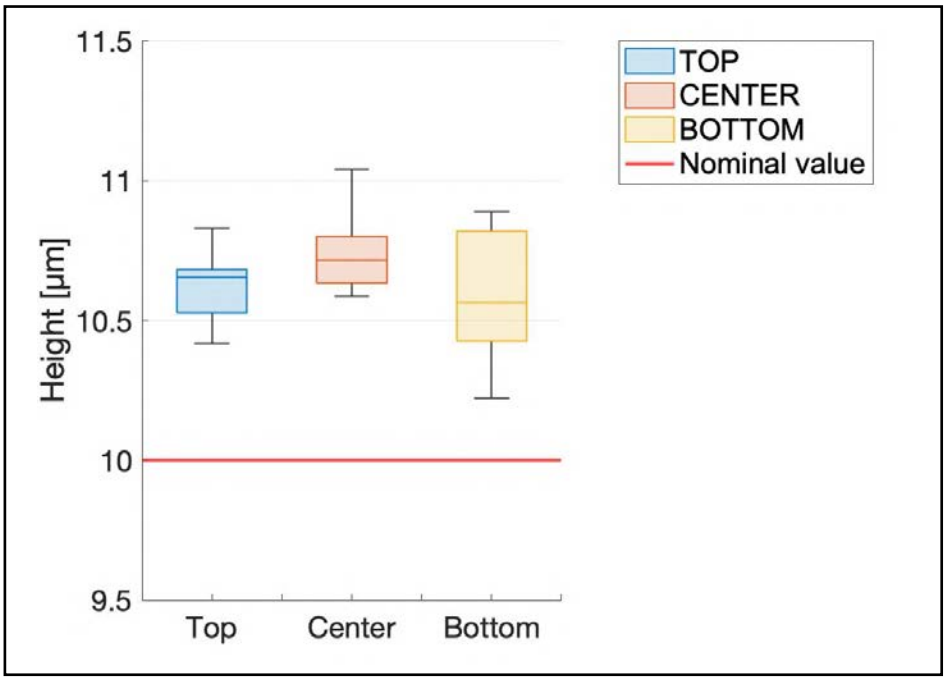


*(b)*

**Figure 3.10** *(a) Box plot of the heights of all 15 channels: in blue the measures of the micro-channel top, in orange the one of the micro-channel center and in yellow the measures of micro-channel bottom. In red the line of the comparison CAD value;(b) Chart zoom.*

## 3.3 Platform production through *replica molding*

The microfluidic platform is produced using PDMS Sylgard®184 (Dow Corning) that is provided as a two-part kit (DOWSILTM 184 Silicone Elastomer kit). It includes a silicone elastomer base and curing agent as it is shown in Figure 3.11. Thanks to this kit is possible to build a part of the microfluidic platform.


**Figure 3.11** *PDMS Sylgard® 184 (Dow Corning), two-part kit: silicone elastomer base on the left, curing agent on the right.*

## 3.3.1 PDMS

PDMS is a silicon-based organic polymer, also known as polydimethylsiloxane, build up by a sequence of the monomer [$SiO(CH_3)_2$], (Figure 3.12).It is the most widely used material in the production of microfluidic platforms for the biological applications, thanks to its low shrinkage and the good ability to replicate microscale features. Apart from microfluidic applications, it is used as a food additive, in shampoo and as anti-foaming agent in beverages or lubricating oils[47]. Lots of advantages makes PDMS a suitable material for microfluidic devices for cell culture production:

- Biocompatibility: it is inert and non-toxic, essential features in a biological environment;
- Gas-permeability, that allows $O_2$, $CO_2$ and $N_2$ to permeate across the material and reach the cell culture;
- Transparency at optical frequencies (240nm-1100nm), that allow the observation of the content thanks to a microscope;
- Low autofluorescence;
- Hydrophobic;
- Low cost.

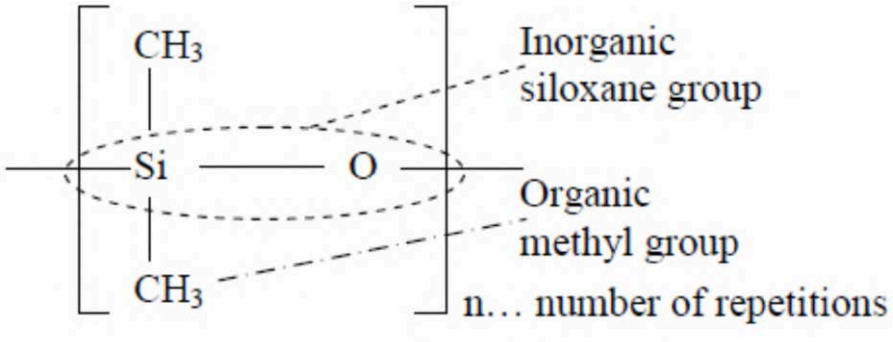


**Figure 3.12** *PDMS structure. Adapted from* [48]

Nevertheless, it has some properties that can create criticism in biological environment:

- Porosity: it can absorb hydrophobic molecules like lipids from the culture media. For this reason, regular replacements of the media are needed;
- Permeability to gases can result in a rapid evaporation of the culture media;
- Not completely toxic: curing step could be the critical one. To overcome this problem chips are also autoclaved to increase the cell compatibility;
- No cells attachment: very often cells are not able to attach the surface of this polymer and for this reason fibronectin, or mixtures like laminin or Matrigel can be used as coating;
- Sensibility to some chemicals such as hydrofluoric acid, sulfuric acid, potassium hydroxide.

### *3.3.2 Replica molding*

In this technique the master is used to produce microfluidic devices. A polymer, usually PDMS, is poured on the master and reticulated at controlled temperature for the required time. Then, PDMS can be easily removed from the master to obtain the microfluidic layer. Figure 3.13 shows the steps of *replica molding*.

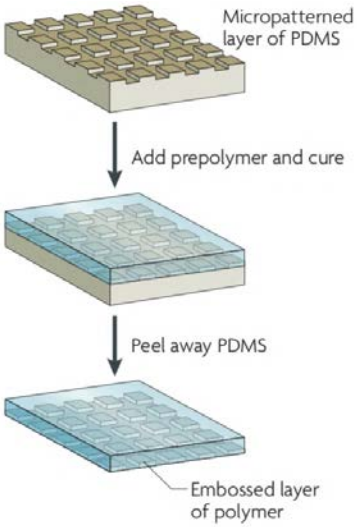


**Figure 3.13** *Key stages of the replica molding technique. Adapted from*[49]

After the obtainment of the PDMS layer, it is typically sealed to a glass slide, or to another layer of PDMS, through a plasma treatment that allows the creation of permanent covalent bonds between the two. In detail, the *replica molding* steps are reported below:

1. In a plastic container PDMS and cross-linking curing agent are energetically mixed in a proportion of 10 parts of 1 part until a homogeneous mixture is obtained;
2. A desiccator connected to a vacuum pump (Figure 3.14) is used to eliminate bubbles formed in the mixture. After 10 minutes the pump is switched off, and the valve of desiccator is opened to return at atmospheric pressure;
3. The content is poured on the master, in order to have a 3 mm thick layer, this parameter is not critical to the success of the molding[50];
4. The master is collocated inside the desiccator as in step 2. The procedure is repeated 4-5 times to remove all bubbles;
5. Curing of the PDMS on the master inside an oven, at 75 °C for 75 minutes;
6. Peeling of the cured PDMS layer from the rigid master.

**Figure 3.14** *Desiccator connected to a vacuum pump in the BIAMET laboratory.*

### 3.3.2.1 *Replica molding* and issues and resolutions

During the production of the platform through the *replica molding*, problems were encountered when the PDMS layer was removed from the mold. The result was the detachment of part of the mold channels (Figure 3.15 in the yellow square). They were later found stuck inside the replica in PDMS, as shown by the image acquired through the optical microscope (Figure 3.16)

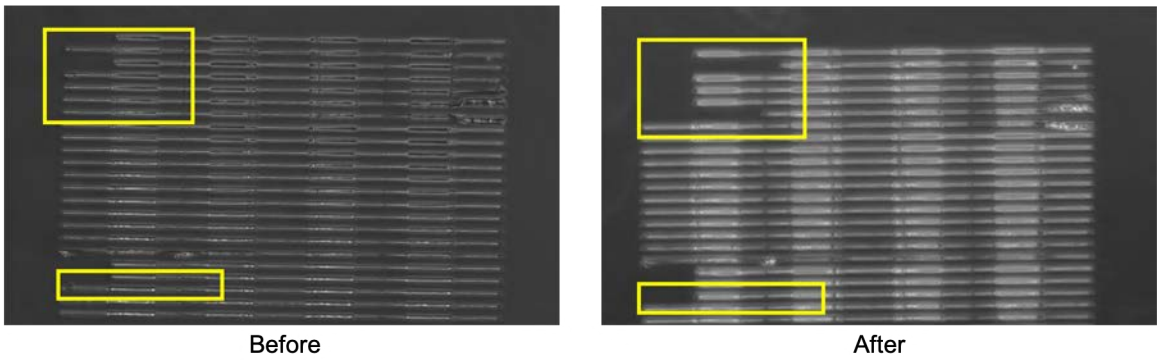


**Figure 3.15** *Detachment of part of the mold channels: before and after the removal.*

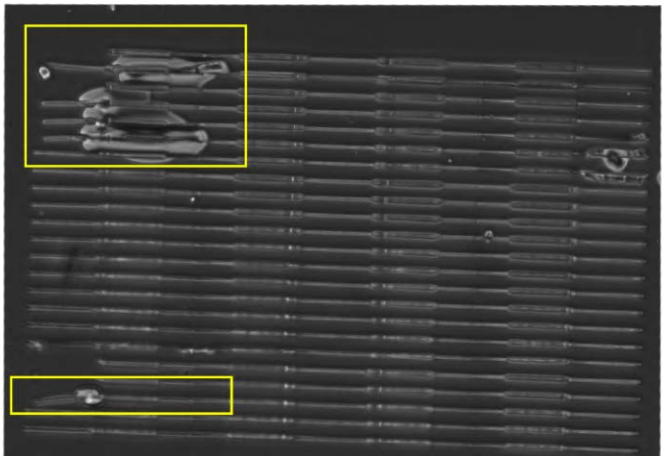

**Figure 3.16** *Channels stuck inside the replica in PDMS.*

Several hypotheses have been proposed to overcome the problem:

- Use chlorotrimethylsilane to silanize the surface for facilitating the detachment of the PDMS from the mold;
- Decrease PDMS thickness over the master to 1.5mm;
- Build a thin resin film under the entire surface.

The first hypothesis was found to be unsuccessful due to the presence of a non-compliant substrate (ITO coated glass) that cannot be replaced. The combination of the last two led to positive results. In Figure 3.17 is possible to see the mold of complete geometry (a) focusing the attention on the micro-channel (b) and on the micro-channel arrays of the master (c). At this point inlets and outlets of the platform are created punching the PDMS layer with a 1 mm diameter biopsy punch. After that, the platform is cut to the desired size and the surface is covered with scotch tape to prevent dust contamination.

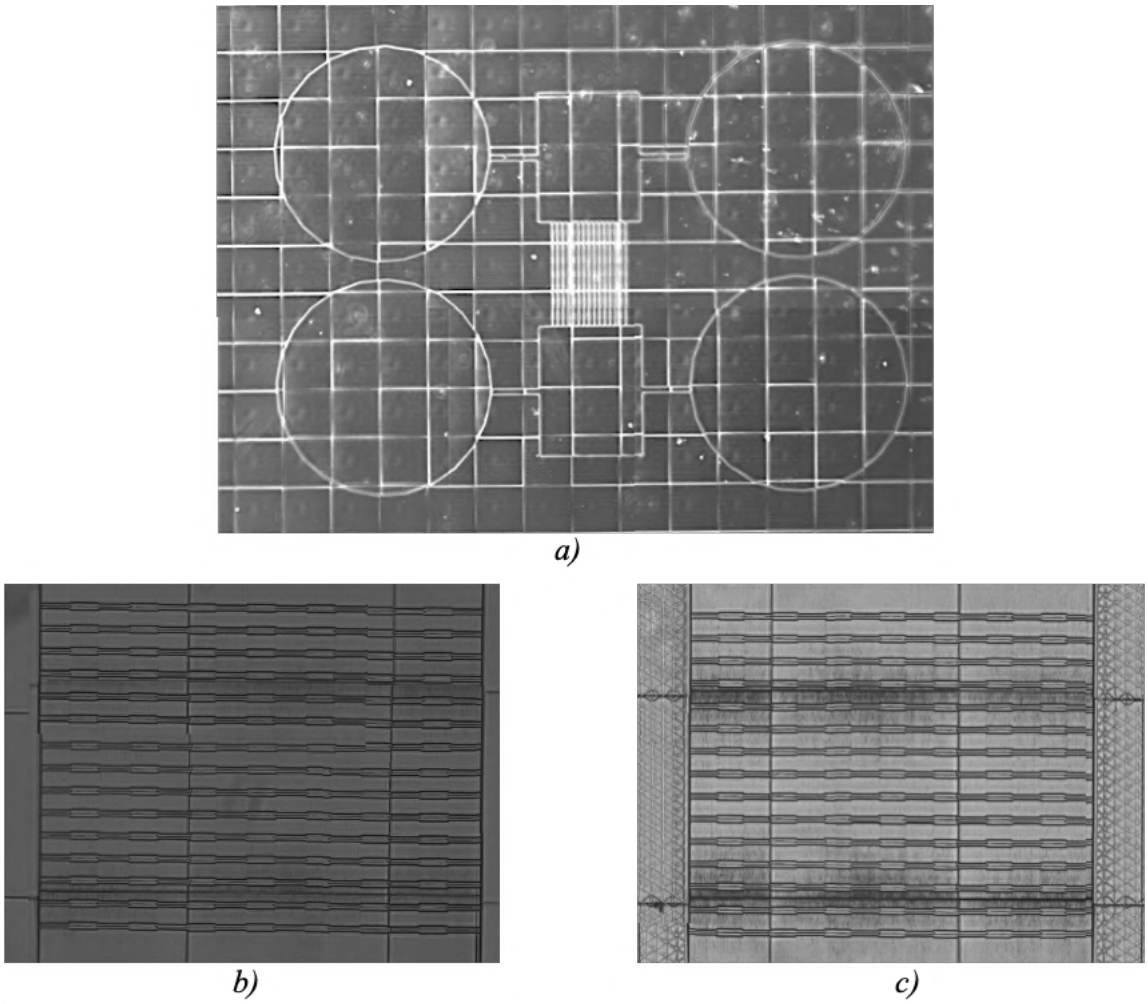


**Figure 3.17** *The complete the mold of complete geometry (a) focusing the attention on the micro-channel (b) and the micro-channel arrays of the master (c).*

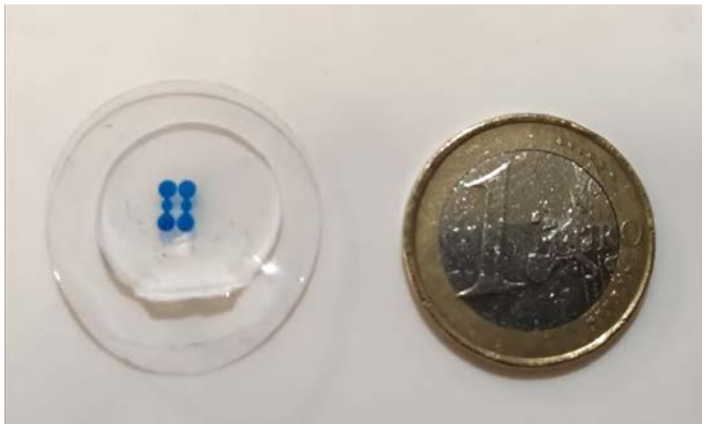

**Figure 3.18** Replica of the final platform filled with blue colorant compared with one-*euro coin.*

### 3.3.3 Metrological analysis of master after 5-10 replicas

To verify how a mold can last over time, it has been subjected to further metrological measurements after 5 and 10 replicas. The values of the individual measurements with the respective channels are shown in Figure 3.19a-b and Figure 3.20

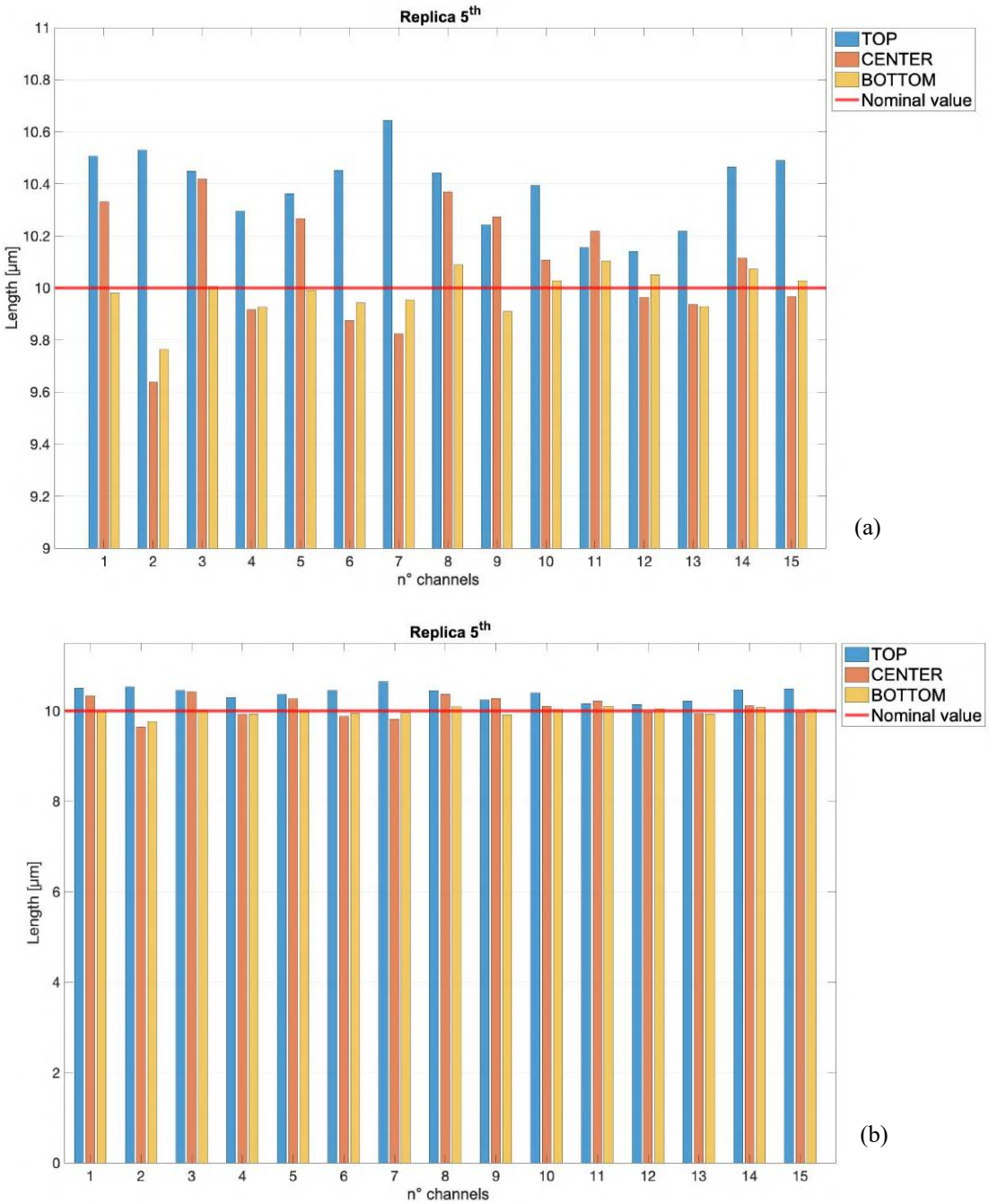


**Figure 3.19** *(a)Metrological characterization of the heights of all 15 channels after 5 replicates: in blue the measures of the micro-channel top, in orange the one of the micro-channel center, in yellow the measures of micro-channel bottom and in red the line of the comparison CAD value;(b)Chart zoom .*

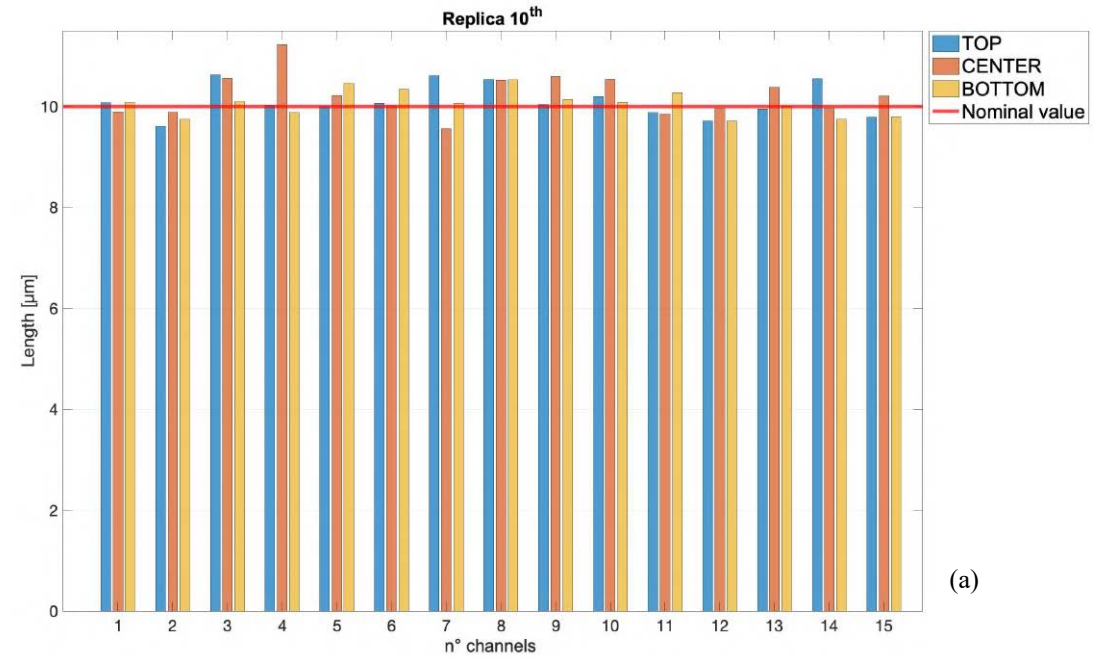


(a)

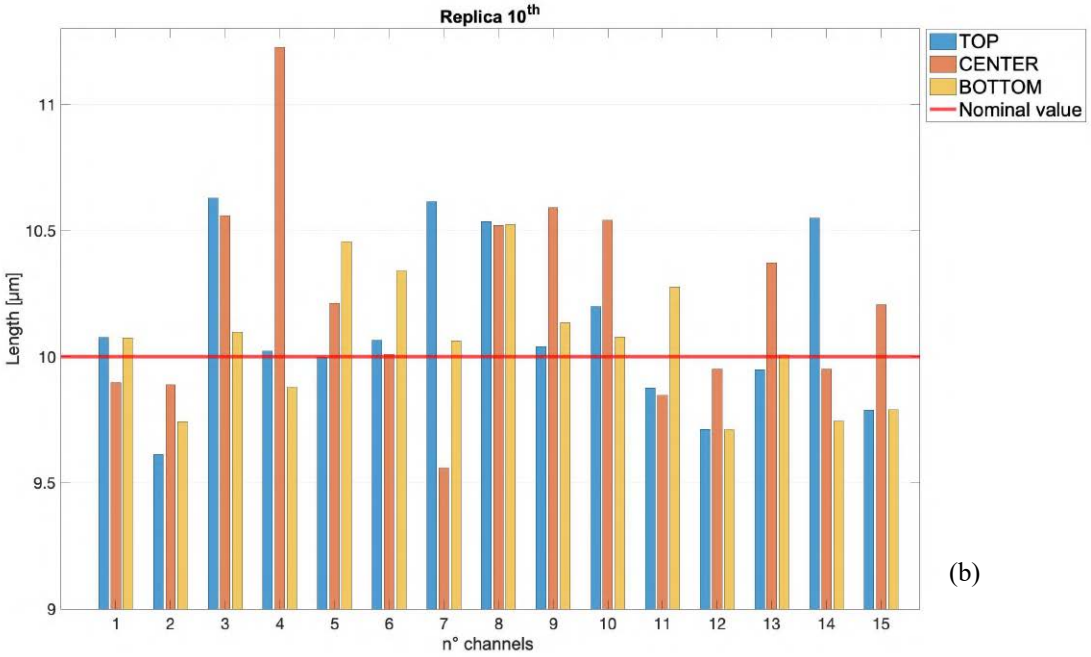


(b)

**Figure 3.20** *(a)Metrological characterization of the heights of all 15 channels after 10 replicates: in blue the measures of the micro-channel top, in orange the one of the micro-channel center, in yellow the measures of micro-channel bottom and in red the line of the comparison CAD value;(b)Chart zoom .*

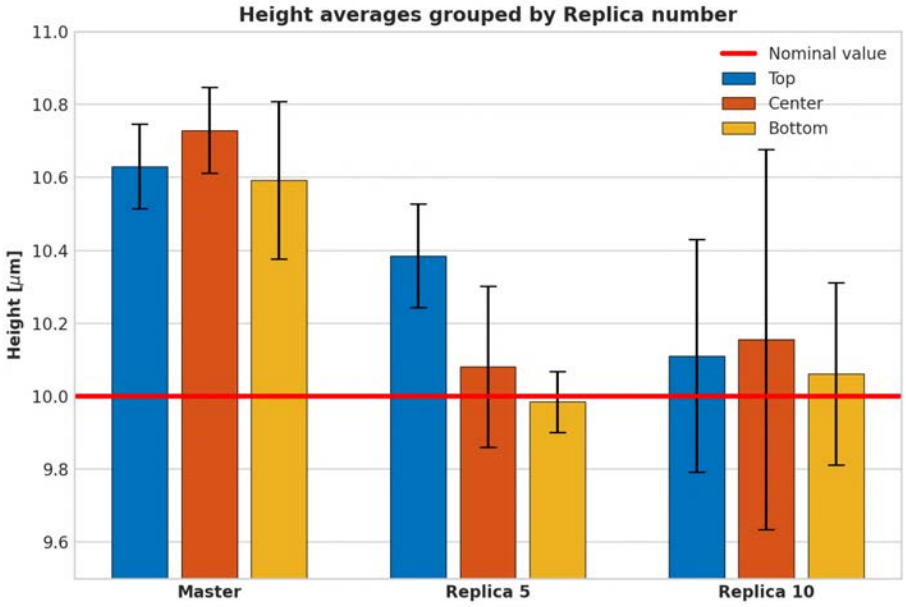


**Figure 3.21** *Length average grouped by replica's number.*

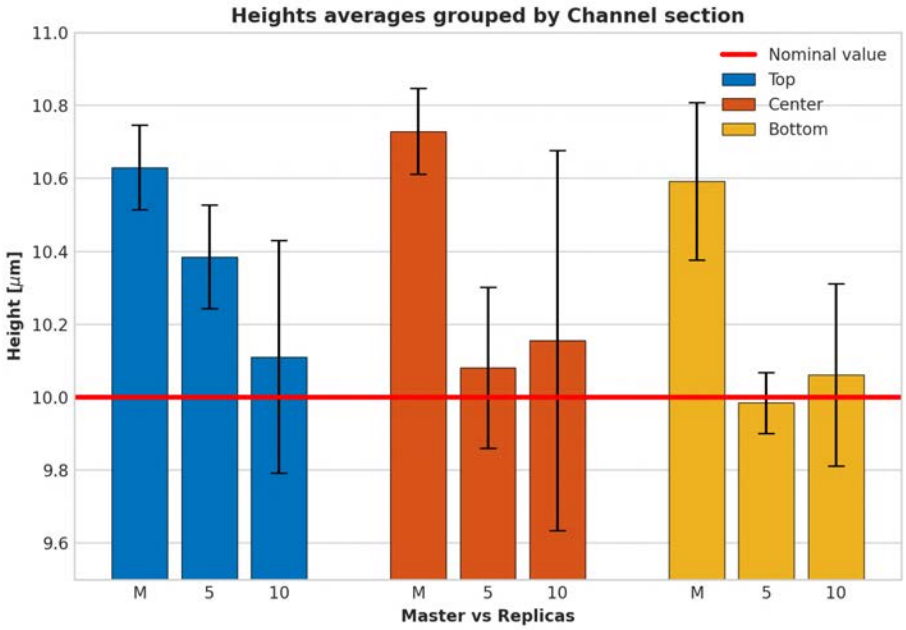


**Figure 3.22** *Length averages grouped by channel section (range of 1.5 μm of height).*

From the values shown in the tables and Figure 3.21 and Figure 3.22 it is clear that:

- Mean value of the initial master always higher than the nominal one;

- Increasing the numbers of replicates also induces errors increase: this means that there is an increase in the difference in height between channels, losing control of the geometry;
- Increasing the number of replicates leads to a decrease of the minimum of errors, confirming the wear phenomenon after each replica.

In conclusion it is possible to state that the realization of the master in IP-S resin can be a good alternative to other building materials such as aluminum, (used in micromilling), because it can be used for the realization of devices in PDMS through the *replica molding*, without significant problems of wear or tear of this.

**Table 3.3** *Mean length as a function of replica's number averaged on all sections.*

| Master vs Replica | Mean length [µm] | STD [µm] |
|---|---|---|
| Master | 10.65 | 0.17 |
| 5 | 10.15 | 0.23 |
| 10 | 10.11 | 0.38 |

**Table 3.4** *Mean length as a function of sections averaged on all replica's number.*

| Section | Mean length [µm] | STD [µm] |
|---|---|---|
| Top | 10.38 | 0.30 |
| Center | 10.31 | 0.44 |
| Bottom | 10.21 | 0.33 |

**Table 3.5** *Mean length for each section as a function on replica's number.*

| Replica | Section | Mean length [µm] | STD [µm] |
|---|---|---|---|
| 0 | Top | 10.63 | 0.12 |
| | Center | 10.73 | 0.12 |
| | Bottom | 10.59 | 0.22 |
| 5 | Top | 10.38 | 0.14 |
| | Center | 10.08 | 0.22 |
| | Bottom | 9.98 | 0.08 |
| 10 | Top | 10.11 | 0.32 |
| | Center | 10.15 | 0.52 |
| | Bottom | 10.06 | 0.25 |

## 3.4 Plasma treatment for irreversible sealing

Plasma is a state of matter in which gas molecules have become ionized (lose one or more electrons) after adding enough energy. The net charge is positive, and plasma incorporates neutral gas atoms, electrons, positive ions, UV light and excited gas atoms, that carry a big amount of internal energy (Figure 3.24)[51]. The plasma treatment is a procedure that improve adhesion, through variation of surface properties, achieving a perfect hydraulic seal in the platform.

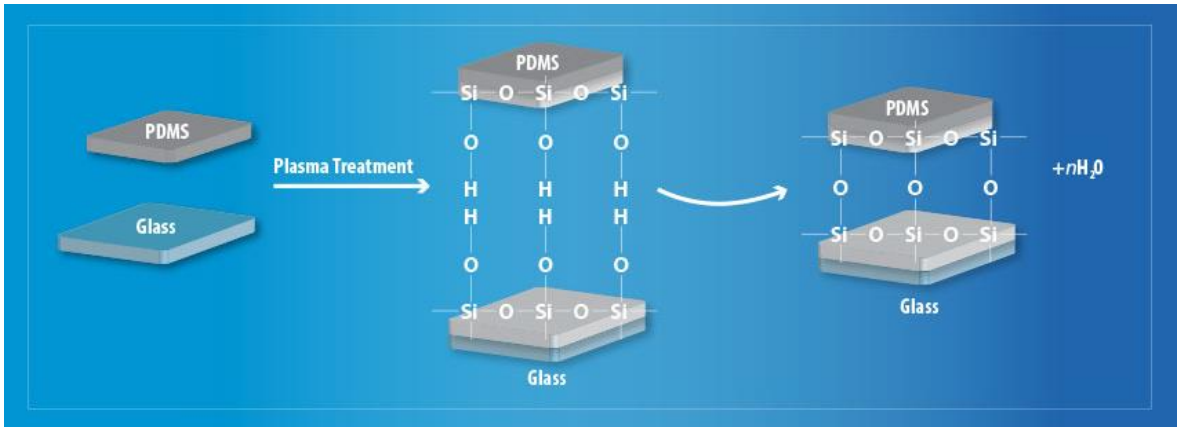


**Figure 3.23** *Schematic diagram of plasma treatment: single elements of glass and PDMS; activated surfaces and bond creation. Adapted from*[51]

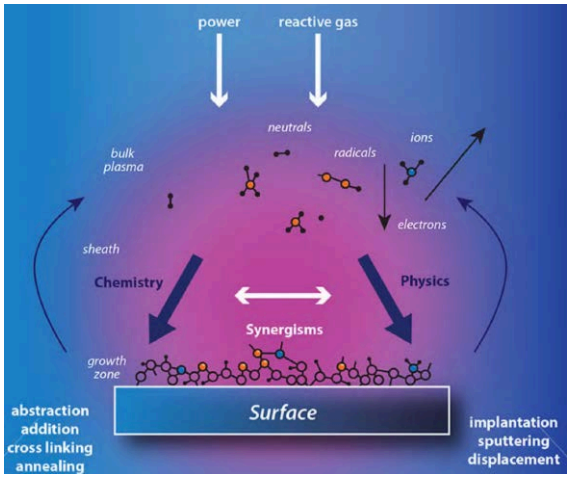


**Figure 3.24** *Plasma treatment technique. Adapted from* [52]

Plasma is generated through a Plasma Cleaner (PDC-002-CE by Harrick Plasma, Figure 3.25 b) with a combination of low pressure, radio frequency oscillating electric field and elastic scattering of electrons. These effects lead to heating of the electrons, that gain kinetic energy in excess of the first ionization threshold in the neutral gas species and then collision lead to further ionization[51].

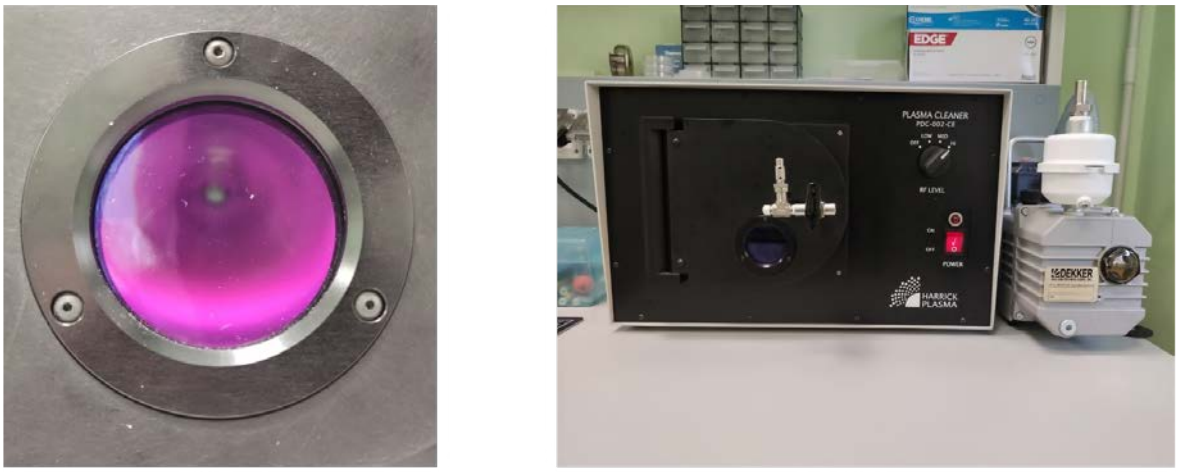


*(a)* *(b)*

**Figure 3.25** *(a) Color of plasma when an adequate quantity of oxygen is present in the chamber; (b) Plasma Cleaner by Harrick Plasma, used in BIAMET laboratory.*

In this case the PDMS layer surface is activated creating covalent bond with a glass side or another PDMS piece (Figure 3.23).The plasma reacts with the materials, creating silicon atoms with one missing electron on the surface. The silicon bonds will connect with hydrogen to create Si-OH bonds on the PDMS and the glass surface. Subsequently, when PDMS is placed on the glass's surface, the initial Si-$CH_3$ bonds recombine to form covalent bond (Si-O-Si) between them, and its strength can reach 5 bar[53]. This method is widely used in biological microfluidic field, precisely because of its advantages[51]:

- It affects the near surface of the material, leaving bulk properties unchanged;
- Plasma forms at about ambient temperature, minimizing risk of damage to heat-sensitive materials;
- It can be applied to many different materials such as semiconductor wafers, polymer scaffolds;

In biological microfluidic devices, the plasma treatment needs to be performed before the insertion of cells in the platforms because it can damage them due to its reactivity[54] .

### *3.4.1 Plasma treatment protocol*

In this case, plasma treatment is used to form the hydraulic seal of the microfluidic platform to a microscope slide (Menzel-Gläser by Thermo Fisher Scientific). Before starting, the inlets and outlets of the fluids are created with a biopsy punch (diameter of 1 mm). After that, the microbioreactor is sealed to another piece of PDMS (to support the needle connected to the syringe pump, then inserted) and subsequently to the glass slide with the following procedure:

1. Cleaning of the device and the glass, or PDMS, base with scotch tape. Dust and any residue in this way are removed;

2. Insertion of the two pieces in the Plasma Cleaner (PDC-002-CE by Harrick Plasma Figure b with the surface that must be activated upwards;
3. Plasma cleaner is closed keeping the valve close (vertical position);
4. Starting the vacuum pump to create vacuum inside the Plasma Cleaner;
5. After approximately 4 minutes, the vacuum is reached, and the Plasma Cleaner is switch on;
6. After 15 seconds plasma appears, and the valve is gently opened to allow the entrance of air (the color should be an intense pink, Figure 3.25a, not violet or blue, both meaning lack of oxygen);
7. Plasma is maintained for 1 minute and 30 seconds;
8. After, Plasma Cleaner and vacuum pump are switched off in this sequence. The valve is slowly opened to return to atmospheric pressure;
9. The door is opened, and the pieces are removed, paying attention to not touching the activated surfaces;
10. Afterwards, surfaces are put in contact and they attach;
11. The new platform is introduced in the oven at 65°C for at least 10 minutes, to promote the formation of covalent bonds.

In this configuration the cells cannot be inserted neither before the plasma treatment, because of its high energy that can damage the culture. An image of the final platform is shown in Figure 3.26.

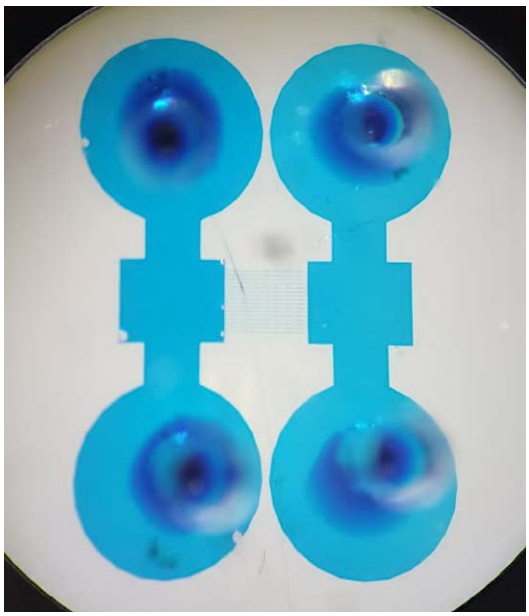

**Figure 3.26** *Final platform: layer of PDMS attached to a glass slide through plasma treatment and filled with blue colorant.*

## 3.5 Hydraulic seal validation

The hydraulic seal of the final platform is validated with colorants and fluorescent tracers to guarantee a proper operation inside the microfluidic device. This validation was favored by the optical properties of PDMS, as its transparency makes it easier to observe under the microscope. The colorants validation is done using a blue food coloring and fluorescent substances solutions prepared by mixing them with PBS or water. A syringe pump is used to infuse the solution inside the micro-bioreactor. The pump PHD Ultra (Harvard Apparatus), in Figure 3.27, is composed by a mechanical multi-rack unit where syringes can be placed and a central body with a display used to set up flow rates syringes types. The fluorescent substances used are fluorescein isothiocyanate-dextrans (SIGMA- ALDRICH®), polymers of anhydroglucose. Their maximum excitation is at a wavelength of 490nm, and the maximum emission is at 520nm. The isothiocyanate-dextran solution is prepared by diluting it in phosphate buffered saline (PBS) or water in a proportion 0.0005g/10mL. For the fluorescent tracers the culture media is not used as a solvent, since it contains phenol red that can interfere with the fluorescence acquisitions.

The experiment procedure consists of the following steps:

- The microfluidic device is filled using the two inlets and outlets of the platform with water to remove all the bubbles of air trapped inside the microbioreactor (this step is called "*debubbling*");
- 5 mL syringes (NYPRO) are filled with the colorant mixtures (particular attention must be taken in covering the syringes with aluminum foil to avoid light-induced damage to the fluorescent tracers): a 21G steel dispensing tip (DRIFTON) is inserted inside a microtube (inner diameter 0.5 mm, outer diameter 1.5 mm, TYGON® TUBING) and then connected to the syringe;
- A flow rate of 5 μL/h is set, the pump is started and once the fluid has completely filled the tube the syringes are connected to the platform, filling it.

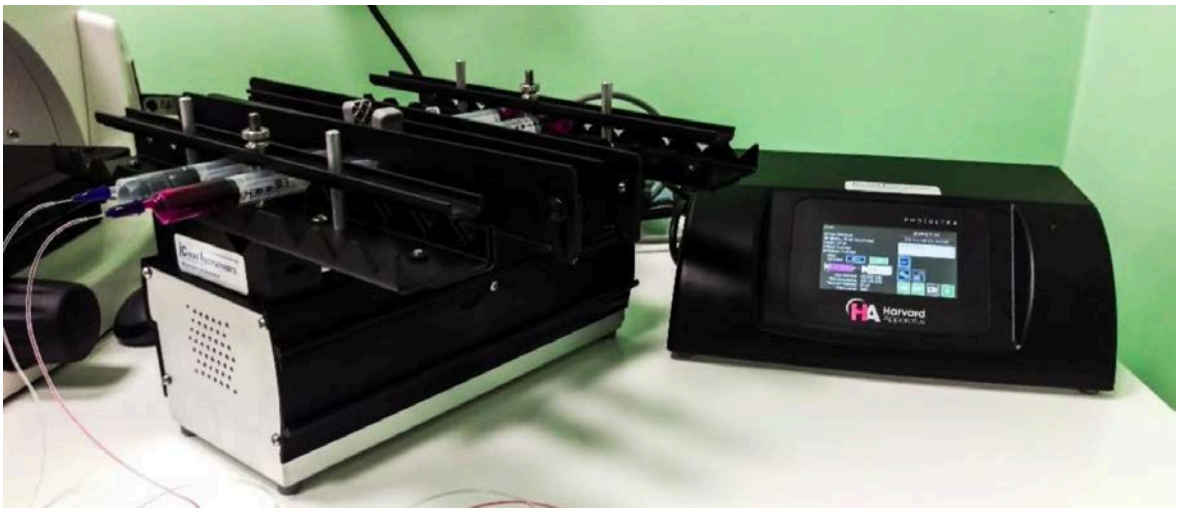


**Figure 3.27** *Pump PHD Ultra by Harvard Apparatus employed in BIAMET laboratory.*

The results of this validation experiments highlighted the perfect hydraulic seal of the platform as it is possible to observe in Figure 3.28 and Figure 3.29. Because of the transparence of PDMS some autofluorescence phenomena are present especially in the input/output area

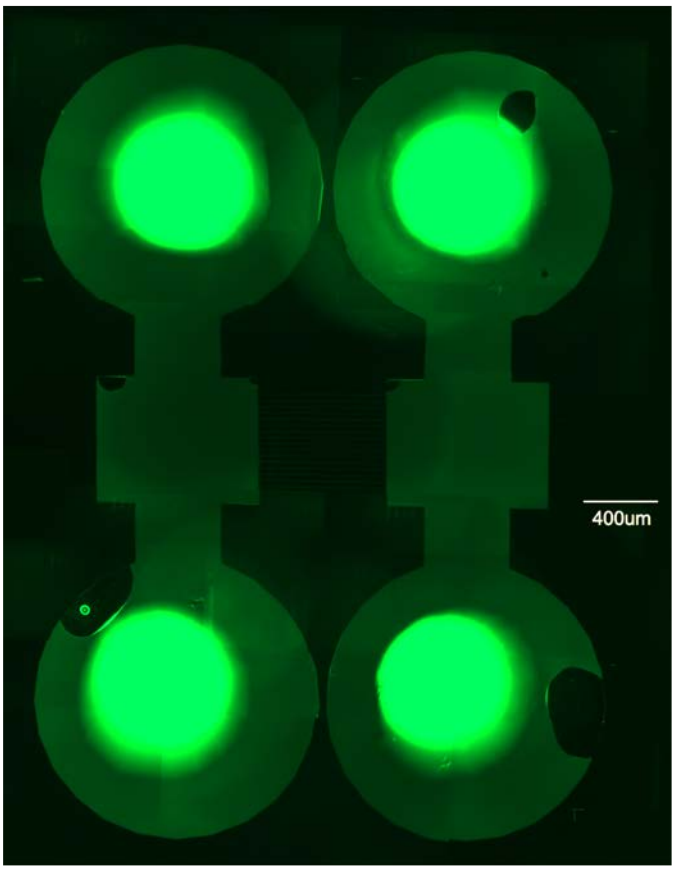


**Figure 3.28** *Final platform: layer of PDMS attached to a glass slide through plasma treatment and filled with fluorescent solution.*

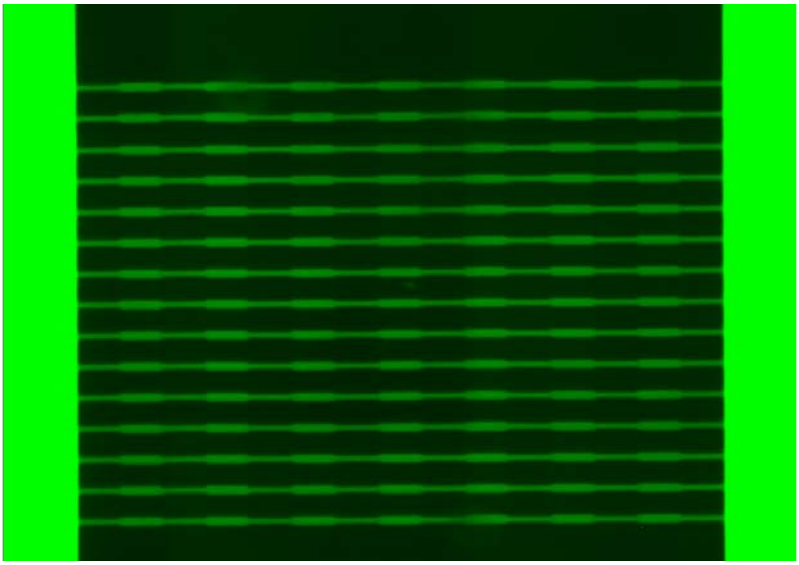

**Figure 3.29** *Channels section: layer of PDMS attached to a glass slide through plasma treatment and filled with fluorescent solution at 10x.*

# Chapter 4

# Biological validation

In this Chapter biological tests performed using SK-N-AS cell line are explained and discussed. Initially, the aim is to verify if cells are able to attach and growth inside the platform produced, and then to verify if the cells move through the channels. In the final part of the chapter the tests to induce migration inside the microfluidic platform are reported.

## 4.1 Biological validation with SK-N-AS cells

The microfluidic platform is first validated using SK-N-AS, (Figure 4.1) a human neuroblastoma cell line. Maintenance of these cells in culture is more difficult and their growth is slower compared to other cell lines typically used for validation experiments. We nonetheless decided to use them because of their biological relevance for Neuroblastoma research. SK-N-AS need a culture medium constituted by specific components that provide nutrients to the cells and allows their growth. The solution is composed by:

- a base medium DMEM (Dulbecco's Modified Eagle Media by Thermofisher Scientific);
- 10% v/v of fetal bovine serum (FBS), 1% v/v of MEM (a modified Basal Medium Eagle media containing higher concentrations of essential nutrients) and 1% v/v of Penstrep (an antibiotic to prevent contamination).

The mixture is then filtered and stored at temperature of 4°C.

### *4.1.1 Cellular culturing and splitting*

This operation allows the continuous growth of the cell population, so that they can be used in the experiments. During splitting, cells can counted be in order to seed precise numbers for the specific experiment planned. Eventually, the cells are seeded in the platform previously prepared. The majority of these actions are carried out under a biosafety cabinet.

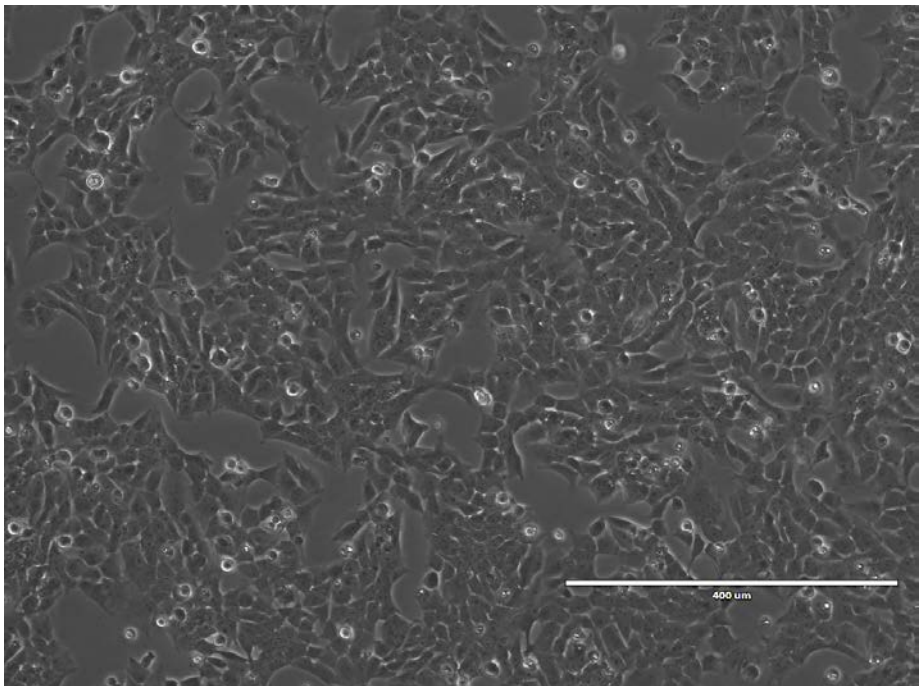


**Figure 4.1** *SK-N-AS cells seeded in a 75cm$^2$ flask.*

Firstly, culture media and Trypsin/EDTA solution (Biochrom GmbH) are warmed in a 37°C waterbath (Bagnomaria Serie Pura, Julabo, Sacco srl). Trypsin is a serine protease used to cut bonding proteins of cells to the flask surface. Then, the flask containing the cells is taken from the incubator and placed in the biosafety cabinet.
The process of splitting is the following:

- The spent medium (7-8 ml) is removed by aspiration with a serological pipet, stored and kept in a 15 mL Falcon tube;
- The bottom surface of the flask is gently washed with 7-8 ml of PBS at room temperature, to remove any trace of serum from culture media, that contains trypsin inhibitors. Subsequently PBS is aspirated and discarded;
- 2 ml of Trypsin are added on the cell layer and the flask is placed in the incubator for 3-4 min. The detachment of cells can be observed by gently hitting the flask;
- 4 ml of the stored spent medium are added in the flask, to inhibit the action of Trypsin. By gentle pipetting, the cells are aspirated from the bottom surface and placed in a 15 ml Falcon tube;
- The Falcon tube is centrifuged at 3000 rpm and 25°C for 5 minutes, setting the soft deceleration. This induces the sedimentation of the cells that form a dense pellet, while the residues remain in the supernatant. The liquid is aspired through a glass Pasteur pipette connected to a vacuum pump;

- The cells are counted, and an appropriate aliquot of cell suspension is added to a new 75 $cm^2$ flask, with 7-8 mL of fresh culture media. An inoculum of $2 \cdot 10^3$ to $6 \cdot 10^3$ cells/$mm^2$ is recommended.

The splitting is usually performed every 3-4 days. The color of the medium is an index of cell growth, shifting from red to brown/yellow because of the pH change due to the depletion of nutrients. This means that if necessary, the splitting process can take place even before the third day.

### *4.1.2 Cellular counting*

The procedure of cellular counting is necessary whenever the total number of cells, suspended in a certain volume of liquid, must be known. This is important during the seeding of cells inside microfluidic platforms, since specific and controlled cell densities inside the chamber are required. For this purpose, a hemocytometer, the Bürker chamber, is used. An example is reported in Figure 4.2: it is formed by a rectangular microscope slide with a rectangular indentation that creates a chamber. This latter is engraved with a laser-etched grid of perpendicular line. The area enclosed by the line is known, as well the volume of the chamber.

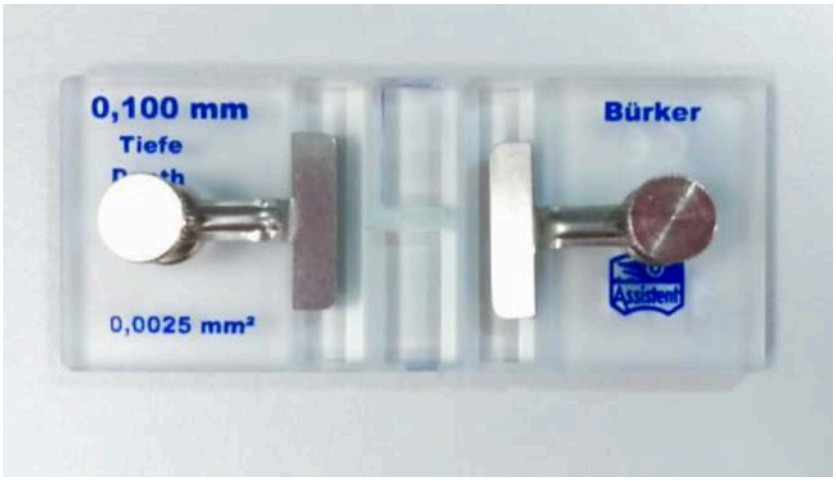


**Figure 4.2** *An example of hemocytometer: the two chambers to count cells are two small rectangles in the middle of the device.*

Therefore, it is possible to count the number of cells present in a specific volume of fluid, and so the total number of cells. The Bürker chamber is formed by two 3x3 mm larger squared cells with a depth of 0.1 mm. Each cell is divided in 9 squares (1 mm side), each one further divided in 16 smaller squares (0.2 mm side).
The chamber is prepared by placing a glass slide over the chamber and locked it with the two lateral latches. To count the total number of cells the main steps are:

- The cell suspension is diluted (commonly 10 times) with some fresh culture media and gently pipetted in order to avoid clustering and sedimentation of cells;
- 10 μL of cell suspension are collected with micropipette and positioned on one side of the Bürker chamber, forming a bubble. Then 10 μL of Trypan Blue (Invitrogen), a cell stain that colors in blue only dead cells, are mixed with the cells by pipetting. Viable cells do not take up this dye, since their membrane is impermeable (dead cells' membrane is permeable and therefore become blue);
- 10 μL of the mixture are inserted between the chamber and the glass slide by capillarity;
- The chamber is observed at the microscope with a 10x objective. Al least 5 squares are considered: the number of live cells is counted for each square, and then the arithmetic mean is calculated.
- At the end, knowing the mean number of cells per square ($N_{mean}$), the concentration of cells can be evaluated as follows in Equation (4.1):

$$N_{cell} = N_{average} \cdot d_1 \cdot d_2 \cdot K \cdot V_{sosp}, \tag{4.1}$$

Where $N_{average}$ is the average cells number counted in one square of the Bürker chamber (Figure 4.3), $d_1$ and $d_2$ are dimensionless numbers that represents the dilution factor of cell suspension and the dilution factor for the Trypan Blue, $K$ [μL $^{-1}$] is a constant related to the geometry of the hemocytometer and $V_{sosp}$ [μL] is the volume of medium culture added to the cells after detachment process.

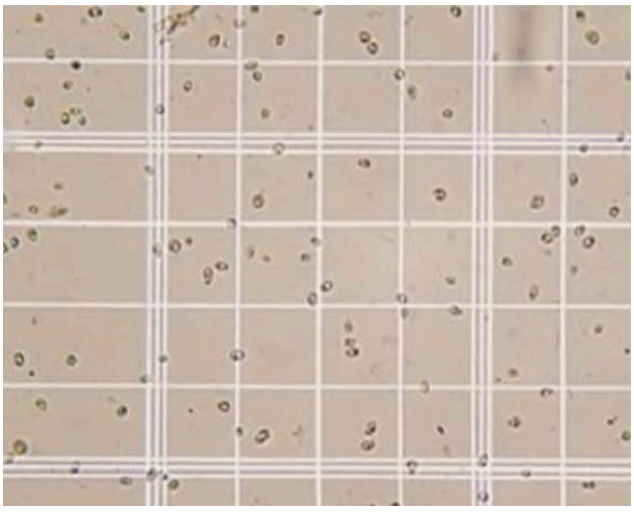

**Figure 4.3** *One of the 9 squares divided by three parallel lines which are present on each of the two chambers; the small points visible inside the squares are cells.*

In this case 10 is the dilution factor of cell in suspension, 2 the dilution factor for the Trypan Blue and 10000 is the constant, that includes information about the geometry and volume of

the chamber (number of squares per mL). The number of cells per mL is obtained, and this value can be multiplied for the total volume to obtain the total number of cells.[8]

## 4.2 Cellular seeding in microfluidic platform

Cells are kept in 75cm$^2$ flasks, immersed in culture media. Overcrowding of cells attached to the flask's bottom surface, must be avoided through a subculturing process, also called cellular splitting. A specific value of confluence must not be exceeded, since cells would not be able to grow further.

### *4.2.1 Viability test*

First of all, the platform is placed inside a 10 cm diameter Petri dish, and prepared to host cells.

The "*debubbling*" step, explained in paragraph §3.5 is performed using sterile physiological solution. In this way the presence of bubbles inside channels is avoided. The preliminary seeding trial consists in introducing cells inside the platform directly on the lateral chamber, previously punched. At this point is important to take a target density $\rho_{target}$ [cells/mm$^2$] in order to calculate the volume of the medium $V_{sosp}$ [µL] in which the cells have to suspended. Then, few µL of this suspension are injected inside the lateral chamber of the platform (Figure 4.4).

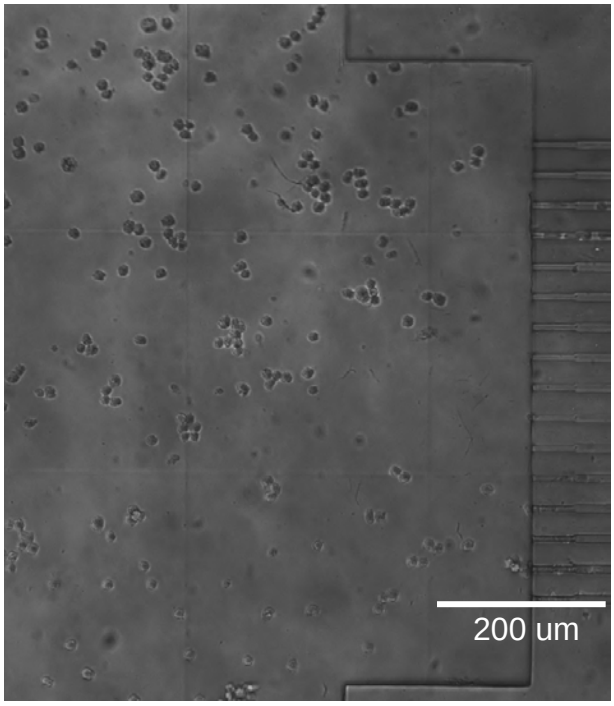


**Figure 4.4** *SK-N-AS seeded in the microfluidic platform.*

At the end, the device is covered by fresh culture medium, and some PBS solution is added to avoid evaporation of the culture medium. In Figure 4.5 is reported the image of cells inside the lateral chamber 36 hours after seeding.

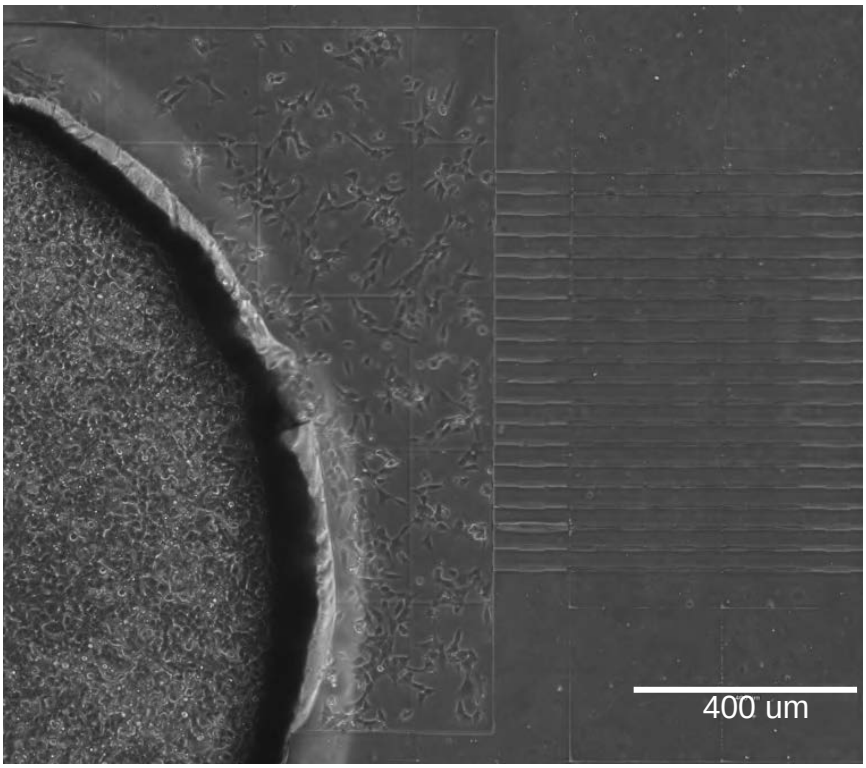


**Figure 4.5** *SK-N-AS seeded in the microfluidic platform after 36 hours.*

The figure shows that cells are attached to the surface of the chamber. It is possible to state that this microfluidic platform is a favorable environment for cell culture applications. However, this preliminary cell viability test was done by injecting cells directly into the side chamber, which was previously punched. In the next paragraph a protocol will be optimized to introduce the cells into the chamber from the previously described entrance doors.

## 4.3 Migration experiments

In order to validate the utility of the fabricated migration chip as *in vitro* model of migration, an excess of Fetal Serum Bovine (FBS) can be introduced as a chemoattractant for cell migration into the opposite chamber. In particular, the solution used as chemoattractant is DMEM base with the adding of 20% of FBS, while the cells are seeded in DMEM only. The idea is that highly migratory cells move to the chamber of the left side (serum-free media) to the other one rich in serum as it shown in the scheme in Figure 4.6.

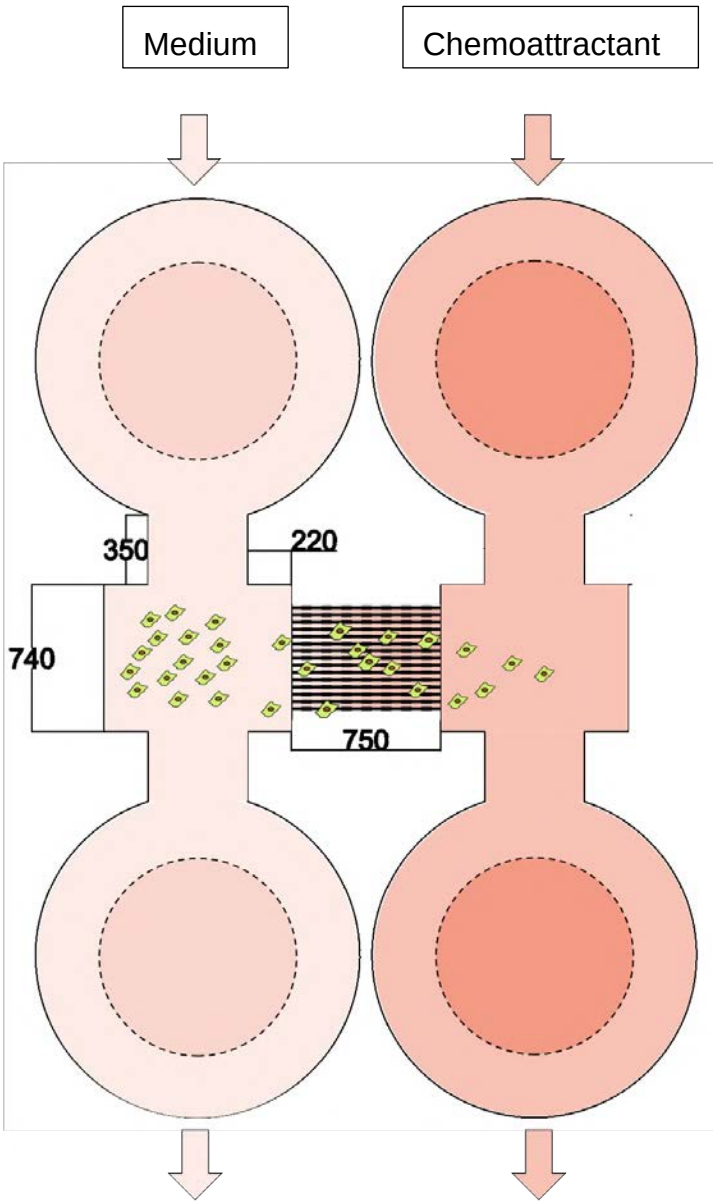


**Figure 4.6** *Scheme of migratory platform. Measures expressed in µm.*

### *4.3.1 Labeling assay*

Non-invasive cell tracking is crucial to fully understand the behavior of the motile cells during the migration processes. The tracer cell used is the Vibrant Dil cell-labeling solution (Thermo Fisher®). Dil is a lipophilic membrane stain that diffuses laterally to stain the entire cell. It is weakly fluorescent until incorporated into membranes. Its maximum excitation is at a wavelength of 520 nm and maximum emission is at a wavelength of 570 nm. This orange-red fluorescent dye is often used as a long-term tracer for neuronal and other cells.

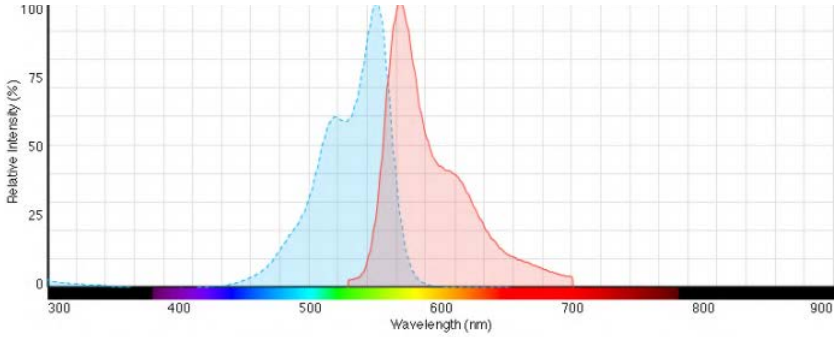


**Figure 4.7** *Fluorescence spectra of DiI: in blue the excitation plot and in red the emission one. Adapted from*[50]

The protocol of labeling of cells in suspension is explained below:

1. Suspend cells at a density of 1 x $10^6$ cells/mL in any chosen serum free culture medium;
2. Add 5 µL of cell-labeling solution supplied per mL of cell suspension. Mix well by gently pipetting;
3. Incubate for 30 minutes at 37°C to obtain a uniform staining;
4. Centrifuge the labeled suspension at 1500 rpm for 5 minutes, preferably at 37°C;
5. Remove the super at ant and gently resuspend the cells in warm (37°C) DMEM (serum-free medium);
6. Repeat the wash procedure (4. and 5.) two more times.

### *4.3.2 Results of migration experiments*

The first step was to calculate the required density for the staining protocol: $10^6$ cells suspended in 1 mL with 5 µL of DiI as explained in paragraph §4.3.1. After staining, the cells were introduced into the platform using a 10-µL micropipette, fixing an entry volume of 1 µL. This to ensure complete chamber filling. The observations under the microscope unfortunately show how the cells, from a fluid dynamic point of view, tend to cluster at the edge of the platform, at inlets and outlets (Figure 4.8).

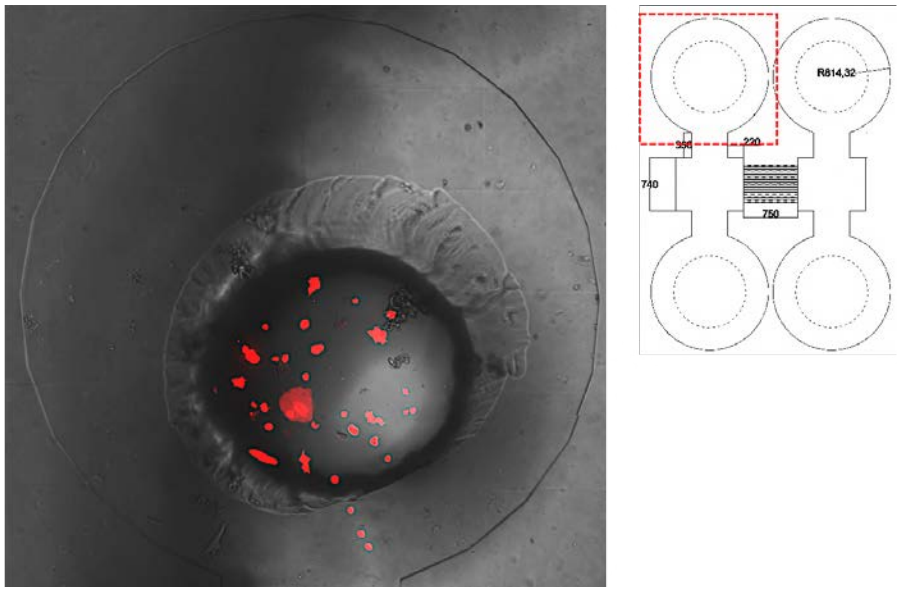


**Figure 4.8** *Cells stained with Dil with a density of $10^6$ cells/mL.*

To overcome the problem, the density of cells was increased to $4x10^6$ cell/mL. The results are also improved by increasing the density of cells in liquid volume. The cells were able to move, and to reach and settle inside the lateral chamber (Figure 4.9-10). Some cells also managed to enter the channels thanks to the difference in pressure, that was generated at the time of seeding (Figure 4.11).

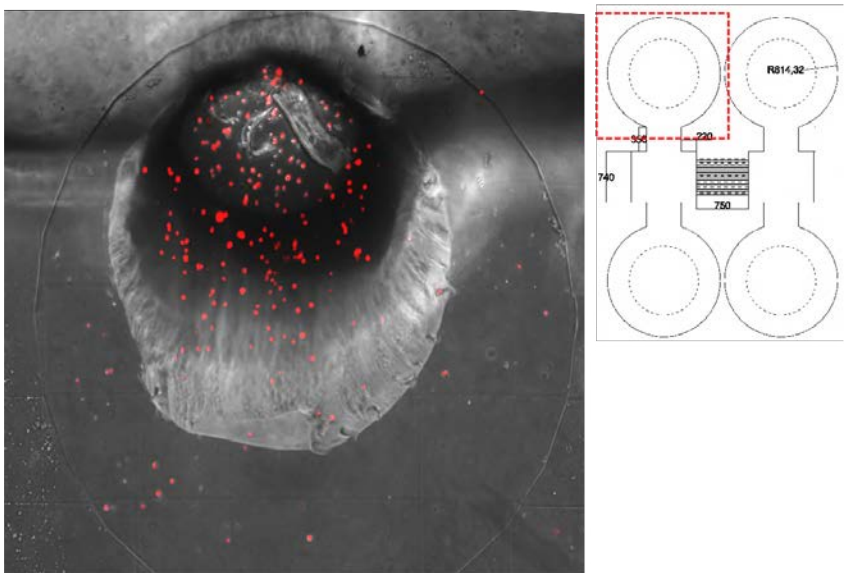


**Figure 4.9** *Cells stained with Dil with a density of $4x10^6$ cells/mL, inlet section.*

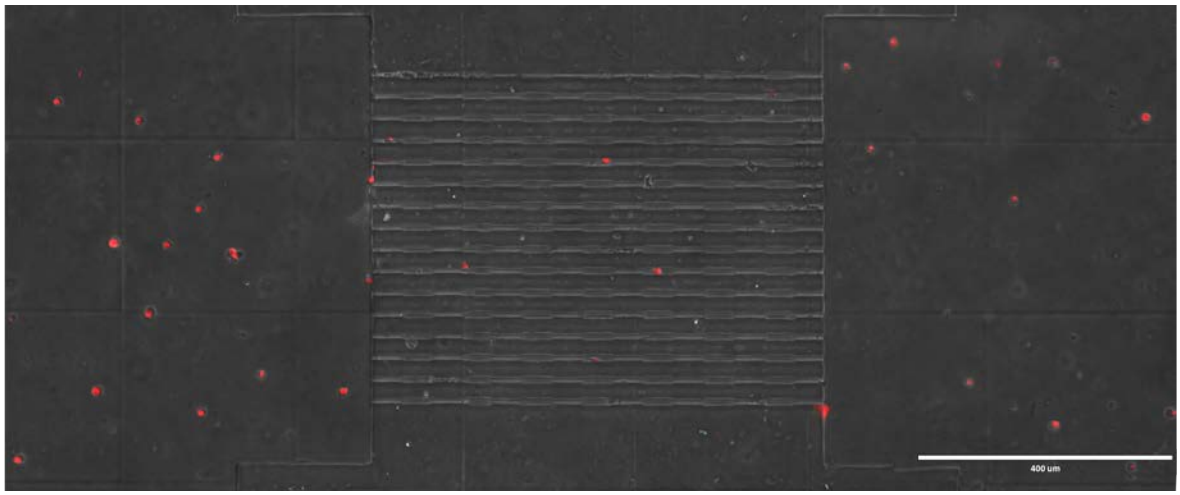


**Figure 4.10** *Cells stained with Dil with a density of $10^6$ cells/mL, chambers section.*

This confirms how the dimensions of the channels, although very small, are suitable for the purpose of the study. Finally, we can say that despite the increased seeding density, cells still have a preferential position at the inlets and outlets of the side area (**Figure 4.1**).

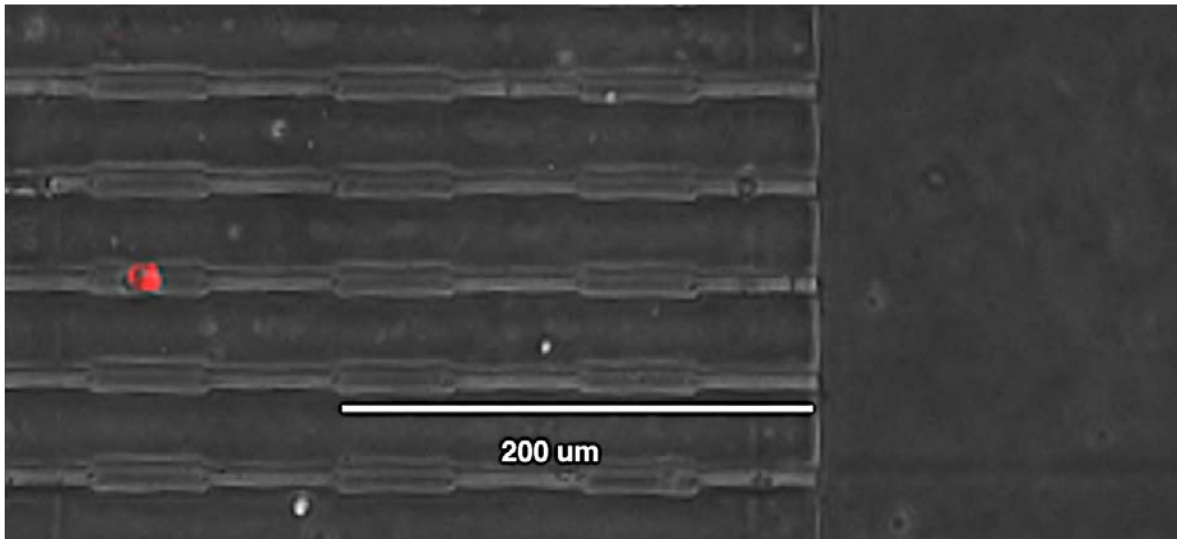


**Figure 4.11** *Cell stained with Dil with a density of $10^6$ cells/mL inside a channel.*

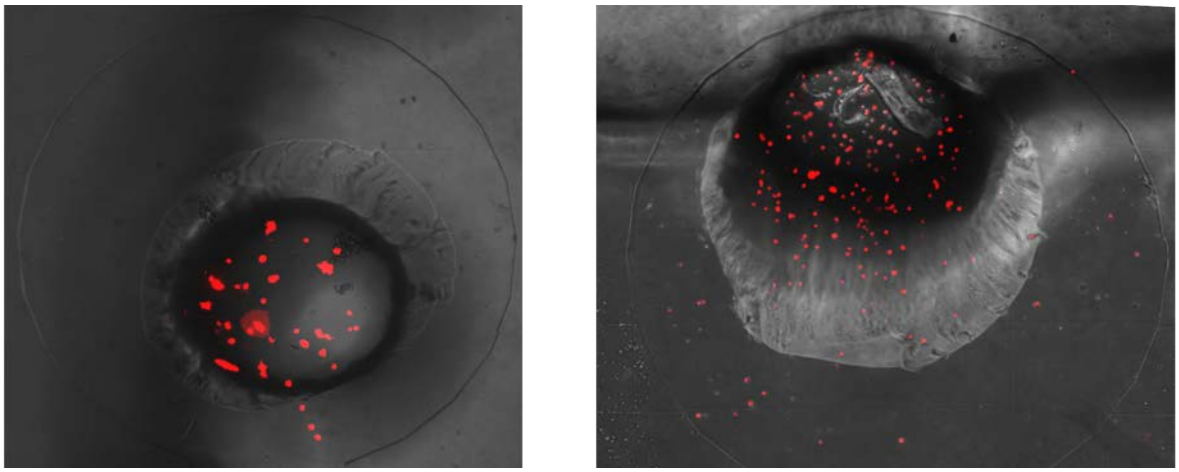

**Figure 4.12** *Comparison between cells stained with Dil with a density of $10^6$ cells/mL and a density of $4x10^6$ cells/mL.*

The hypothesis of the addition of a new exclusive door for the seeding has been proposed, as shown in Figure 4.13. This should allow better directing of the seeded cells to the side chamber.

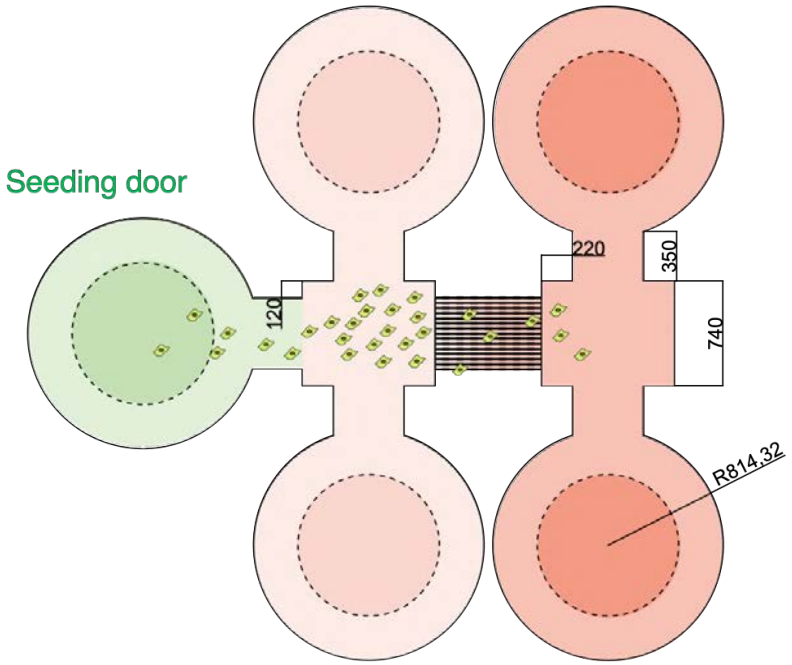


**Figure 4.13** *Scheme of the migratory platform with the additional seeding door. Measure expressed in µm.*

#### 4.3.2.1 Seeding door geometry results

Before introducing the cells inside the microfluidic platform, the *"debubbling"* process was carried out as explained in the paragraph §3.5. A target density of 20 cell/mm$^2$ was taken in order to calculate the volume of the medium $V_{sosp}$ [µL] in which the cells have to suspended.

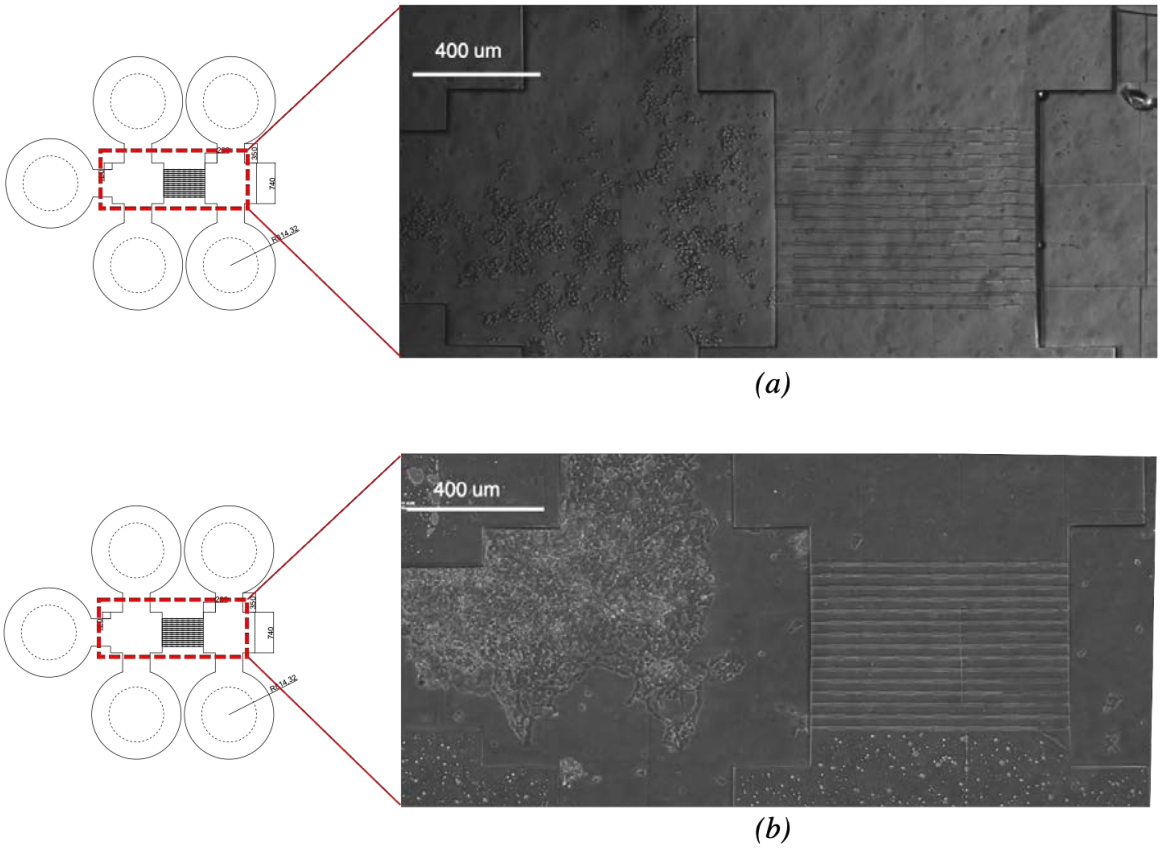


**Figure 4.14** *SK-N-AS cells inside the chamber: (a) Cells immediately after the seeding; (b) Cells after 24 hours from seeding.*

Then, the cells were resuspended in medium serum-free and introduced gently inside the platform with a micropipette (Figure 4.14 a). The cells after 24 are visibly alive and attached to the surface of the slide, inside the chamber, without the need of adhesion promoter over the glass surface (Figure 4.14 b), reconfirming the biocompatibility of the environment. In conclusion, it can be confirmed that the presence of the added seeding door is essential for the correct introduction of cells into chamber.

# Conclusions

This thesis aimed to design an innovative microfluidic device that would allow studying the migration of cancer cells to a *"single-cell"* resolution and based on a novel production technology: two-photon polymerization. The device presents a series of micro-channels in which the cell is free to migrate when subjected to chemical or biological stimuli. The key element is the structure of the micro-channels that, designed with shrinkages and larger sections, recall the shape of lymphatic vessels, the main migration ducts. The numerical solutions, performed using COMSOL Multiphysics® software, allowed an optimization of the geometry, mainly on the size of the narrowing, to obtain a better performance of the platform. The results also prove the feasibility of obtaining a stable concentration gradient within the micro-channels. This will ensure the study of migration for chemotaxis, i.e. directional migration process, guided by gradients of chemo attractive or repulsive substances.

All the proposed designs were fabricated employing *Nanoscribe Photon Professional GT*, a precision nano-metric 3D printer. A 3D construction of the micro-channels in acrylate resin does not allow to have a rigid structure and a favorable environment for the growth and migration of the cells. The two-photon technology was thus reworked to produce the master of the device, that, combined with *replica molding*, would lead to obtain the final platform. The heights of the channels were measured with the Sensofar S Neox profilometer. It was concluded that it is possible to build a master with nano-metric features that successfully transfer to the replica molded devices.

This new method resulted in a reduction of time, costs, and quantities of substances compared to established master production methods such as photolithography and micromilling. The result is a microfluidic platform, which successfully replicated the required micro- and nano-metric sizes and dimensions. With its excellent hydraulic sealing and very good cellular biocompatibility, this device can be, for all intents and purposes, a valuable tool for the study of cancer cell migration.

# Appendix

## A.1 Additional data of COMSOL® Multiphysics.

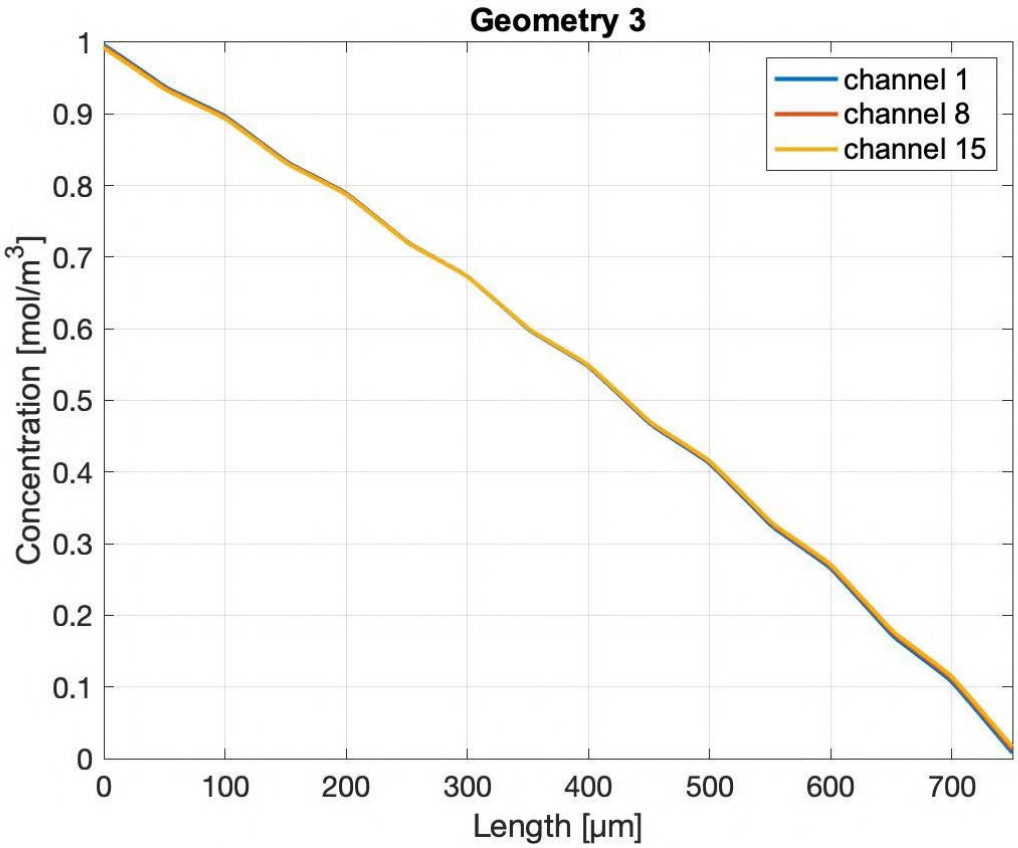


**Figure A.1** *Geometry 3: Expected concentration along the first, eighth and fifteenth channels of the platform.*

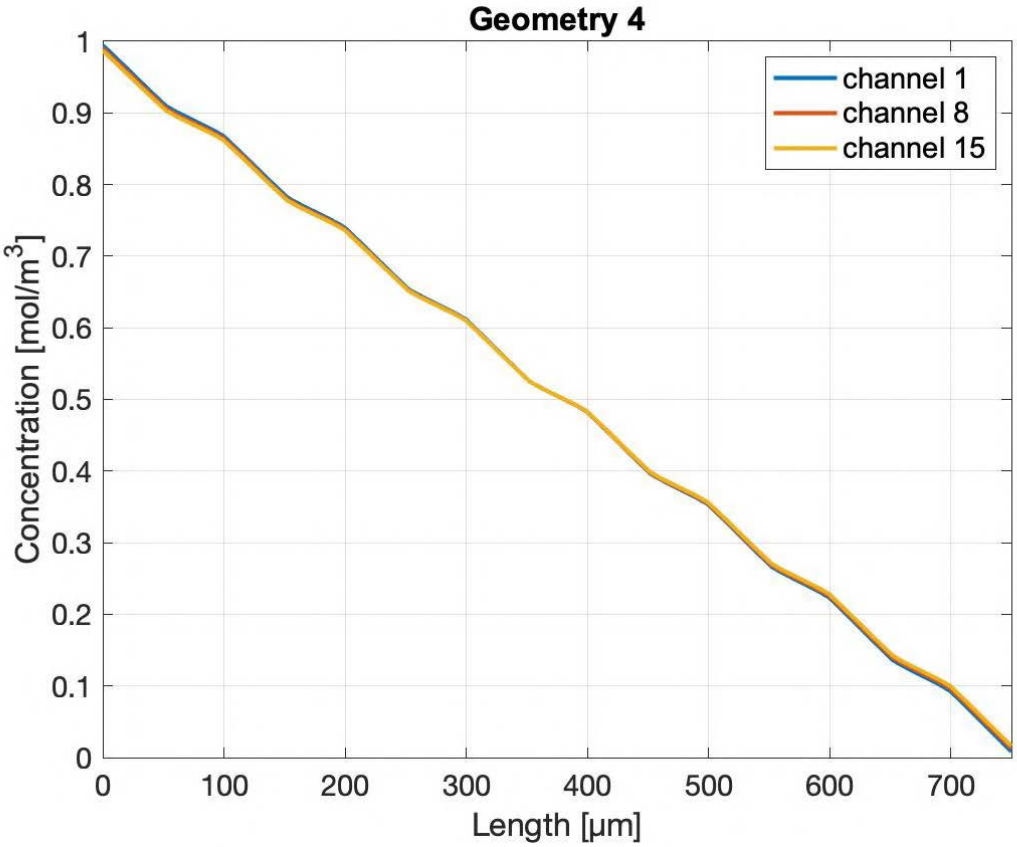


**Figure A.2** *Geometry 4: Expected concentration along the first, eighth and fifteenth channels of the platform.*

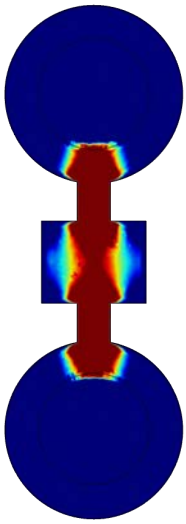

**Figure A.3** *Channel 2 : results of the COMSOL simulation for the velocity magnitude.*

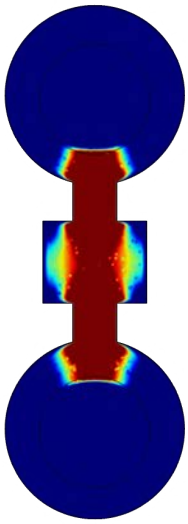

**Figure A.4** *Channel 4: results of the COMSOL simulation for the velocity magnitude.*

# References


1.Nguyen, N.-T. & Wereley, S. T. *Fundamentals and applications of microfluidics*. (Artech House, 2006).

2.Whitesides, G. M. The origins and the future of microfluidics. *Nature* **442**, 368–373 (2006).

3.Cimetta, E. *et al.* Microfluidic bioreactor for dynamic regulation of early mesodermal commitment in human pluripotent stem cells. *Lab Chip* **13**, 355–364 (2013).

4.Squires, T. M. & Quake, S. R. Microfluidics: Fluid physics at the nanoliter scale. *Rev. Mod. Phys.* **77**, 977–1026 (2005).

5.Galeotti - Modeling-based design optimization of microfluidic.pdf.

6.Bird, R. B., Stewart, W. E. & Lightfoot, E. N. *Transport phenomena*. (J. Wiley, 2002).

7.Beebe, D. J., Mensing, G. A. & Walker, G. M. Physics and Applications of Microfluidics in Biology. *Annu. Rev. Biomed. Eng.* **4**, 261–286 (2002).

8.Battaiotto, G. Design, development and validation of microfluidic platforms for biomedical applications. 114.

9.Breslauer, D. N., Lee, P. J. & Lee, L. P. Microfluidics-based systems biology. *Mol. Biosyst.* **2**, 97 (2006).

10.Cimetta, E. *et al.* Microfluidic bioreactor for dynamic regulation of early mesodermal commitment in human pluripotent stem cells. *Lab Chip* **13**, 355–364 (2013).

11.Galeotti, C. Modeling-based design optimization of microfluidic gradient generator and validation with cell cultures. 108.

12.Bhawalkar, J. D., He, G. S. & Prasad, P. N. Nonlinear multiphoton processes in organic and polymeric materials. 32.

13.Wu, S., Serbin, J. & Gu, M. Two-photon polymerisation for three-dimensional micro-fabrication. *J. Photochem. Photobiol. Chem.* **181**, 1–11 (2006).

14.Fischer, J. & Wegener, M. Three-dimensional optical laser lithography beyond the diffraction limit: 3D optical lithography off limits. *Laser Photonics Rev.* **7**, 22–44 (2013).

15.Xiong, W. *et al.* Simultaneous additive and subtractive three-dimensional nanofabrication using integrated two-photon polymerization and multiphoton ablation. *Light Sci. Appl.* **1**, e6–e6 (2012).

16.Niesler, F. & Hermatschweiler, M. Two-Photon Polymerization - A Versatile Microfabrication Tool: From maskless lithography to 3D printing. *Laser Tech. J.* **12**, 44–47 (2015).

17.Maruo, S. & Fourkas, J. T. Recent progress in multiphoton microfabrication. *Laser Photonics Rev.* **2**, 100–111 (2008).

18.You, S. *et al.* Nanoscale 3D printing of hydrogels for cellular tissue engineering. *J. Mater. Chem. B* **6**, 2187–2197 (2018).
19.Farsari, M., Vamvakaki, M. & Chichkov, B. N. Multiphoton polymerization of hybrid materials. *J. Opt.* **12**, 124001 (2010).
20.Waheed, S. *et al.* 3D printed microfluidic devices: enablers and barriers. *Lab. Chip* **16**, 1993–2013 (2016).
21.Kim, A. & Makariou, E. Metastatic neuroblastoma. *Applied Radiology* (2006).
22.Galarza, S., Kim, H., Atay, N., Peyton, S. R. & Munson, J. M. 2D or 3D? How cell motility measurements are conserved across dimensions *in vitro* and translate *in vivo*. *Bioeng. Transl. Med.* **5**, (2020).
23.Friedl, P. & Gilmour, D. Collective cell migration in morphogenesis, regeneration and cancer. *Nat. Rev. Mol. Cell Biol.* **10**, 445–457 (2009).
24.Disanza, A. *et al.* Is cell migration a selectable trait in the natural evolution of cancer development? *Philos. Trans. R. Soc. B Biol. Sci.* **374**, 20180224 (2019).
25.Hou, Y. Orchestrating cancer cell migration: Quantatitive analysis of protrusion, adhesion and contraction dynamics regulated by epidermal growth factor and collagen. 4615852 (Iowa State University, Digital Repository, 2013). doi:10.31274/etd-180810-3610.
26.Chen, H.-C. Boyden Chamber Assay. in *Cell Migration* vol. 294 015–022 (Humana Press, 2004).
27.https://www.merckmillipore.com/IT/it/life-science-research/antibodies-assays/assays-overview/cell-invasion-migration-assays/boyden-chamber-technique/I0qb.qB.KSMAAAFANtY.1ZcQ,nav.
28.Fisher, J. P. H. & Tweddle, D. A. Neonatal neuroblastoma. *Semin. Fetal. Neonatal Med.* **17**, 207–215 (2012).
29.Davidoff, A. M. Neuroblastoma. *Semin. Pediatr. Surg.* **21**, 2–14 (2012).
30.Li, W. *et al.* Role of exosomal proteins in cancer diagnosis. *Mol. Cancer* **16**, 145 (2017).
31.Braicu, C. *et al.* Exosomes as divine messengers: are they the Hermes of modern molecular oncology? *Cell Death Differ.* **22**, 34–45 (2015).
32.Agnes Dobos, Jasper Van Hoorick, Wolfgang Steiger, Peter Gruber, Marica Markovic, Orestis G. Andriotis, Andreas Rohatschek, Peter Dubruel, Philipp J. Thurner, Sandra Van Vlierberghe, Stefan Baudis, Aleksandr Ovsianikov. Bioprinting: Living cells in a 3D printer. *ScienceDaily* https://www.sciencedaily.com/releases/2019/10/191021103905.htm (2019).
33.Versteeg, H. K. & Malalasekera, W. *An introduction to computational fluid dynamics: the finite volume method*. (Pearson Education Ltd, 2007).
34.Introduction to Application Builder. 382 (2019).
35.Welty, J. Fundamentals of Momentum, Heat and Mass Transfer, 5th Edition. 729.
36.CFD Module Users Guide.pdf.
37.Chen, Y.-C. *et al.* Single-cell Migration Chip for Chemotaxis-based Microfluidic

Selection of Heterogeneous Cell Populations. *Sci. Rep.* **5**, 9980 (2015).
38.Hsieh, S.-S., Lin, C.-Y., Huang, C.-F. & Tsai, H.-H. Liquid flow in a micro-channel. *J. Micromechanics Microengineering* **14**, 436–445 (2004).
39.M., Cimbala, John. *Fluid mechanics : fundamentals and applications.* (2006).
40.BasicTraining_Nanoscribe.pdf.
41.User_Manual_digital_Nanoscribe.pdf.
42.Campbell, J. H. *et al.* Three-dimensional printing and deformation behavior of low-density target structures by two-photon polymerization. in *Nanoengineering: Fabrication, Properties, Optics, and Devices XIV* (eds. Campo, E. M., Dobisz, E. A. & Eldada, L. A.) 66 (SPIE, 2017). doi:10.1117/12.2274193.
43.https://www.uni-muenster.de/imperia/md/content/mnf/ip-dip_photoresist.pdf.
44.https://www.uni-muenster.de/imperia/md/content/mnf/ip-s_photoresist.pdf.
45.https://www.sensofar.com/metrology/products/sneox/.
46.Passalacqua, L. Additive manufacturing and injection molding for rapid prototyping of meso-scale devices for biomedical studies. 103.
47.PDMS and Microfluidics. Available at: https://www.elveflow.com/microfluidic-tutorials /microfluidic-reviews-and-tutorials/the-poly-di-methyl-siloxane-pdms-and- microfluidics/.
48.Kuncova-Kallio, J. & Kallio, P. J. PDMS and its Suitability for Analytical Microfluidic Devices. in *2006 International Conference of the IEEE Engineering in Medicine and Biology Society* 2486–2489 (IEEE, 2006). doi:10.1109/IEMBS.2006.260465.
49.Weibel, D. B., DiLuzio, W. R. & Whitesides, G. M. Microfabrication meets microbiology. 10 (2007).
50.LaFratta, C. N. *et al.* Replication of Two-Photon-Polymerized Structures with Extremely High Aspect Ratios and Large Overhangs. *J. Phys. Chem. B* **108**, 11256–11258 (2004).
51.https://harrickplasma.com/what-is-plasma/.
52.https://www.azom.com/article.aspx?ArticleID=14346.
53.https://plasmatreatment.co.uk/pt/plasma-technology-overview/plasma-treatment-explained.
54.https://www.elveflow.com/microfluidic-reviews/soft-lithography-microfabrication/pdms-soft-lithography-plasma-cleaner/.
55.Squires, T. M. & Quake, S. R. Microfluidics: Fluid physics at the nanoliter scale. *Rev. Mod. Phys.* **77**, 977–1026 (2005).

Websites:

https://www.merckmillipore.com (Accessed 23/07/2020)

https://www.sciencedaily.com/releases/2019/10/191021103905.htm (Accessed 10/08/2020)

https://www.uni-muenster.de/imperia/md/content/mnf/ip-dip_photoresist.pdf. (Accessed 12/07/2020)

https://www.uni-muenster.de/imperia/md/content/mnf/ip-s_photoresist.pdf. (Accessed 23/07/2020)

https://www.sensofar.com/metrology/products/sneox/. (Accessed 30/07/2020)

https://www.comsol.it/model/flow-through-a-pipe-elbow-12221 (Accessed 04/10/2020)

https://harrickplasma.com/what-is-plasma/ (Accessed 17/11/2020)

https://www.elveflow.com (Accessed 01/12/2020)